University of Washington
Department of Civil and Environmental Engineering

TREES, SNOW AND FLOODING: AN INVESTIGATION OF FOREST CANOPY EFFECTS ON SNOW ACCUMULATION AND MELT AT THE PLOT AND WATERSHED SCALES IN THE PACIFIC NORTHWEST

Pascal Storck

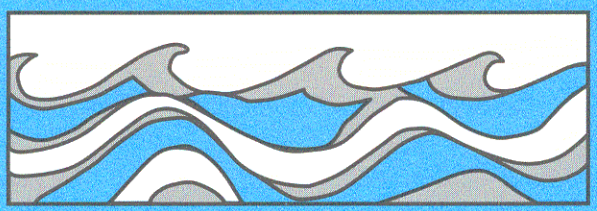

Water Resources Series
Technical Report No.161
March 2000

Seattle, Washington
98195

Department of Civil Engineering
University of Washington
Seattle, Washington 98195

TREES, SNOW AND FLOODING: AN INVESTIGATION OF FOREST CANOPY EFFECTS ON SNOW ACCUMULATION AND MELT AT THE PLOT AND WATERSHED SCALES IN THE PACIFIC NORTHWEST

Pascal Storck

Water Resources Series
Technical Report No. 161

June 1999

ABSTRACT

Concerns about the extent to which major Pacific Northwest floods over the last decade might have been exacerbated by logging have heightened the need for a better scientific understanding of the role of forest maturity on snow accumulation and melt. To address this need, a multi-scale field and modeling study of the effects of forest canopies on snow accumulation and melt was conducted. Over a three year period, weighing lysimeters and cut-tree experiments were used to measure the processes controlling snow interception and its fate at a site in the Umpqua National Forest, OR (elevation 1200 m). Continuous observations of below-canopy snowpack evolution were made over the same period. Over the study period, approximately 60 percent of annual snowfall was intercepted by the canopy (up to a maximum of 40 mm water equivalent). Approximately 72 percent and 28 percent of the intercepted snow was removed as meltwater drip and large snow masses, respectively. Apparent average sublimation rates from the intercepted snow were less than 1 mm per day and totaled approximately 100 mm per winter season. Observed differences in snow interception and release between trees of different species were minimal.

These data, along with ancillary observations including standard micrometeorology, were used to construct, calibrate, and test an energy balance model of snow as affected by the forest canopy. Although initially implemented and tested on the Umpqua data, the model was designed for use in spatially distributed hydrology models designed to be applied at larger scales. Intercepted snow load was modeled as a function of Leaf Area Index and adjusted for the effects of air temperature. Removal of intercepted snow by sublimation, melt-water drip and mass release was explicitly modeled. A fractional canopy coverage parameter was used to scale from the plot to the stand scale. To support application in distributed hydrology models, a computationally efficient atmospheric stability correction was developed. The model was calibrated against one year of weighing lysimeter data and was tested at the plot scale against two

years of weighing lysimeter data and at the stand scale against three years of snow course data taken over an area of 26 ha at the Umpqua site.

The snow model was incorporated into the Distributed Hydrology Soil Vegetation Model (DHSVM) to explore the effect of forest canopy removal on floods during Rain-On-Snow (ROS) events in maritime climates like the Pacific Northwest. A sensitivity analysis of the 10 largest flood between 1988 and 1996 on the Snohomish River, which drains an area of 4000 km^2 of the western slopes of the Cascade Mountains in Washington State, was conducted. Predicted peak streamflow was increased by an average of 3 percent with the current vegetation cover relative to the historic land cover. Larger increases (> 10 percent) were predicted for headwater basins (Tolt River, average increase over all ten flood events of 8.9 percent), in which forest harvest has been concentrated, and events with a large snowmelt contribution. Overall, the average predicted increase in peak streamflow for current land cover relative to historic was below the minimum that could be detected in paired catchment studies.

Table of Contents

List of Figures

List of Tables

Acknowledgements

The research described in this report is based on the Ph.D. dissertation of the author, funding for which was provided through a NASA Earth Systems Science Fellowship. The field component of this work was a part of the Demonstration of Ecosystem Management Options Project, funding for which was provided by the USDA Forest Service PNW Research Station. Additional financial support was provided by the University of Washington Puget Sound Regional Synthesis Model (PRISM) project.

I would like to thank the members of my supervisory and reading committees for their encouragement and comments during the course of this research. Special thanks go to Walt Megahan for his careful review of the final manuscript, Susan Bolton for making feasible the inclusion of a substantial field campaign in my research, Stephen Burges for all of his encouragement and "chats", and finally Dennis Lettenmaier for keeping me on track, focused on the big picture, and introducing me to the topic. Additional thanks go to all the individuals that assisted with the field campaign. The assistance of Travis Kern was instrumental during all phases of the field campaign. At the Toketee Ranger Station, the support of Rick Abbot, Joe Brett and many others was greatly appreciated. I would also like to thank my colleagues at the University of Washington for all of their help, especially Bart Nijssen and Ken Westrick.

Chapter 1. Introduction

1.1. Background

During the winters of 1986, 1990, 1995, 1996 and 1997, the major rivers draining the western Cascade Mountains of Washington and Oregon experienced flooding events with estimated return periods that exceeded 100 years in some watersheds. These events have led to a widespread perception that the frequency and severity of extreme floods in the Pacific Northwest have increased. Although these perceived increases may be due to climate variability, the severity of the events has nevertheless focused attention on the possible causal links with land use changes, especially related to forest harvesting. This dissertation explores the effect of canopy removal due to forest harvest on peak streamflow during major floods in maritime mountainous watersheds such as those found on the western slopes of the Cascade Mountains in the Pacific Northwest.

Possible connections between forest harvest and peak streamflows have long been debated in the scientific literature (e.g., Anderson and Hobba 1959; Rothacher 1973; Harr and McCorison 1979; Harr 1981, 1986; Christner and Harr 1982; Jones and Grant 1996; Thomas and Megahan 1998; Bowling et al. 2000). Most investigations of forest harvest effects on floods have followed one of two paths of inquiry.

The first seeks to address the issue at the watershed scale, typically from 1 to 1000 km^2. These studies compare observed peak streamflows against a control series. The control series is typically obtained from observations of streamflow in an adjacent basin with a contrasting land use history or from a computer simulation of peak flows for the test basin with a fixed level of forest harvest (see e.g. Rothacher 1973, Harr and McCorison 1979, Harr 1981, Connelly et al. 1993, Storck et al. 1995, Jones and Grant 1996, Thomas and Megahan 1998, Bowling et al. 2000). The overall consensus of these studies is that land use changes related to forest harvesting have increased streamflows for smaller events (i.e. those that occur several times per year). Due

to the large natural variability and the small sample size associated with larger peak streamflow events (i.e. > 2 year return period), the results of these studies have been mostly inconclusive for larger events (Bowling et al. 2000). Another limitation of these studies is that it is difficult to isolate the effects of a single process (such as changes in snowmelt rates as opposed to changes in antecedent snow accumulation) on possible changes in streamflow and, therefore, difficult to develop predictive models that can be applied to other watersheds. Review of recent findings of watershed-scale investigations of peak streamflow can be found in Jones and Grant (1996), Thomas and Megahan (1998), and Bowling et al. (2000).

The second approach, which is pursued here, is to investigate and quantify canopy processes that can increase runoff response at the plot scale (the area beneath a single or several trees) during flood events and then scale up to the watershed scale. The effects of forest canopy removal on peak streamflow can be assessed by incorporating a numerical model of canopy effects in a watershed-scale hydrologic simulation. Since this method of investigation is based on an explicit model of canopy processes, the methodology can be easily applied to many watersheds. However, the validity of the predicted changes in peak streamflow depends on the model formulation of the water and energy balance at the plot scale.

1.2. Current understanding of forest harvest effects at the plot scale

Forest harvest can impact streamflow through a number of mechanisms, which are reviewed by Jones and Grant (1996). These include: increased evaporation from the soil due to higher water tables and increased energy transfer; decreased transpiration due to canopy removal; decreased interception of rain, snow and fog due to canopy removal; increased snow accumulation due to decreased snow interception; increased snowmelt due to larger antecedent accumulations of snow and increased energy exchange; increased interception of subsurface flow by the forest road network; and decreased infiltration on road surfaces.

Motivated by the observations that large flood events in the Pacific Northwest occur during storms in which significant rainfall occurs simultaneously with snowmelt (Harr 1981), the

focus in this dissertation is on possible increases in peak streamflow due to changes in snow accumulation and melt as a consequence of canopy removal. These events are commonly described as rain-on-snow (ROS) although it is the turbulent transfer of latent and sensible heat to the snowpack that drives snowmelt. During ROS events, the severity of the flood response, and consequently the possible magnitude of enhancement due to forest harvest, depends on the presence of snow before the flood event, its condition, and the rate of snowmelt during the rain storm.

Figure 1.1 shows how canopy removal can affect ground snow accumulation and melt (e.g. USACE 1956, Miller 1962, Satterlund and Haupt 1970, Harr 1981). Snow can be intercepted by the forest canopy where it is sublimated, melted or released as snow from the canopy (e.g. Miller 1967, Satterlund and Haupt 1970). While sublimation represents a direct loss from the soil-snow system, drip of melt-water from the canopy is either stored by the snowpack or routed directly to the soil (depending on the snowpack temperature and liquid water content). Snow released from the canopy adds directly to the water equivalent of the snowpack.

Removal of the forest canopy affects the melt rate of the ground snowpack by altering the near-surface energy balance. The canopy attenuates short-wave radiation to the ground surface and modifies long-wave radiation transfer (Black et al. 1991). Short-wave radiation absorbed by the canopy can be re-radiated to the snowpack as long-wave radiation. The canopy shelters the snowpack from the prevailing winds, thereby reducing the turbulent exchanges of latent and sensible heat, which depend directly on windspeed and the near surface gradients of temperature and humidity. During conditions in which short-wave radiation or turbulent energy fluxes prevail, canopy removal enhances the rate of snowmelt.

An example of how changes in antecedent snow accumulation and melt rate can affect total water delivery to the soil is shown in Figure 1.2 for two ROS events: February 1996 (Storck et al. 1999) and February 1984 (Berris 1984). Prior to the ROS event from 5 February to 9 February 1996, which was observed at an elevation of 1000 m in the Gifford Pinchot National Forest, Washington, heavy snowfalls during unusually cold conditions deposited nearly

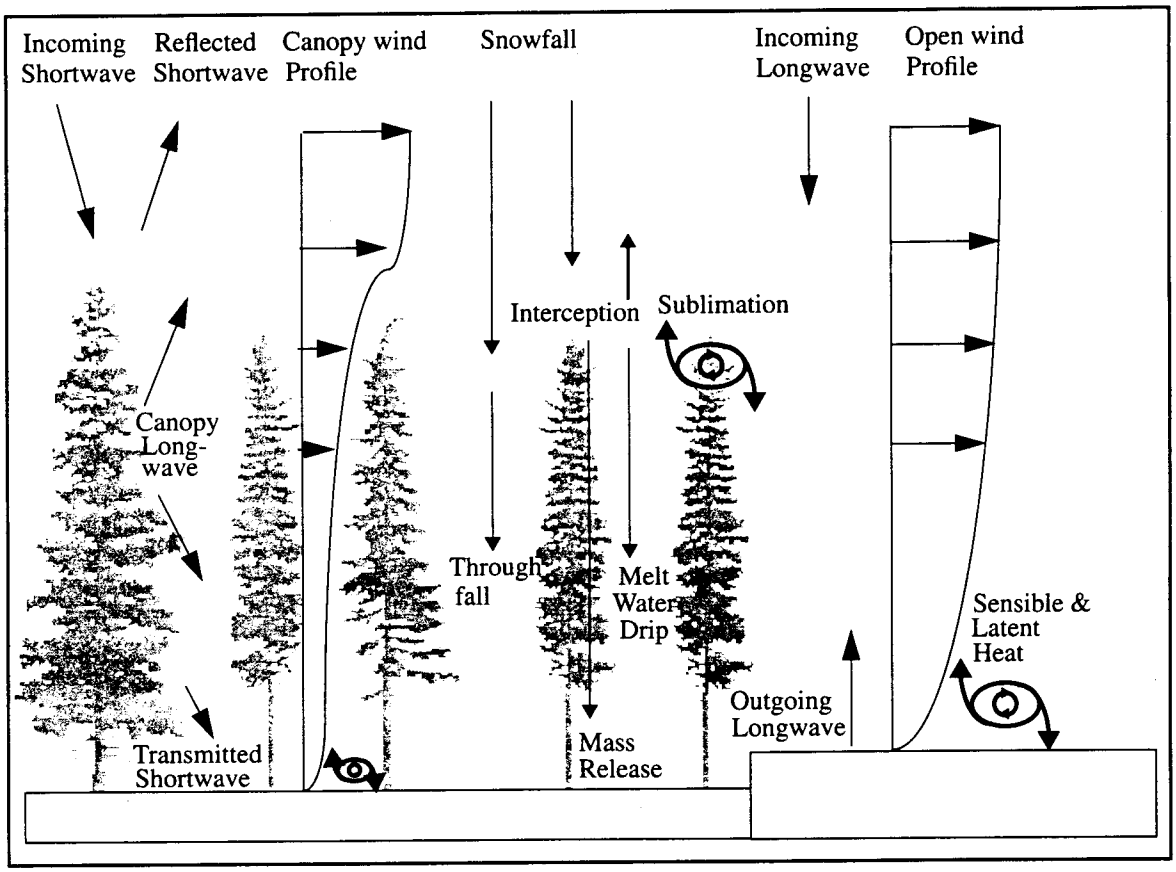

Figure 1.1. Overview of processes controlling the difference in snow accumulation and melt below a forest canopy and in a clearing. The canopy alters the radiation balance and shelters the snowpack from turbulent heat exchange driven by the wind. The canopy reduces snow accumulation due to canopy interception of snow. Intercepted snow can be sublimated or released from the canopy as snow parcels or meltwater drip.

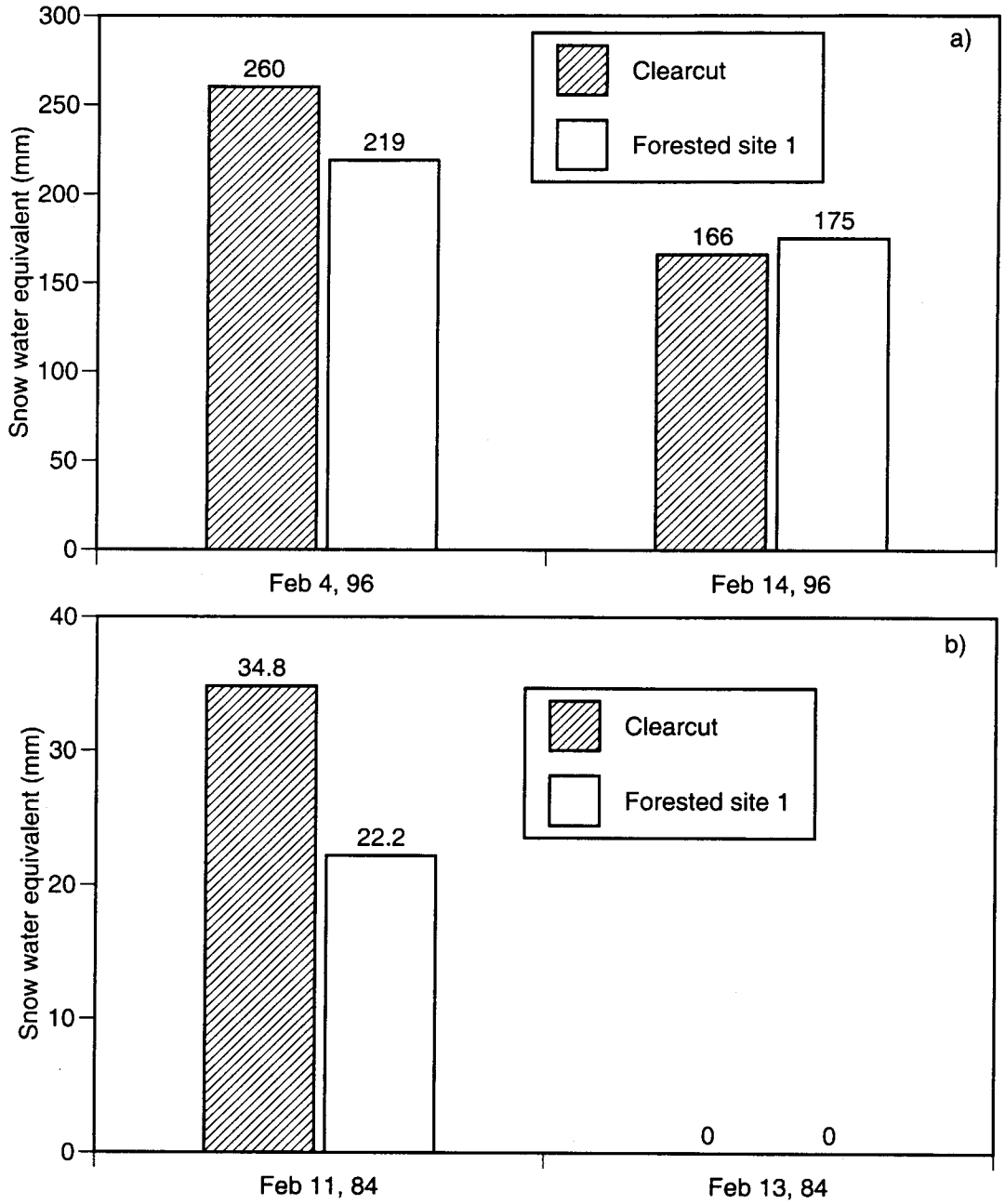

Figure 1.2. a) Observed changes in snow water equivalent (SWE) in a clearcut and beneath a mature forest stand during the ROS event of February 1996 in the Gifford Pinchot National Forest (elevation of 1000 m) (Storck et al. 1999). b) same as a), but for a ROS event during February 1984 in the H.J. Andrews Experimental Forest (elevation of 900 m) (Berris 1984).

equal accumulations of snow beneath the forest canopy and in an adjacent clear-cut (219 and 260 mm of SWE, respectively). During the ROS event, 94 mm of SWE was lost in the clear-cut while 44 mm SWE was lost beneath the forest canopy. Total event snowmelt was increased by 114 percent. This increase could be attributed entirely to an increase in the melt rate. Differences in antecedent snow accumulation did not contribute to the increased snowmelt during the event.

Differences in antecedent condition were entirely responsible for the enhanced melt due to forest canopy removal for the second event shown in Figure 1.2. Prior to the ROS event of February 1984 (observed at an elevation of 900 meters in the H.J. Andrews Experimental Forest, Oregon), 34.8 mm of SWE accumulated in the clearcut. Canopy interception processes limited snow accumulation beneath the canopy to 22.2 mm of SWE. During a two day ROS event, the entire snowpack at both sites melted. Total event snowmelt was increased by 57 percent due to canopy removal.

These two events are a small sample of the available data in the Pacific Northwest on changes in total snowmelt due to forest harvest during ROS events (Beaudry and Golding 1983, Berris 1984, Berris and Harr 1987, Coffin and Harr 1992, Wetherbee 1995, Adams et al. 1996, Storck et al. 1999). Despite problems with instrumentation and sampling error (see Section 4.2 for a detailed discussion), the combined evidence of these studies has shown that total snowmelt during ROS events can be increased due to forest harvest. In all of the indicated studies, two main factors have been identified as contributing to increased melt response; increased snow accumulation before events and increased energy transfer during events. While these studies provide a clear understanding of how canopy removal alters the energy balance of the ground snowpack, the effects of a forest canopy on snow accumulation are not well understood in maritime climates like the Pacific Northwest. The main reason behind the limited understanding of snow interception processes is the scarcity of data relevant to this region (Bunnel et al. 1985). A more complete understanding of canopy processes is essential to the development of a predictive model of canopy removal on peak streamflow at the watershed scale. Therefore, a field campaign to measure these processes at the plot scale is a central part of this dissertation.

Chapter 2. Science questions and objectives

Two fundamental science questions are addressed in this dissertation: a) Has canopy removal due to forest harvest increased peak streamflow during ROS events in the maritime mountainous climate of the Pacific Northwest? and b) To what extent are changes in antecedent snow accumulation responsible for increases in streamflow?

These questions are motivated by previous investigations of forest harvest effects at the watershed and plot scales. Watershed scale investigations have suggested that peak streamflows have increased during smaller ROS events (e.g. Jones and Grant 1996, Thomas and Megahan 1998). Significant trends for larger events have not been detected due to a decrease in sample size for the largest events coupled with the natural variability of observed streamflows (Bowling et al. 2000). Previous plot scale investigations have shown that total water delivery to the soil can be increased after forest harvest (e.g. Beaudry and Golding 1983, Berris and Harr 1987). Although these studies have shown that increases are due to both increased melt rates and increased antecedent snow accumulation, only those processes controlling increased melt rates (i.e. changes in the energy balance of the snow surface) are understood well enough to be explicitly incorporated in numerical models for describing forest harvest effects in the Pacific Northwest. The data to construct and test a numerical model of canopy interception processes on antecedent snow accumulation are not available (van Heesjwick et al. 1996, Marks et al. 1998). Therefore, to address the science questions proposed above, the work in this thesis is organized around three distinct objectives.

1) To quantify snow interception by the canopy, the removal of snow from the canopy, and the overall impact of canopy removal on ground snow accumulation and melt in the maritime climate of the Pacific Northwest at both the plot (single or several trees) and forest stand (>10 ha) scales.

2) To develop, calibrate, and test an energy balance model of snow interception and canopy effects on ground snowpack accumulation and melt at both the plot and forest stand scales.

3) To incorporate the canopy-snow model within a watershed scale hydrology model to investigate the relative contributions of increased snow accumulation and increased melt rate to possible increases in peak streamflow.

The translation of near-surface meteorology (i.e. air temperature, wind speed, humidity and radiation) into snowmelt is well understood for a large variety of climates including the maritime Pacific Northwest. As a consequence, numerical models that explicitly represent the energy balance of the snow surface have been developed (Anderson 1976, Price and Dunne 1976, Jordan 1991, Wigmosta et al. 1994, Tarboton et al. 1995, Marks and Dozier 1988, Price 1988, Marks et al. 1998). Despite differences in computational complexity, these models are remarkably similar in their basic formulation and their prediction of average plot scale SWE for areas unaffected by a forest canopy. Therefore, the focus of the data collection and the discussion in this dissertation is on canopy effects related to snow interception and the fate of intercepted snow. Process data collected in this thesis on the evolution of the ground snowpack are used primarily to formulate and test numerical models of snow interception processes. These data are used secondarily to test the current understanding of the snowpack energy balance formulations beneath the forest canopy.

This dissertation is divided into six additional chapters: Chapter 3 provides a detailed review of previous studies on snow interception. Chapter 4 describes the field campaign to study canopy interception and the effect of the canopy on ground snowpack dynamics. Chapter 5 presents the results from the field campaign. Chapter 6 presents the development, calibration, and testing of the canopy-snow model. A sensitivity analysis of key model formulations and parameters is also presented. Chapter 7 presents the watershed scale modeling investigation and explores the relative contribution of increased snow accumulation and increased melt rates due to

forest canopy removal to changes in peak streamflow. Chapter 8 summarizes and concludes the discussion.

Chapter 3. Snow interception – current understanding

A qualitative description of snow interception processes was presented in the early 1960's in a series of papers by Miller (1962, 1964, 1966, 1967). Based on literature available at the time (limited primarily to experiments conducted by the Japanese Government Forest Experiment Station, JGFES 1952), Miller (1964) hypothesized that three principle factors would affect snow interception by the forest canopy. These factors are morphological characteristics of the canopy, air temperature, and wind speed. Miller (1967) also suggested that three major mechanisms act to remove intercepted snow from the canopy: evaporation, mechanical-thermal removal (resulting in mass release), and meltwater drip. These processes are shown schematically in Figure 1.1.

The main mechanisms and processes proposed by Miller are used to organize the review of the current understanding of snow interception processes in the remainder of this chapter. The factors that control snow interception by the canopy (including tree morphology, air temperature and windspeed) are examined first, followed by a review of previous studies on mechanisms that remove snow from the canopy.

3.1. Factors controlling snow interception

3.1.1. Canopy morphology

One of the most fundamental questions regarding snow interception is how differences in canopy morphology affect storage capacity. Early attempts to understand the mechanisms of interception focused primarily on rainfall and it was long thought that snowfall would behave almost identically. Horton (1919) presented one of the first comprehensive discussions of the subject and proposed that the interception loss (the difference between above and below canopy precipitation over the course of an event) is the sum of the storage of water on the canopy and the

evaporation from the canopy storage during the event. Based on this representation and the available data, Merriam (1960) suggested:

$$L=S(1-\exp(-P/S)+RET \qquad 3.1$$

Where: P is the precipitation during the storm,

L is the interception loss over the projected area of the canopy,

S is the maximum water stored on the vegetation,

R is the ratio of vegetation surface area to projected area of the crown,

E is the evaporation rate during the storm,

T is the duration of the storm.

Eq 3.1 represents the loss of precipitation due to interception (L) as increasing at a decreasing rate during a given storm and, in the absence of evaporation, it approaches its maximum value (S) asymptotically. Although Merriam (1960) found that Eq 3.1 agreed well with observed data on rainfall interception loss, he questioned the applicability of Eq 3.1 to snowfall events. Unfortunately, the data available at the time reinforced the perception that rain and snow interception were equivalent in magnitude and net effect.

Johnson (1942) analyzed over 140 precipitation events during summer and winter months by sampling precipitation with standard rain gages at 6 points under the canopy and 6 points in a nearby large openings. On average, 30 percent of rain and 20 percent of snow were lost due to interception. Rowe and Hendrix (1951) performed a similar study at an elevation of 1000 m in California where approximately 30 to 40 percent of annual precipitation is snow. Interception loss was determined to be 4 percent greater for rainfall than snowfall.

Among the first evidence that rainfall and snowfall interception are fundamentally different in magnitude is found in a study at the Japanese Government Forest Experiment Station (JGFES 1952). The weight of a cut cedar tree (*Cryptomeria*) was measured immediately after several snowfalls events (Figure 3.1). Total snowfall was measured by collected falling snow on a flat board. During several of the smaller snowfall events, nearly 85% of total snowfall was intercepted.

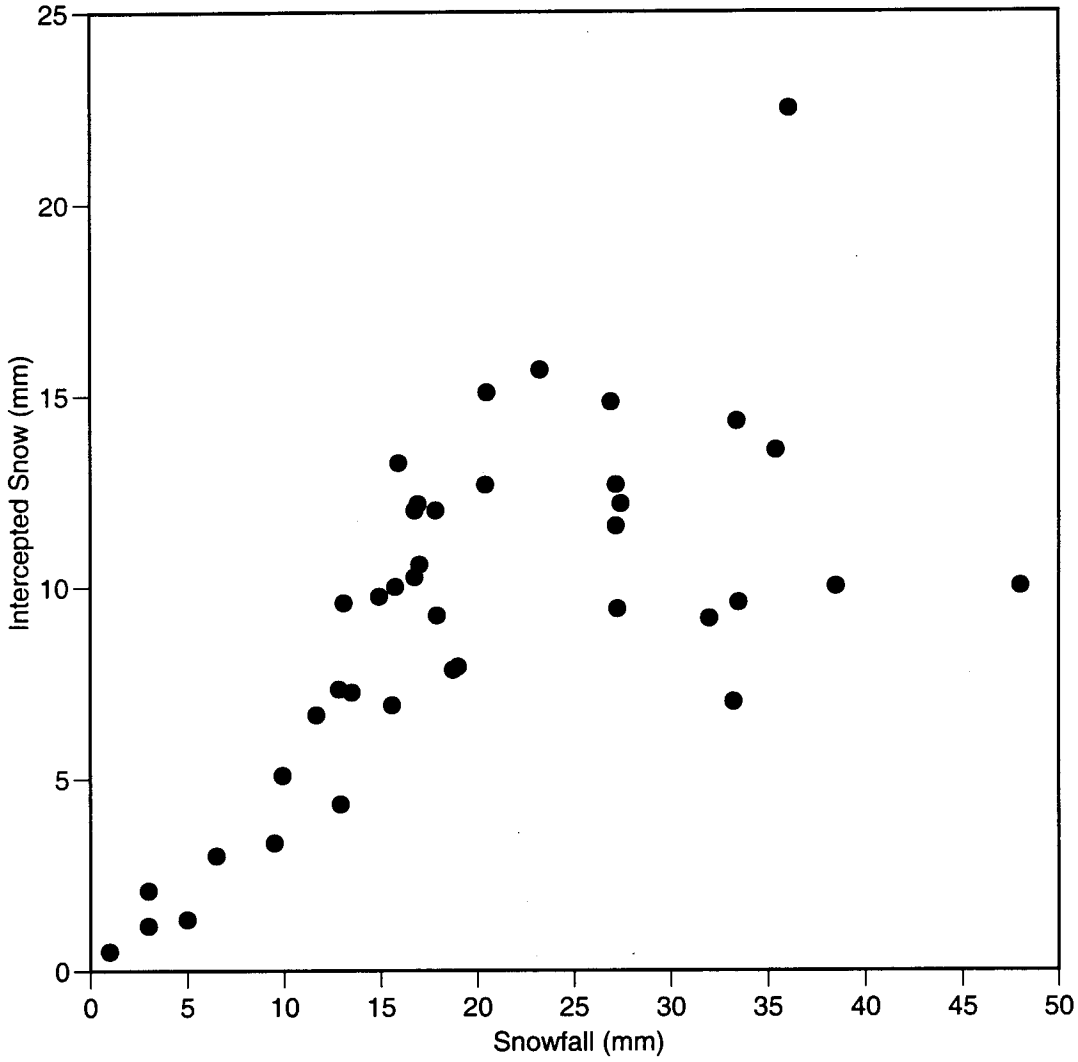

Figure 3.1. Observations of intercepted snow on a cedar tree immediately after several snowfalls. Data are from JGFES 1952.

The JGFES experiment was replicated in the Priest River Experimental Forest of Idaho (Satterlund and Haupt 1967). Douglas-fir (*Pseudotsuga menziessii*) and western white pine (*Pinus monticola*) trees that were approximately 4 m tall were weighed continuously during two separate snowfall events (Figure 3.2). During both events, air temperature was just below freezing. A sigmoidal growth curve of the following form provided was found to provide the best agreement with observations (Satterlund and Haupt 1967).

$$I=S/(1+\exp(-k(P-P_0))) \qquad 3.2$$

where I = intercepted snow (mm)

S = maximum intercepted snow (mm)

P = snowfall (mm)

k = constant expressing rate of interception storage

P_0 = inflection point of sigmoidal curve

The poor fit of the simple exponential model is explained by the difference in mechanisms controlling rain and snow interception (Satterlund and Haupt 1967). During rainfall, interception is controlled by surface tension. As branches accumulate a thin film of water, surface tension is exceeded and further wetting of the branches does not enhance interception. During snowfall, initial interception efficiency is low as snowflakes do not adhere to bare branches. As snowflakes lodge between needles and branches or adhere to the canopy, interception efficiency is increased due to cohesion of snowflakes to intercepted snow and the increased effective projected area of the canopy. As snowfall continues, branches bend downward under increasing weight. This causes a decrease in projected area. If adhesion of the intercepted snow to the canopy is overcome then sliding of intercepted snow from the canopy may occur. Steady state is reached as new snow interception balances snow release. Due to the small sample size of the study, conclusions about inter-species or inter-storm differences could not be made.

Hoover and Leaf (1967) conducted similar experiments on lodgepole pine (*Pinus contorta*) at an elevation of 2750 m in Colorado. Average conditions were cold with nighttime temperatures frequently falling below –25°C. Under these conditions, snow adhesion to the

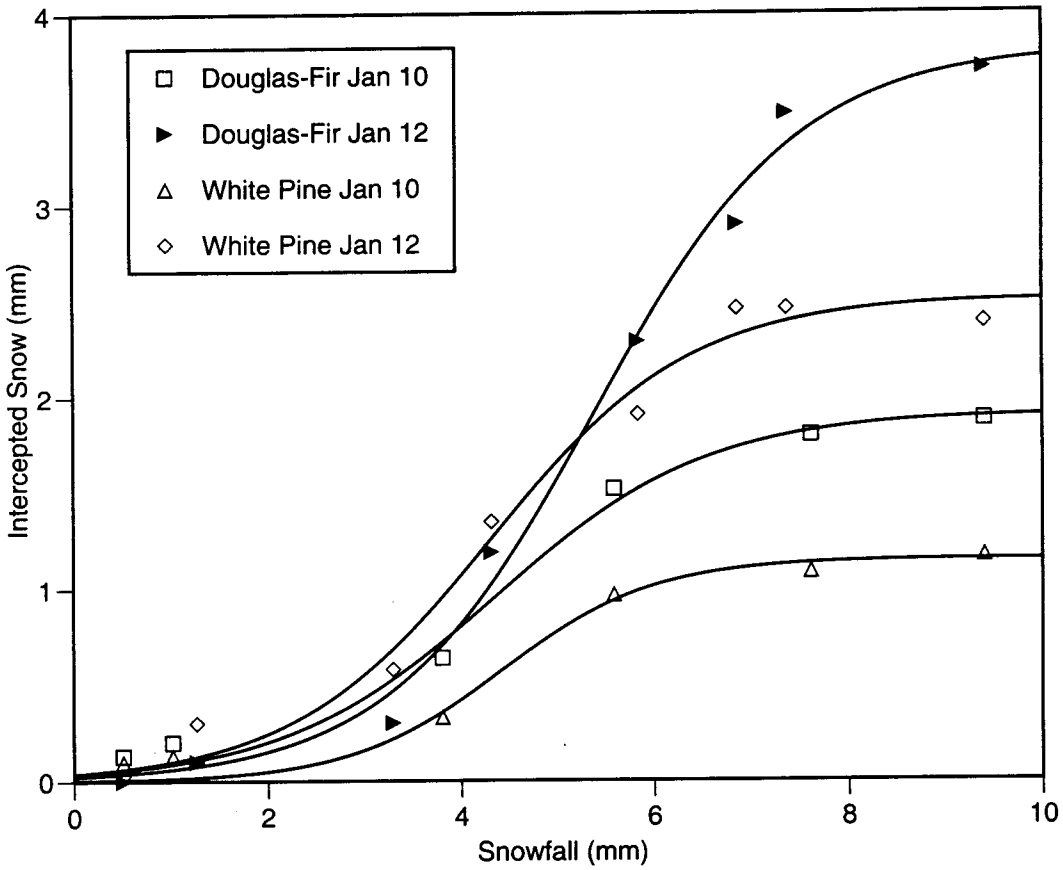

Figure 3.2. The growth of intercepted snow on Douglas-fir and white pine trees during two snowfall events. Sigmoidal growth curves are fitted to all four data sets. Data are from Satterlund and Haupt (1967).

foliage was not observed. Interception commenced as snow crystals lodged into the base of needles. Snow interception was accelerated by cohesion (driven, at extremely cold temperatures, by vapor diffusion). In effect, snow did not adhere to the canopy, but simply rested on it. Intercepted snow loads approached a maximum after approximately 3 mm of precipitation.

The contrast in the magnitude of observed snow interception and dominant interception mechanism between maritime and continental climates suggests that micrometeorology can exert a strong control on snow interception. These controls on interception are expected given the differences in density of fallen snow due to crystal structure and aggregate formation between maritime and continental climates (Bunnel et al 1988). Differences in canopy morphology between conifers have not been shown to exert as strong a control on snow interception. Evidence for the dominance of micrometeorological effects over morphological effects of the canopy can be found in the study of Schmidt and Gluns (1991). Cut branches of Engelmann spruce (*Picea engelmannii*), sub-alpine fir (*Abies lasiocarpa*), and lodgepole pine (*Pinus contorta*) were weighed during snowfall (average air temperatures ranging from –1 °C to –16°C), at sites in Colorado (2740 m elevation) and British Columbia (1680 m elevation). No significant difference in snow interception between the three branch species was found. Initial snow accumulation was slow on all three species until the needles and branch tips were bridged by snow. Accumulation accelerated due to cohesion of snowfall to the intercepted snow and the increased surface area of the branch. Snow interception decreased and eventually ceased due to branch bending.

Additional evidence for the dominance of climate over morphology is presented in Satterlund and Haupt (1970). Douglas-fir and western white pine trees were weighed continuously through the course of two winters (1966 to 1968) at the Priest River Experimental Forest in Idaho. Despite considerable differences in the morphology of the two species, no significant difference was observed in the amount of snow intercepted during the winter. The Douglas-fir intercepted 32.1 percent of snowfall. The western white pine intercepted 35.5 percent.

3.1.2. Temperature effects on snow interception

A weak relationship between decreased air temperature during snowfall and decreased percent interception on a cut cedar tree was reported in the study of JGFES (1952). In a series of experiments designed specifically to remove the variability of natural canopy crowns, snow interception was measured on a series of long, narrow boards (1, 2, 4, 8 and 16 cm. wide) (JGFES, 1952). Interception, expressed as the snow interception on each board relative to the 16 cm wide board, was found to decrease with decreasing air temperature. This effect was most pronounced for the narrowest board. The 8 cm wide board showed no decrease in interception as air temperature decreased.

In a series of similar experiments, Kobayashi (1987) investigated the effect of air temperature on boards that were 0.5, 1, and 2 cm wide. Snowfall was simulated by sieving ice crystals onto the boards. These experiments were conducted in a cold room to allow precise control of air temperature. Results were similar to those described above. As the board width decreased, the amount of interception decreased. The most pronounced effect was observed at the smallest board widths. At temperatures above -0.9°C all boards intercepted approximately 75 percent of snowfall. At temperatures below minus 3°C, the 0.5 cm board did not intercept any snow, the 1 cm board intercepted only 10 percent and the 2 cm board intercepted 30 percent of snowfall.

Although the results of these two studies at first seem identical, there is a significant difference. No effect of lower air temperature was found for boards that were 8 cm wide. In both studies, snow interception on boards narrower than 8 cm was strongly affected by air temperature. Thus, the effective width of the interception surfaces on the canopy becomes an important factor in determining the degree to which air temperature controls snow interception. Interception by deciduous trees, which can be conceptualized as a collection of narrow boards, should depend strongly on air temperature with minimum interception at low air temperatures. This argument is supported by the data of Ohta et al. (1993). No difference in maximum spring snow accumulation

was observed between open and deciduous sites over two winter seasons. As interception surfaces become wider, interception should become less dependent on air temperature.

3.1.3. Wind

It is impossible to isolate the effect of wind on snow interception during snowfall unless a direct measurement of snow interception is made. Unfortunately, only a few studies have observed snow interception in the canopy directly (e.g. by weighing a cut tree) and most have not observed enough interception events to isolate the effect of wind. No significant effect on maximum intercepted snow load was found for wind speeds ranging from calm to 1.5 m/s (JGFES 1952). At wind speeds above 2 m/s, a sharp reduction in maximum intercepted snow load was observed. However, there were too few observations at wind speeds above 2 m/s to draw any conclusions.

3.2. Mechanisms for the removal of intercepted snow

Intercepted snow can be removed from the canopy by sublimation, mass release, or melt water drip. All three of these can occur simultaneously, complicating the measurement of any single mechanism. The first study to measure the disposition of snow from conifer crowns in the Pacific Northwest was conducted by Satterlund and Haupt (1970). Douglas-fir and western white pine saplings were weighed continuously during two winters at the Priest River Experimental Forest in Idaho. Interception was directly measured from changes in tree weight. Throughfall, mass release, and drip from the canopy were collected by a large plastic sheet under each tree and the total volume was measured by melting the catch. Mass release events were identified as rapid decreases in the weight of the tree. During the experiment, 220 mm of snowfall occurred. The two largest events of the year were not included in the analysis due to instrument malfunction. Approximately 30 percent of snowfall was temporarily retained in the canopy crown. Of the initial snowfall, 208 mm or 95 percent eventually reached the ground. Direct throughfall accounted for 70 percent, 15 percent was washed off by rain, and 10 percent was released during

large mass release events. Only 5 percent was identified as meltwater drip. Loss from intercepted snow due to sublimation was estimated at 5 percent of total snowfall. While these percentages are sensitive to the amount of snowfall, these results suggest that the majority of intercepted snow is eventually added to the ground snowpack as snow (as opposed to meltwater).

3.2.1. Evaporation of intercepted snow

Of all the mechanisms that can remove intercepted snow from the canopy, sublimation has been the most studied. Experiments in which real or artificial trees were continuously weighed reveal that high sublimation rates occur from intercepted snow. Lundberg (1993) reported rates as high as 0.3 mm per hour (over 7 hours) from continuous weight measurements of a cut 6 m tall spruce tree in Norway during conditions of relatively low wind speed but high vapor pressure deficits. Schmidt (1991) reported rates as high as 1.5 mm/day from continuous weight measurements of artificial trees in cold, dry climates. Average evaporation rates (over 7 hour periods) of 0.2 mm per hour were observed by Calder (1990) and Lundberg (1998) with maximum observed hourly rates of 0.5 mm per hour (equivalent to a radiant energy input of approximately 400 Watts per square meter).

In an analysis of the data collected by Calder (1990), Schmidt (1991) and Lundberg (1993), Lundberg et al (1998) found that high rates of snow sublimation from the canopy were sustained by both net radiation and the sensible heat flux. These rates were well predicted by a simple energy balance model provided that the aerodynamic resistance governing the flux of vapor from the snow surface was specified correctly. Based on a comparison of predicted rates of intercepted snow sublimation to intercepted rain evaporation, intercepted snow was found to increase the aerodynamic resistance of the canopy by an order of magnitude. This result suggests that turbulent exchange between the atmosphere and the canopy is reduced as the canopy becomes aerodynamically smoother due to snow cover.

3.2.2. Mass release of intercepted snow

Mass release of intercepted snow from the canopy occurs by two mechanisms. The first is due to the shaking action of the wind and is purely mechanical. As the adhesion of intercepted snow to the tree becomes more important (i.e. during snowfall at or just below freezing), it would be expected that pure mechanical removal of intercepted snow via wind would be exceedingly rare. The second mechanism for mass release is driven by melt and can occur in the absence of wind. As intercepted snow melts, it destroys the adhesive bonds of the snow to the canopy and mass release by slippage from the canopy can occur. This phenomenon was observed during the JGFES (1952) experiments. During periods of snowfall with light winds in which temperatures rose slightly above freezing (increasing from -2°C to 1°C), the snow load accumulated on a cedar (Cryptomeria) tree decreased from 25 mm to 2 mm over 7 hours. Small increases in energy supplied to the intercepted snow were capable of destroying the adhesive bonds to the tree and triggering mass release of snow from the branches.

Sliding of snow from the upper branches, where the fluxes of turbulent and radiant energy are highest, will dislodge snow from lower branches. Even the casual visitor to the forests of the Pacific Northwest during winter has witnessed these large cascading mass releases. Unfortunately, no quantitative data are available that describe when these events are most likely to occur or how much mass they deposit to the ground snowpack. Since this process is likely to be the dominant mechanism of transfer of intercepted snow to the ground snowpack, the conditions under which it occurs are important to assessing the length of time intercepted snow remains in the canopy and is vulnerable to sublimation.

3.2.3. Meltwater drip

Most researchers have discounted the importance of meltwater drip because it does not constitute a direct loss of water from the snow/soil system and consequently does not affect the annual water balance. Regarding meltwater drip, Miller (1962) wrote, "Is this a transport that by

reason of its nuisance to field men is reported beyond its hydrologic magnitude?" Miller (1962) describes melt from intercepted snow in Oregon as "like a showerbath."

Kittredge (1953) measured meltwater drip over a period of 5 years in the Sierra Nevada. During 57 snowfalls, only 25 percent of storms produced measurable meltwater drip and only 4 storms produced more than 2 mm of drip. For those events during which drip occurred, the average amount of meltwater drip was 0.8 mm out of an average total snowfall of 40 mm. Satterlund and Haupt (1970) report that meltwater drip accounted for less than 5 percent of the snow removed from the canopy.

3.3. Snow interception by forest stands

Extraordinary efforts are required to measure snow interception by mature stands (i.e. at the scale of several mature trees). Direct measurement by weighing seems impossible, and inference of snow interception from differences in ground snow accumulation requires diligent sampling immediately after snowfall ends. The limited data available suggest that the amount of intercepted snow in a mature stand departs considerably from that in an individual tree (Fitzharris 1975, Calder 1990).

Fitzharris (1975) reports the results of extensive measurements of snow interception by a mature canopy during eighty snowfall events between an elevation of 500 and 1200 m on Mt Seymour, British Columbia. Snow interception was inferred as the difference in snow accumulation in clearings and beneath the forest canopy during each event as measured by snow courses. Results showed that apparent snow interception often exceeded 40 mm of SWE and was best described as a linear function of snowfall. This result implies that snow interception by stands is equally efficient at all times during snowfall. No upper asymptote to snow interception by the mature stands was found. Kittredge (1953) found similar results in a study in the California Sierra Nevada Range. Although an upper asymptote to snow interception by stands must exist, this value has not yet been identified in maritime climates like the Pacific Northwest.

Calder (1990) reports results from gamma ray attenuation studies of a mature spruce forest of the highlands of Scotland. By measuring the attenuation of gamma radiation as it passed through the canopy, the storage of water on the canopy could be monitored continuously. Snowfall interception was best described as a linear function of snowfall depth. The maximum reported snow interception was approximately 20 mm of water equivalent during a snowfall of 30 mm (i.e. 66 percent interception efficiency).

Chapter 4. Measurement of processes controlling snow interception, ground snowpack accumulation and ablation

The main goal of this study is to determine possible increases in peak streamflow due to forest canopy removal during Rain on Snow (ROS) produced floods. Previous field studies have shown that forest canopy removal can increase the total water delivery to the soil by increasing the antecedent accumulation of snow prior to a ROS event and the snowmelt rate during the event. While the processes that affect the melt rate are well understood and have been incorporated into various numerical models of the ground snowpack, the canopy processes that control snow interception and antecedent accumulations are less well understood. Therefore, a detailed field measurement program to quantify canopy snow interception and its influence on ground snowpack accumulation and melt is a major part of this study.

This chapter describes the field campaign. Results of the field campaign are described in Chapter 5 and the energy balance model for snow interception by the canopy and ground snowpack accumulation and melt is presented in Chapter 6.

4.1. Field campaign objectives

The objectives of the field campaign were:

1. To measure canopy processes that control snow interception.
2. To measure the various transport processes of snow from the canopy, which include sublimation, mass release, and meltwater drip.
3. To provide data necessary to develop and test an energy balance model of beneath-canopy snowpack accumulation and melt.

4.2. The need for additional measurements and new instrumental designs

Currently available data to address the above objectives are limited in maritime mountainous climates like the Pacific Northwest. The few field campaigns that have been conducted in maritime climates have reported small interception capacities (Satterlund and Haupt 1967, 1970) even though much larger snow interception loads have been reported elsewhere (JGFES 1952, Calder 1990).

Data on the ultimate fate of intercepted snow are even more limited. Results from relatively cold climates have shown that the sublimation of intercepted snow is an important process. Data to confirm the importance of this process in maritime climates, where retention of intercepted snow is usually relatively short-lived, are not available. A deficiency of previous studies is the absence of data partitioning mass release and meltwater drip. These two removal mechanisms are, most likely, the dominant transport mechanism for removing intercepted snow from the canopy in maritime climates. The lack of snow interception data has created an unsupported perception that the process can be ignored.

The development and testing of energy balance models of beneath-canopy snow accumulation and melt is complicated by the extreme difficulty in collecting basic data. Most investigations of forest canopy effects have used non-weighing lysimeters to measure snowpack outflow and snow courses to measure antecedent snow accumulation. Both of these measurement techniques have biases that can lead to significant errors in the measurement of canopy processes.

The lysimetery technique is difficult even under ideal conditions (e.g. radiation-dominated melt of shallow snowpacks) due to preferential flow-paths of meltwater through the snow matrix. Considering the variability in canopy throughfall, the value of data collected using small lysimeters (less than the scale of the entire canopy of a single tree) should be questioned seriously (Beaudry and Golding, 1983). In a study of throughfall variability, Johnson (1990) found that throughfall increased from 40 to 130 percent of above-canopy precipitation as collectors were placed at increasing distances from the canopy stem. Therefore, the location and number of small lysimeters used to characterize beneath canopy snowpack outflow is critical.

Using small lysimeters placed toward the canopy edge can overestimate outflow. Placing a small lysimeter closer to the stem will underestimate outflow. To obtain a robust estimate of snowpack outflow requires either a single extremely large lysimeter or many smaller ones.

Estimates of snowmelt obtained from an analysis of outflows from a non-weighing lysimeter can also be subject to considerable error due to the difficulty in measuring precipitation. Since snowmelt accompanied by precipitation must be estimated as the difference between outflow and precipitation, errors in the measurement of both terms are transferable to errors in calculated snowmelt. The uncertainty in the inferred melt rates has lead to difficulty in using currently available plot scale data to verify existing energy balance formulations of snowmelt beneath a forest canopy (van Heesjwick et al. 1996, Marks et al. 1998).

The spatially variability of canopy throughfall can also bias beneath-canopy measures of SWE obtained by snow courses. An example of the possible errors in snow course measurement under a forest canopy is given by Kolesov (1985). Sample plots were established in open and forested sites (canopy cover between 80 and 90 % spruce) at the Russian Research Institute of Silviculture and Forestry at Pushkino (near Moscow). In each plot, fifteen 1 m x 1 m pixels were established. Snow water equivalent was determined in each plot using a standard snow course to determine both depth and density in each pixel at five points. To determine the true SWE of each grid, the entire mass of snow was removed from each 1 m^2 pixel and weighed. Snow water equivalent was underestimated by as much as 15% by the standard snow course, even when sampling density was as high as 5 points per square meter. Maximum differences were found directly underneath the canopy crowns and were attributable to the high variability of snow falling from the canopy. At open sites, SWE determined by both methods was nearly identical. These results demonstrate that current techniques of sampling snow water equivalent under a forest canopy can lead to considerable underestimation of SWE. It appears that the only viable method for accurate measurement of under-canopy snow water equivalent is to weigh the snowpack directly at a scale not affected by canopy throughfall variability.

Given the possible errors associated with current techniques for measuring below-canopy snow accumulation and melt, a series of new experimental devices were developed to satisfy the objectives of the field campaign. Four measurement requirements guided the design of these devices:

1. Direct measurement of canopy interception.
2. Continuous measure of spatial average ground snowpack water equivalent.
3. Continuous measure of snowpack outflow.
4. Continuous measure of the driving variables in the energy balance (i.e. precipitation, radiation, wind, temperature, and humidity).

A two tiered approach was developed to satisfy all four requirements. Large weighing lysimeters were used to measure the ground snowpack water equivalent and outflow. Cut-tree experiments were conducted to measure canopy processes including sublimation, mass release and meltwater drip directly. Differences in snow water equivalent and outflow between weighing lysimeters placed beneath a forest canopy and in a clearing were used to estimate canopy dynamics including interception, sublimation, melt water drip and mass release. Direct measurements of interception on small trees were then used to check the validity of inferred interception by the mature canopy. The weighing lysimeters and the cut-tree experiments are described in detail in Section 4.4 and 4.5, respectively.

4.3. Site description

The intensive field campaign of this study was conducted as a part of the Demonstration of Ecosystem Management Options (DEMO) experiment (Aubry et al. 1999). The DEMO study seeks to quantify the effect of alternative forest harvest strategies on vegetation, wildlife, snow hydrology and fungi.

The snow hydrology component of the DEMO experiment was located northwest of Crater Lake in southwestern Oregon (see Figure 4.1). The field site was located at an elevation of 1200 m. (placing it in the upper range of the rain-on-snow zone) in the Umpqua National Forest.

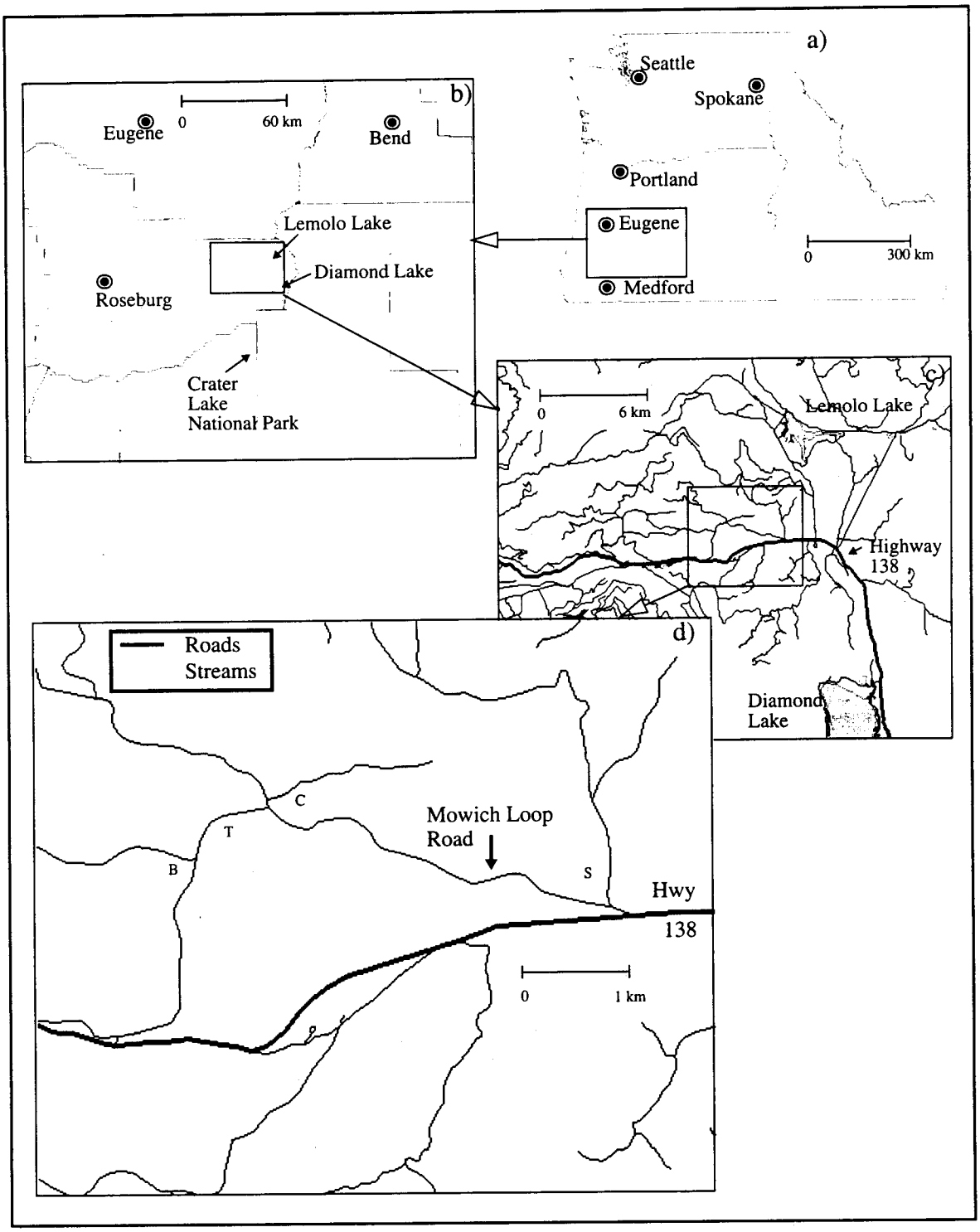

Figure 4.1. Location of field site with respect to the Pacific Northwest, Crater Lake National Park and Oregon Highway 138 (a - c), d) location of instrumentation at field site: B, C and S were the beneath-canopy, clear-cut and shelterwood weighing lysimeters, T was the cut tree experiment and the shaded areas were the snow course survey areas.

The annual precipitation at the site is approximately 2 meters, 70 percent of which falls between October and April. The first snowfall typically occurs in late October. Significant snow accumulation usually begins in late November. Snow cover is generally present in clearings throughout the winter with annual average maximum water equivalents of 350 mm in clearings. Average winter temperatures are often near freezing. The snowpack is maintained throughout the winter by occasional heavy snowfalls. Mid-winter melt is common and final melt occurs in late April or early May. The location of the site on the southern Oregon Cascade Crest exposes the site to frequent rain-on-snow events as well as a pronounced radiation-dominated melt season each spring.

Mature forest stands at the site range in age from 110-130 years. The canopy is dominated by Douglas-fir (*Pseudotsuga menziesii*) although; white fir (*Abies concolor*), western hemlock (*Tsuga heterophylla*), Ponderosa pine (*Pinus ponderosa*) and Lodgepole pine (*Pinus contorta*) are also present. The variety of species makes the area ideally suited for studying morphological effects on maximum snow interception. Basal areas (cross sectional area of tree trunks at breast height per unit area of forest) range from 36 to 52 m^2/ha (Halpern et al.1999). The average tree heights approach 40 meters.

Five sites were selected for intensive investigation of canopy interception and ground snow accumulation and ablation (Figure 4.1). Three sites were instrumented with weighing lysimeters: two weighing lysimeters were placed beneath a mature canopy (location B in Figure 4.1), one was placed in a clear-cut (C), and one was placed in a shelterwood (S). The shelterwood has a green tree retention (i.e. live trees left after harvest) of approximately fifteen percent. The cut tree experiments (T) were conducted in a natural regeneration area. Stand level snow accumulation and melt were measured by snow courses over a 26 ha area adjacent to the beneath canopy weighing lysimeters (shaded area in Figure 4.1). All five sites were selected as close to one another as possible while retaining direct vehicle access during snow free periods and restricting the maximum winter access distance (via skis or snowshoes) to approximately 3 km. The remainder of this chapter discusses the individual experiments in more detail.

4.4. Weighing lysimeter

To measure snowpack dynamics in open areas and beneath the forest canopy, a series of weighing lysimeters was deployed. Each weighing lysimeter was capable of continuous measurement of the ground snowpack water equivalent and outflow. Beyond the performance criteria described above, practical considerations controlled much of the lysimeter design. The overriding concern was that the lysimeter withstand snow loads of up to 800 mm of SWE – equivalent to a mass of 10,000 kg of water over a 12.5 m^2 lysimeter. A second consideration was that the entire device had to be carried by hand from the nearest road to the final installation site. Thus the individual pieces of the device had to be light enough for transport while allowing the final structure to hold significant loads. Given the remote nature of the sites (i.e. no source of AC power) storage batteries were required during winter operation. The dense canopy ruled out the possibility of solar cells.

The weighing lysimeter consisted of six main parts, each of which is shown as a distinct layer in Figure 4.2 and schematically on Figure 4.3. These were: 1) water flow measuring tipping buckets, 2) load cells and base supports, 3) steel substructure to transfer the load directly to the load cells, 4) wood structure to ensure proper slopes for drainage to the tipping buckets, 5) a plywood skin and a waterproof liner, and 6) face panels to isolate the lysimeter's snowpack and outflow from the surrounding snowpack.

4.4.1. Load cells

The lysimeter was weighed continuously using four load cells positioned under the center of each quadrant of the lysimeter. Each load cell was a standard shear beam deflection design. These load cells were chosen specifically to limit temperature bias. Based on manufacturer testing under controlled conditions, overall temperature bias was less than 0.004 percent of the full scale reading per degree Celsius change in temperature. The effects of non-linearity and hysteresis increased expected error for each load cell to 0.05 percent of the full-scale reading. This was equivalent to an error of approximately 0.36 mm SWE for each load cell.

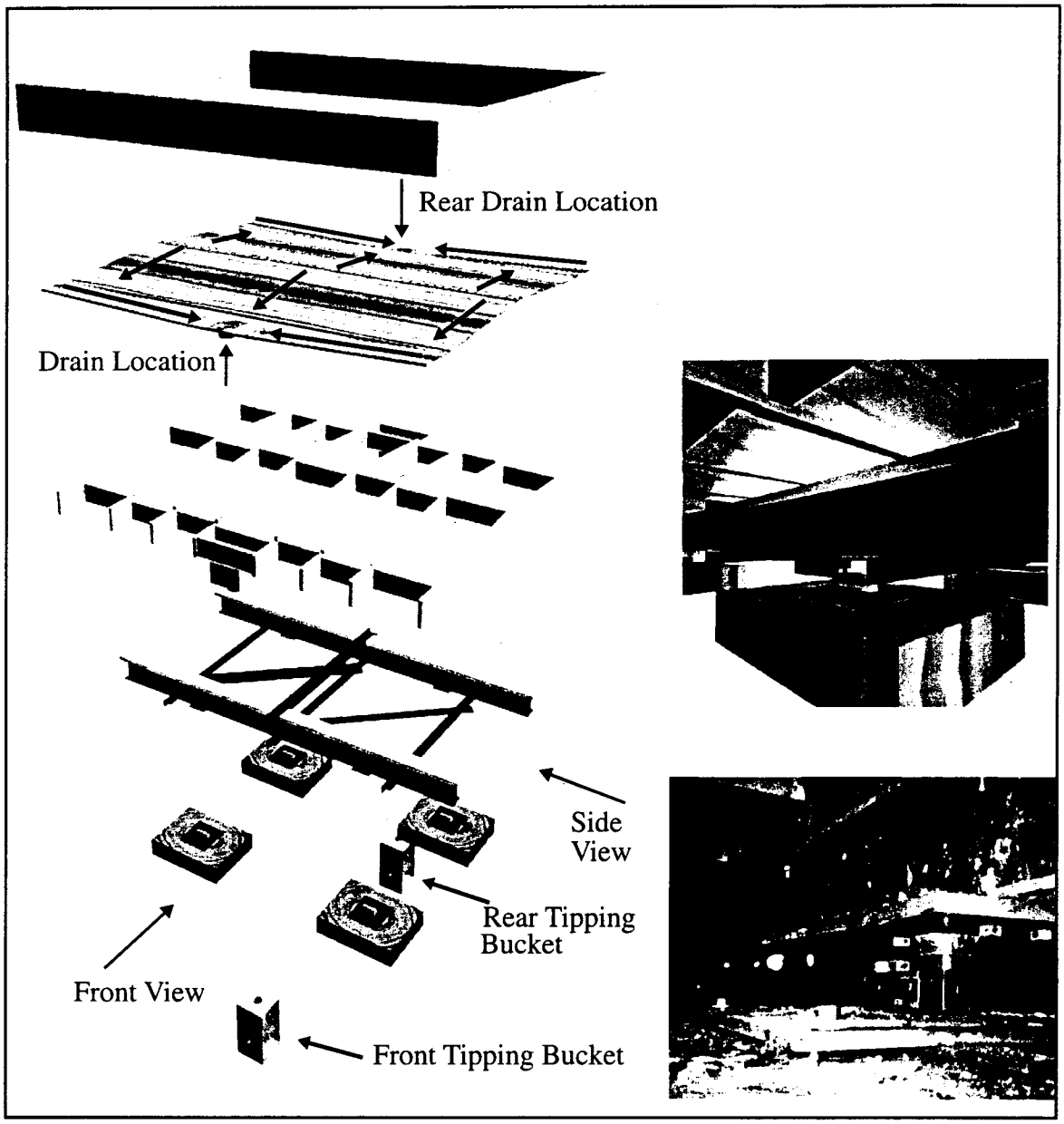

Figure 4.2. Exploded perspective drawing showing layered structure of weighing lysimeter including (from top): face planking, plywood decking (arrows indicate flowpaths), wood joists, steel subframing, load cell platforms and tipping buckets. Inserts to the right show load cell interface with the steel subframe.

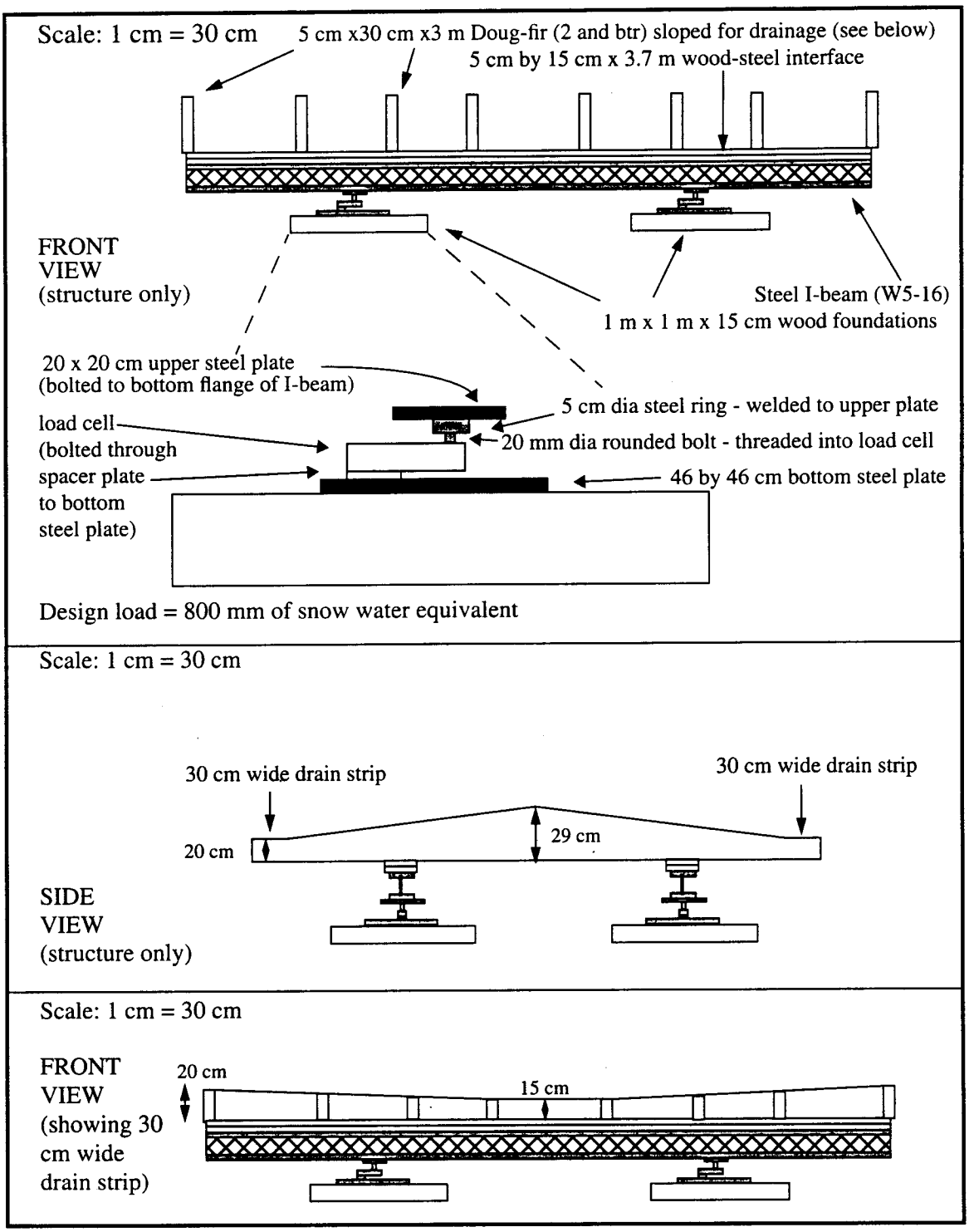

Figure 4.3. Schematic of a 12 m^2 weighing lysimeter including steel and wood substructure and load cell installation. Location of drains and orientation of front and side views are shown on Figure 4.2.

Each load cell was bolted through a spacer plate to a 12 mm thick steel plate. To distribute the load of the snowpack to the soil more uniformly, each steel plate rested on a 1 m^2 pressure treated wood platform. Load transfer from the lysimeter to the load cell occurred via a single 20 mm diameter high tensile strength (ASTM Grade 8) steel bolt that was threaded through the load cell (see Figure 4.3 and top panel of Figure 4.2). By resting the entire lysimeter platform on four rounded bolts, any possible bending moment transfer to the load cells was minimized. To ensure stability of the lysimeter on the load cells, the rounded head of the bolt was positioned inside a steel ring that was welded onto the underside of the upper steel plate. The upper steel plate was in turn bolted to the underside of the steel substructure.

4.4.2. Steel substructure

Given the design capacity of the lysimeter and the necessity to support this load at 4 points, a steel substructure transferred the weight of the platform to the load cells. This substructure consisted of two parallel steel I-beams (W 5 by 16). Each I beam was 3.7 m long. Lateral stability between the two I-beams was provided by a series of interlocking pieces of L-steel on both the top and bottom flanges of the I-beam (see Figure 4.2). The interface between the I-beams and the wood joists consisted of dimensional lumber bolted to the top flange of the I-beam.

4.4.3. Wood Superstructure

To provide effective drainage of meltwater from the lysimeter, a wood superstructure with joists running perpendicular to the I-beams was used. Each joist was 3 m long and was sloped away from the lysimeter center toward 30 cm wide drain strips along the two outside faces of the lysimeter. The ends of each joist were in turn sloped toward the center of each outside face (see front and side views on Figure 4.3). The slope in each direction was approximately 0.05 m/m. The drainage surface consisted of 20 mm exterior grade plywood attached directly to the joists. To isolate drainage from the lysimeter, as well as minimize edge effects on the

measurement of SWE, dimensional lumber (5 cm by 30 cm) was attached to each face of the lysimeter. A 72 mil water-proof liner (polyethylene) reinforced with a nylon mesh was draped over the entire structure. This design ensured that each tipping bucket drained exactly half of the lysimeter's surface area while outflow was concentrated into each of the drainage strips. Lateral stability between joists was achieved using spacers of dimensional lumber.

4.4.4. Drains and tipping buckets

Drains to the two water flow measuring tipping buckets were located in the center of each drainage strip (see Figure 4.2). Although the drain design would at first appear to be a relatively simple issue, drainage leaks have plagued previous lysimeter designs (Berris and Harr 1987, Coffin and Harr 1992, Wetherbee 1995, and Storck et al. 1999). The majority of leaks occurred due to failures in the adhesive during frequent freeze-thaw cycles and the relatively small diameter of the drain (typically 38 mm to 50 mm diameter). The primary concern in the drain design, therefore, was to maintain a completely waterproof seal between the polyethylene liner and the drain that was not dependent on adhesive or caulking. The final drain design (shown in Figure 4.4) used a combination of compression fittings and roofing tar. The drain was constructed from a 10 cm diameter plastic (Schedule 40 ABS – Acrylonitrile Butadience Styrene) floor drain and a matching ring. The air gap between the drain and the collection basin ensured that a proper weight measurement in the lysimeter could be obtained even if the pipe leading to the tipping bucket froze. The wax toilet bowl ring prevented water from being stored in the base of the collection basin.

Outflow from each collection basin was measured directly by a one-liter capacity tipping bucket. Each tipping bucket was installed below grade in a cubic plywood enclosure that measured 1 m on each side. The roof of the tipping bucket enclosure was insulated to prevent freezing. The one-liter capacity tipping bucket yielded a resolution of 0.083 mm. Field tests showed that inflow rates that caused the tipping bucket to exceed 10 tips per minute resulted in water being lost between tips. This limitation translated to a maximum outflow capacity from the

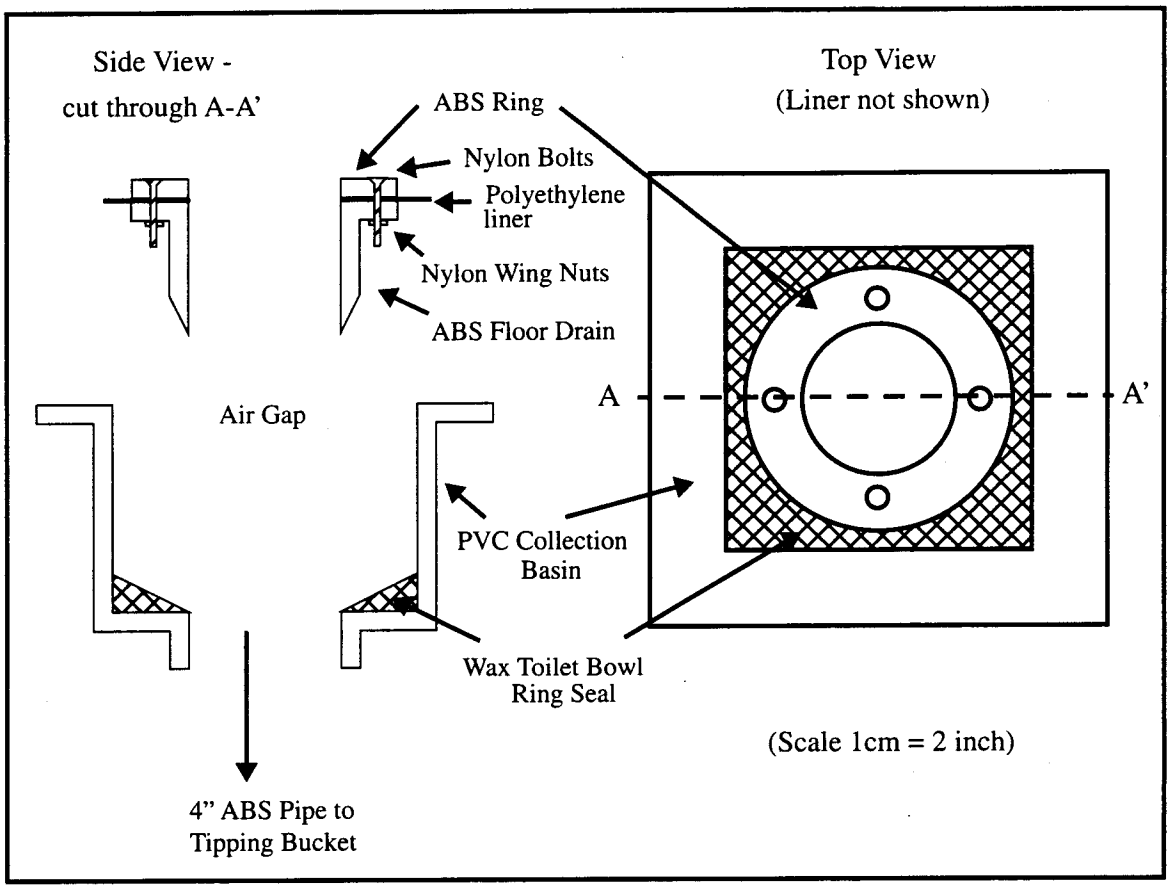

Figure 4.4. Schematic of drain design and air gap. Side view is taken as the cross section through A-A'

entire lysimeter of 100 mm per hour (or 50 mm per hour per tipping bucket). This rate was not exceeded during three years of continuous winter observation.

4.4.5. Differences in weighing lysimeter design between sites

The weighing lysimeter described above was installed at all harvested sites where there was no canopy overhead. This included the clearcut (see Figure 4.5) and shelterwood sites (locations shown on Figure 4.1). The lysimeter liners at these sites were painted white. To minimize the effect of canopy throughfall variability on the observed outflow records, weighing lysimeters installed beneath the forest canopy had a surface area of 24 m^2 and were constructed around an individual Douglas-fir tree such that all throughfall was collected (see Figure 4.5). To reduce bias due to differences of individual trees, two independent lysimeters were installed around adjacent Douglas-fir trees. Edge effects due to placement of the lysimeter beneath the canopy were minimized by the large sampled area and the similarity of surrounding canopy cover. Field observations showed that mass release and drip from each tree was caught by the weighing lysimeters. Stem flow was routed into the lysimeter via a drip skirt fastened to each trunk but was not measured separately

The overall design of the beneath-canopy lysimeters was identical to that described above except that the I-beams and joists were all 4.9 m in length. SWE was measured by four 4500 kg load cells while outflow was measured by four one liter capacity tipping buckets. Because the surface area, number of tipping buckets, and load cell capacities were all twice that of the smaller lysimeter, the outflow resolution and maximum outflow and weight capacities were unchanged.

4.5. Cut-tree experiments

Simultaneous investigation of sublimation, meltwater drip and mass release of intercepted snow requires continuous measurements of intercepted snow and the water equivalent and outflow of the ground snowpack. While the weighing lysimeters yielded continuous measurements of ground snowpack dynamics, they could not provide a direct measure of snow

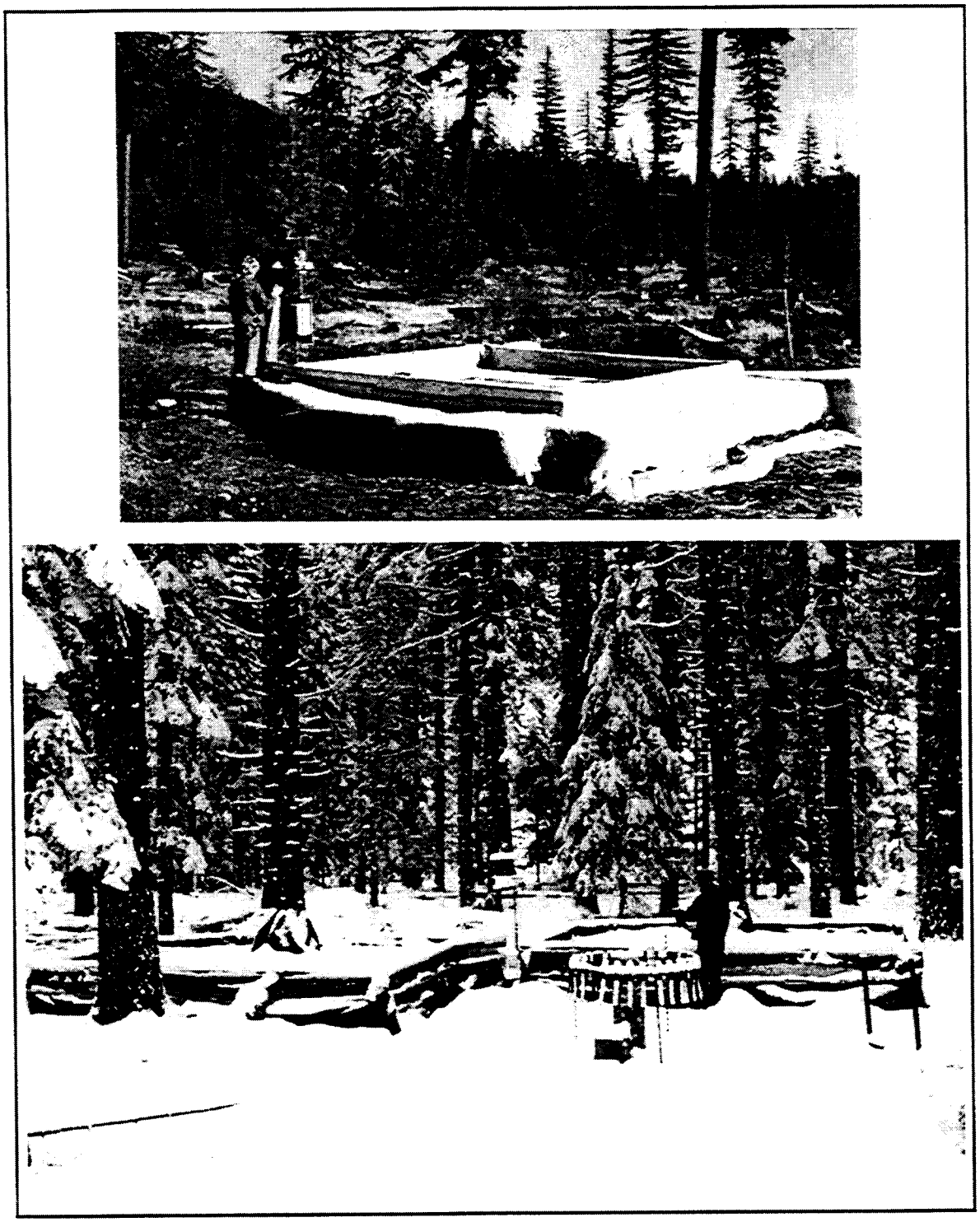

Figure 4.5. Photograph of clearcut weighing lysimeter (top) and beneath-canopy weighing lysimeters (bottom). A shielded precipitation gauge is shown in the foreground.

interception by the canopy. To measure snow interception directly, a series of cut-tree experiments were conducted in a plantation near the weighing lysimeters (see Figure 4.1). The cut-tree technique has been applied previously in the investigation of snow interception (Lundberg 1993, Schmidt 1991; Satterlund and Haupt 1967, 1970; Hedstrom and Pomeroy 1998).

An overview of the cut-tree experiment is shown in Figure 4.6 after a significant snowfall event. Weighing lysimeters were located beneath each of the cut trees. These weighing lysimeters were identical in design to those described previously and had a plan area of 6 m^2. Outflow from the lysimeter was measured by a single one liter capacity tipping bucket. Four 1100 kg load cells weighed the lysimeter. Each weighing lysimeter was constructed around a tree such that its trunk protruded directly through the center of the lysimeter. After the tree was cut and removed, the remaining stump was used to anchor the tree weighing device. Snow released from the tree fell directly into the weighing lysimeter. Meltwater drip was caught by the lysimeter and routed to a tipping bucket.

Figure 4.7 shows an 3-d isometric schematic of the tree weighing device. This device differed from previously developed devices for weighing a cut-tree and was developed specifically to be easily portable, to hold the tree only at its cut end, and to be insensitive to wind loading. The tree weighing device consisted of a pair of nested steel tubes. The interior tube, which held the cut tree, had a 15 cm outside diameter (OD) with 10 mm thick walls. The exterior tube had an 20 cm OD tube with 10 mm thick walls. A 30 cm square, 20 mm thick steel plate was welded to the bottom of the exterior tube. The bottom of the interior tube was welded closed using a 13 cm diameter steel plate. High density polyethylene slats reduced the interior clearance between the two tubes to approximately 0.5 mm. The close tolerance of the design minimized potential for binding while the polyethylene greatly reduced interior friction.

A single 1100 kg load cell was placed through a hole cut in the side of the exterior tube such that the load axis was directly beneath the center of the interior tube. The load cell was bolted through a spacer plate directly to the lower steel plate. Load was transferred from the

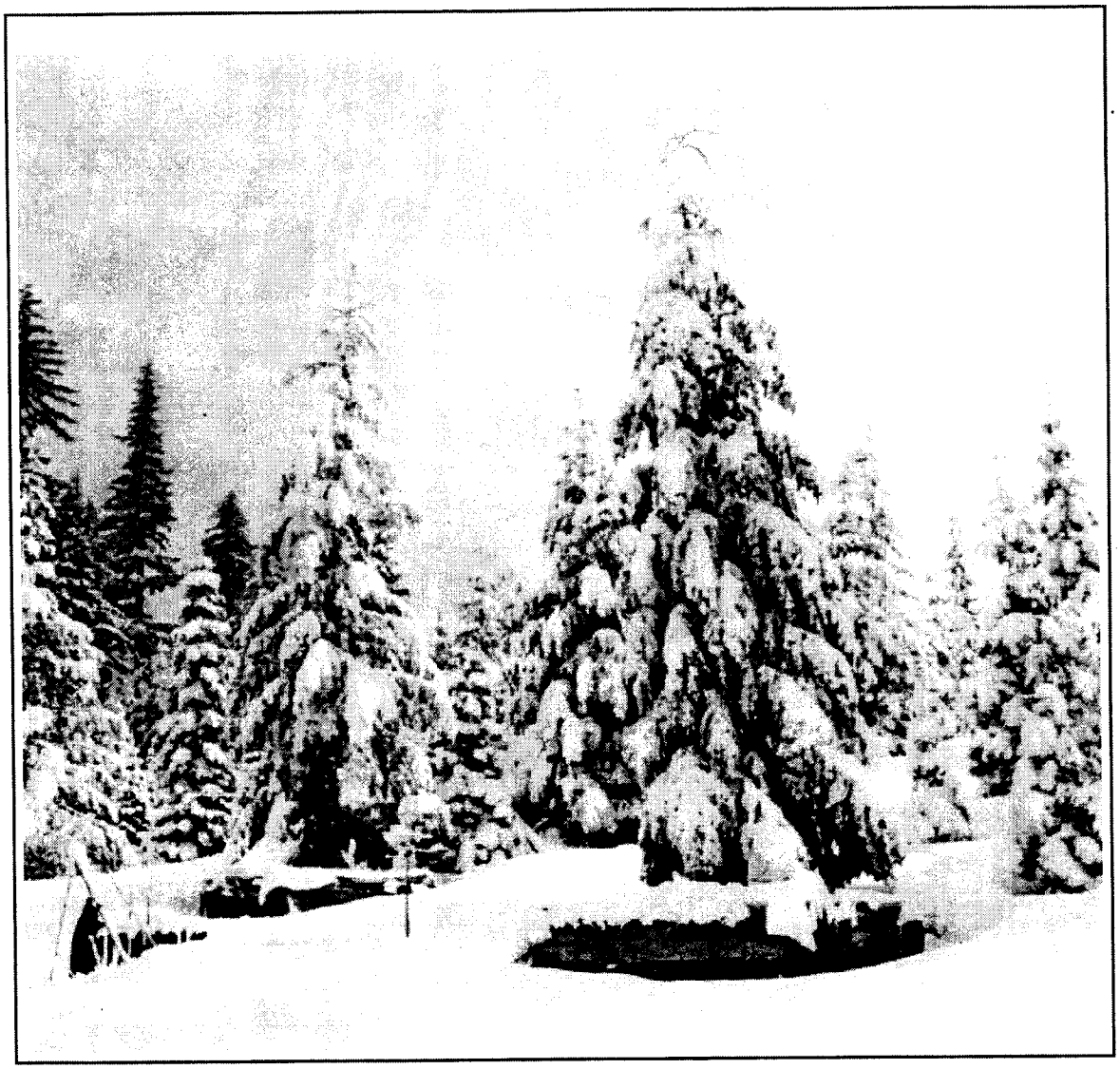

Figure 4.6. Photograph of cut-tree experiment site after a significant snowfall. Both trees are Douglas-fir, the foreground tree is 8 m tall, the background tree is 11 m tall.

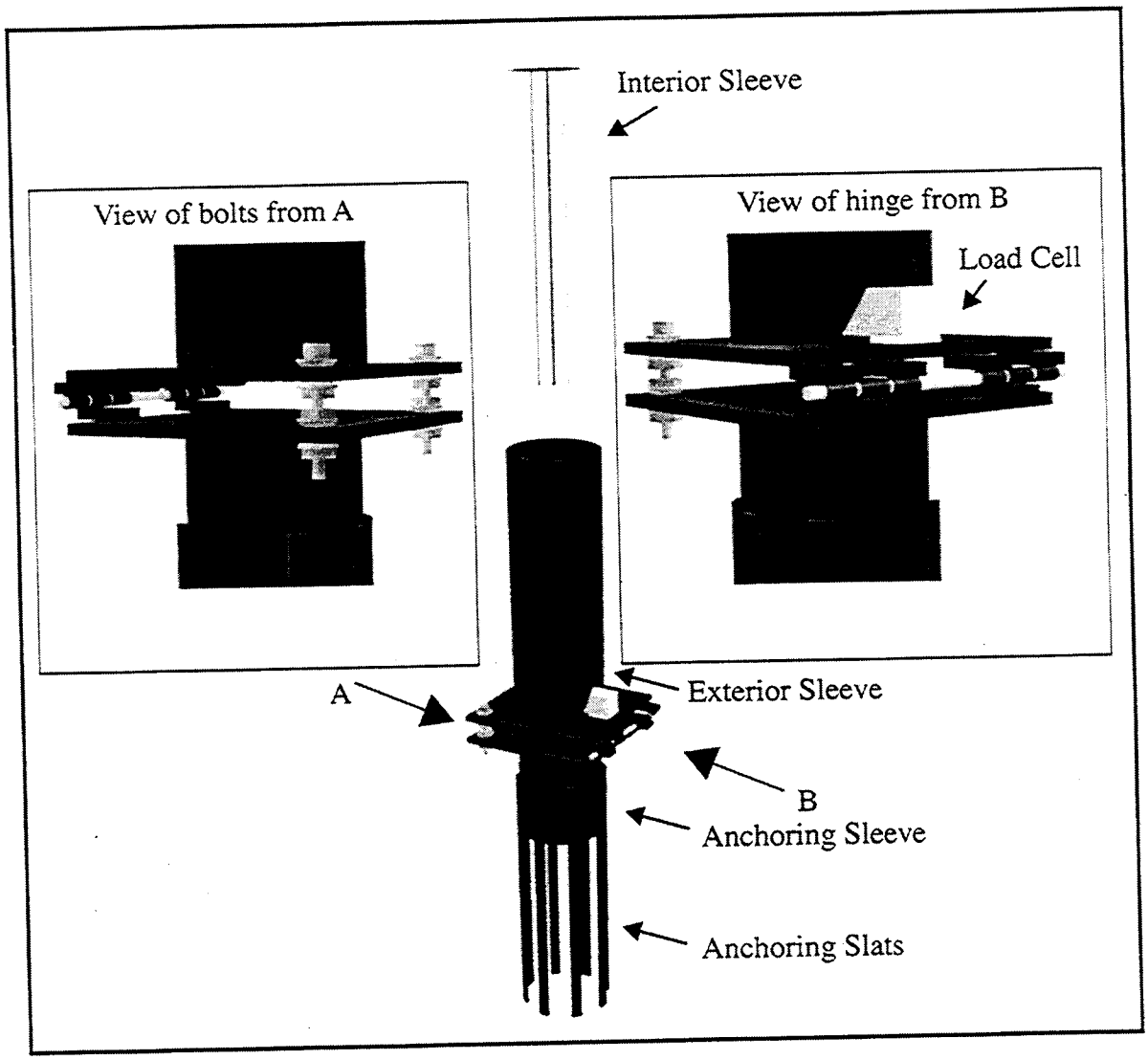

Figure 4.7. Rendering of tree weighing device showing nested tube construction and anchoring sleeve. Side perspectives of the hinge and leveling bolts are also shown.

bottom of the interior tube to the load cell via a 10 mm diameter high tensile strength steel bolt with a rounded head.

A support sleeve was used to anchor the cut-tree weighing device to an existing stump. This sleeve consisted of a 30 by 30 cm, 20 mm thick steel plate welded to a 20 cm OD steel tube with 10 mm walls. This sleeve was placed over the existing stump and anchored in place through 1 meter long perforated slats welded to the exterior of the sleeve. Lag bolts were used to anchor the slats to the stump.

The base plate of the exterior tube and the base plate of the anchor were connected with a single long hinge along one side of the steel plates and two bolts along the opposite side (Figure 4.7). The design was hinged to facilitate insertion of the inner tube (bearing the full load of a tree) into the outer tube. Once the inner tube was completely inserted, the cut tree was pushed into position using a series of long poles with the hinge serving as a fulcrum point. The typical procedure involved in raising a cut-tree is shown in Figure 4.8. The tree was leveled using the combination of nuts and spherical washers as shown in Figures 4.7 and 4.8. The nested tube design ensured that all vertical loading (i.e. changes in the weight of the tree) were applied directly to the load cell. All bending moments due to wind loading were transferred directly to the exterior tube to the support sleeve and stump. To investigate differences in snow interception between tree species, four cut-tree weighing devices were installed in the field. However, only two of these included weighing lysimeters.

4.6. Precipitation gauges

Precipitation was measured with a resolution of one millimeter by a series of unheated tipping bucket gauges. Each gauge consisted of a 30.5 cm diameter PVC pipe (1.2 m in length) attached to a rigid PVC base. The gauge was filled to a depth of approximately 25 cm with an antifreeze solution that was a 3:2 mixture of propylene glycol and ethanol (McGurk 1992) topped with a thin layer of 10-30 weight motor oil, which prevented ethanol evaporation. The antifreeze was recharged after 500 mm of precipitation to limit dilution and thereby prevent freezing.

Figure 4.8. Typical procedure for installing cut tree into weighing device (clockwise from top left): (1) Cut end of tree is trimmed to fit interior sleeve, both are then inserted into the exterior sleeve. (2) Long poles are used to push the tree into position. (3) Once vertical, the top sleeve is bolted in position and the tree is leveled.

Precipitation falling into the gage melted in the antifreeze reservoir and displaced an identical volume of antifreeze into a tipping bucket. To limit catch deficiencies, each gauge was shielded from the wind. Five precipitation gauges were used in conjunction with the weighing lysimeters and cut tree experiments. Two were located at the shelterwood site, one at the cut-tree experiments and two in small clearings near the beneath-canopy weighing lysimeters.

4.7. Snow courses

The SWE and outflow measurements from the weighing lysimeters were point observations taken beneath a full canopy cover (i.e. 100% canopy closure). To provide data for testing a snow accumulation and melt model at scales approaching the horizontal spatial resolution of a typical hydrologic model (~ 100 m), weekly snow courses were conducted at 40 points on a uniform grid (80 by 80 meter spacing) over an adjacent 26 ha forest stand (Figure 4.1). Average canopy closure over the snow course area was approximately 70 percent.

4.8. Energy balance

Environmental sensors, from which the components of the energy balance were estimated, were installed above the snow at each site. Measurements of wind speed, air temperature, relative humidity, and incoming short- and long-wave radiation were taken 2-m above the soil surface and summary statistics were recorded every 30 minutes (Figure 4.9). Wind speed was measured with R.M. Young photochopper totalizing anemometers. These measured wind passage each minute and integrated the wind speed over the observational interval. To prevent snow accumulation on the anemometers, housings of a 30 by 30 cm square of Plexiglas® were constructed and were positioned approximately 15 cm above the anemometer (Figure 4.9). Comparison of paired anemometers, with and without housings, showed no noticeable difference in wind speed when the unprotected anemometer was free of snow. Incoming short-wave radiation was measured with Epply® pyranometers. Reflected short-wave radiation, measured

with Licor® silicon cell pyranometers, was used to estimate albedo and to correct the Epply® pyranometers when they were covered with snow. Incoming long-wave radiation was measured with Epply® pyrgeometers. Air temperature and relative humidity were measured with Campbell Scientific Vaisala probes, which were protected from direct and reflected radiation by six plate shields.

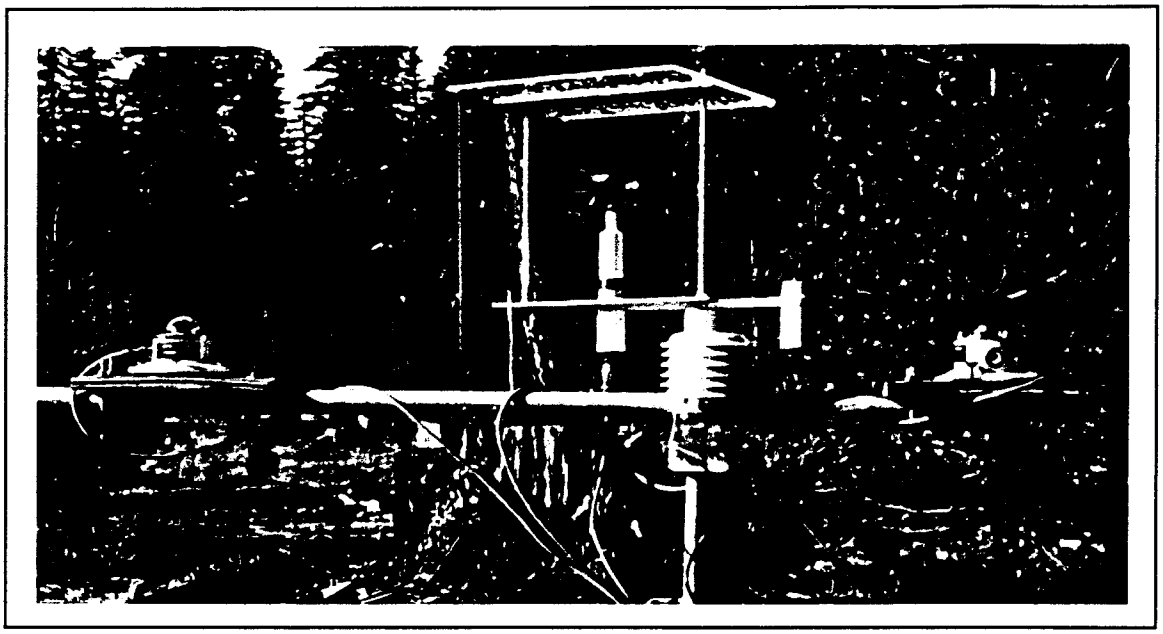

Figure 4.9. Typical micrometeorological tower used to measure energy balance at each site. From left to right, sensors are: shortwave radiation, wind speed (with a snow shield), air temperature and relative humidity (both housed in a 6 plate radiation shield), and longwave radiation.

Chapter 5. Results of the field campaign

This chapter presents the results of the field campaign as they relate to the goal of this dissertation, which is to develop, test and apply an energy balance model of forest canopy effects on ground snowpack accumulation and ablation to assess the impacts of forest canopy removal on peak streamflow. Due to the large quantity of data collected, a detailed accounting of each melt event and the differences in snow water equivalent and outflow between sites is beyond the scope of this discussion. Instead, the collected data are presented in a manner to allow identification of individual processes (to the extent possible) for model development. These field data also form the basis for calibration and testing the model described in Chapter 6. The model is applied at the watershed scale in Chapter 7.

This chapter is organized as follows: First, an overview of the weighing lysimeter and cut-tree data from three winter seasons is presented to highlight overall trends in the data and differences between each season. Next, these data are analyzed to determine micrometeorological and morphological controls on processes governing the rate and limits on snow interception by a mature canopy and cut trees. Data that provide information on the fate of intercepted snow are presented last.

5.1. Overview

Figures 5.1, 5.2 and 5.3 show the observed beneath-canopy, shelterwood and clearcut (when available) snow water equivalent for three winter seasons (1996/97, 1997/98 and 1998/99), respectively, as well as daily total precipitation and average daily air temperature and wind speed observed at the shelterwood site. These figures also show the observed intercepted SWE on the cut-tree experiments for each season. Below canopy SWE is taken as the average of the two beneath-canopy weighing lysimeters. Figure 5.3 compares data from both beneath-canopy

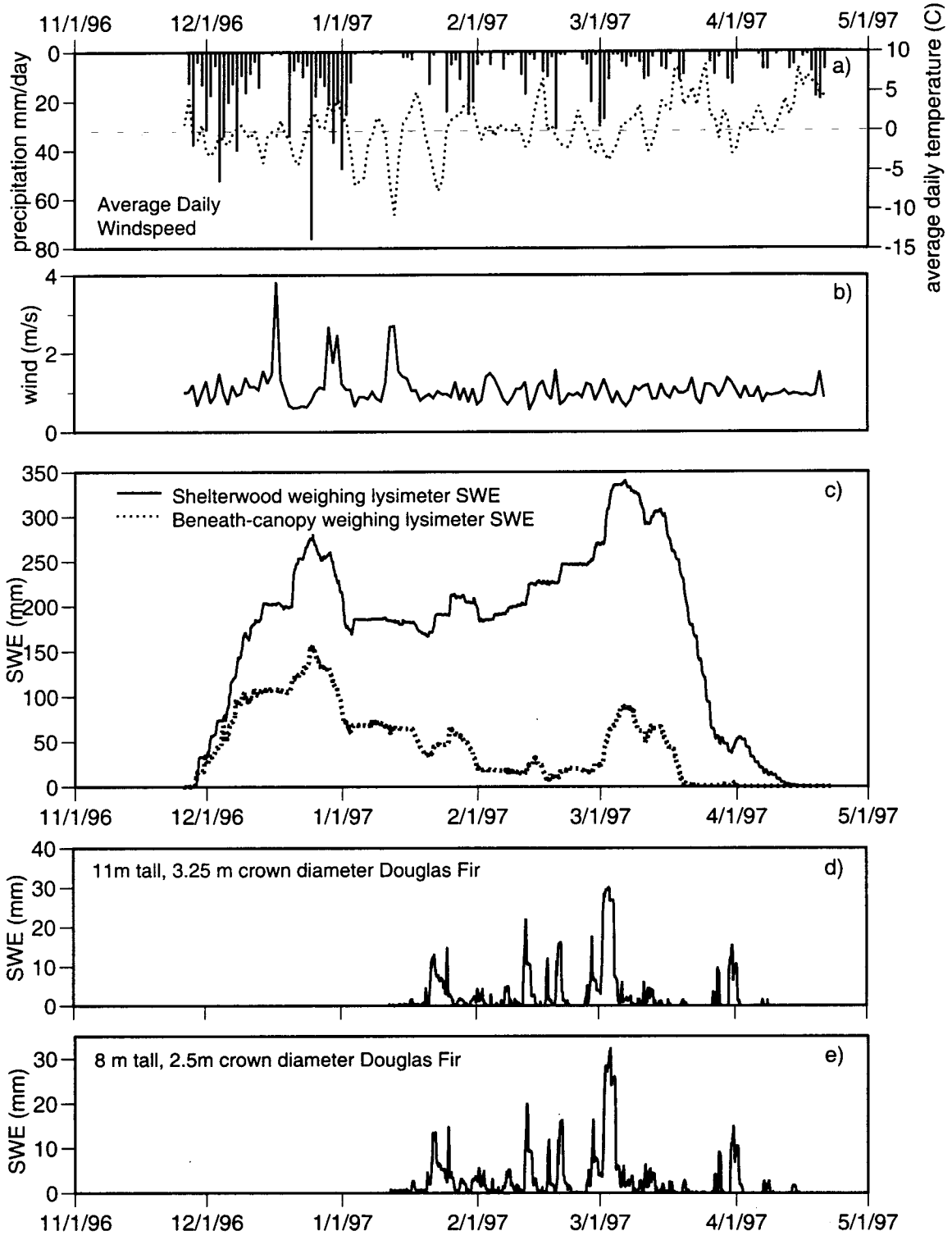

Figure 5.1. Summary results for 1996-97 snow season. a) daily average air temperature and total daily precipitation, b) daily average wind speed, c) shelterwood and beneath-canopy SWE, and d,e) intercepted snow load on two Douglas-fir cut trees.

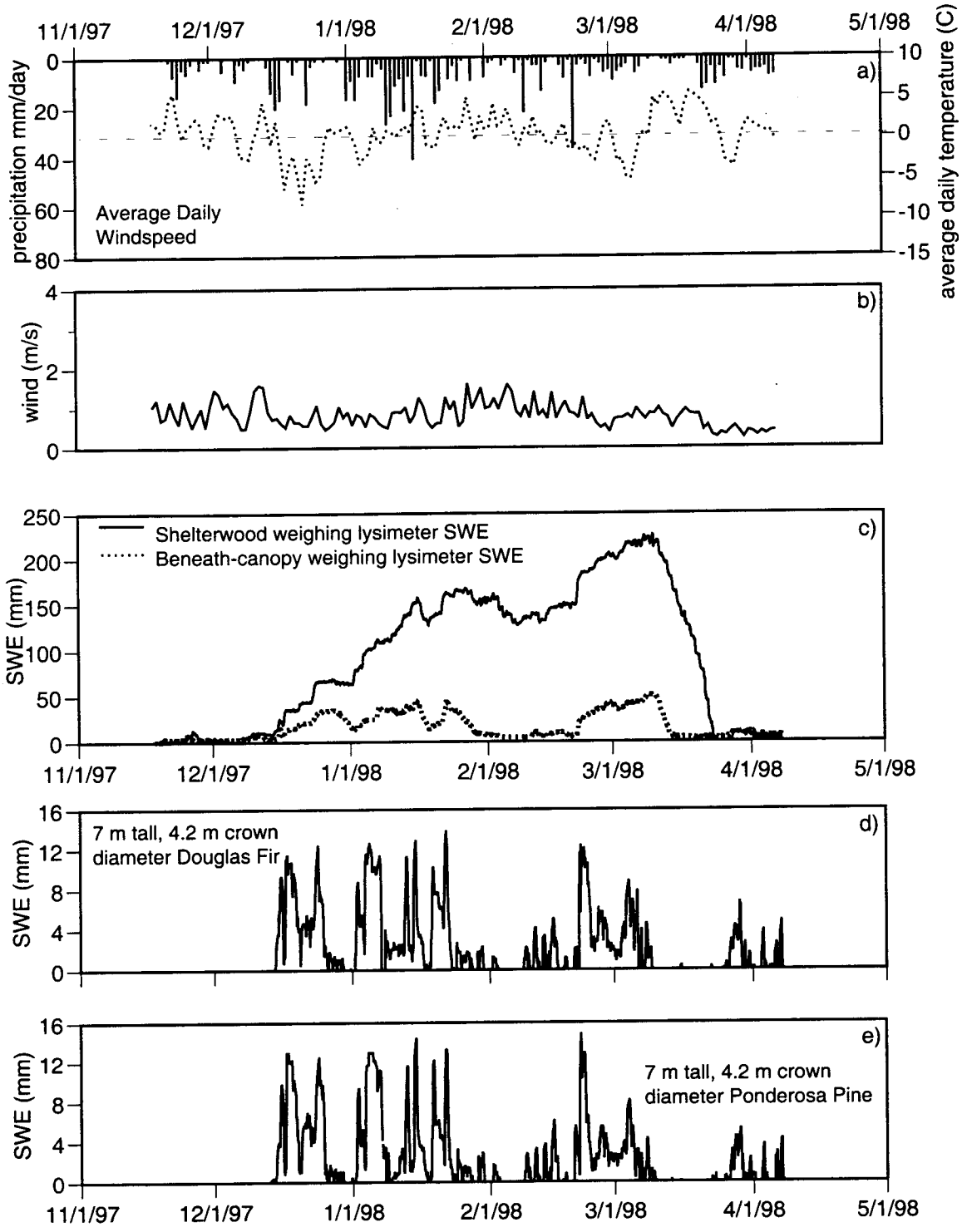

Figure 5.2. Summary results for 1997-98 snow season. a) daily average air temperature and total daily precipitation, b) daily average wind speed, c) shelterwood and beneath-canopy SWE, and d) intercepted snow load on Douglas-fir (d) and ponderosa pine (e) cut trees.

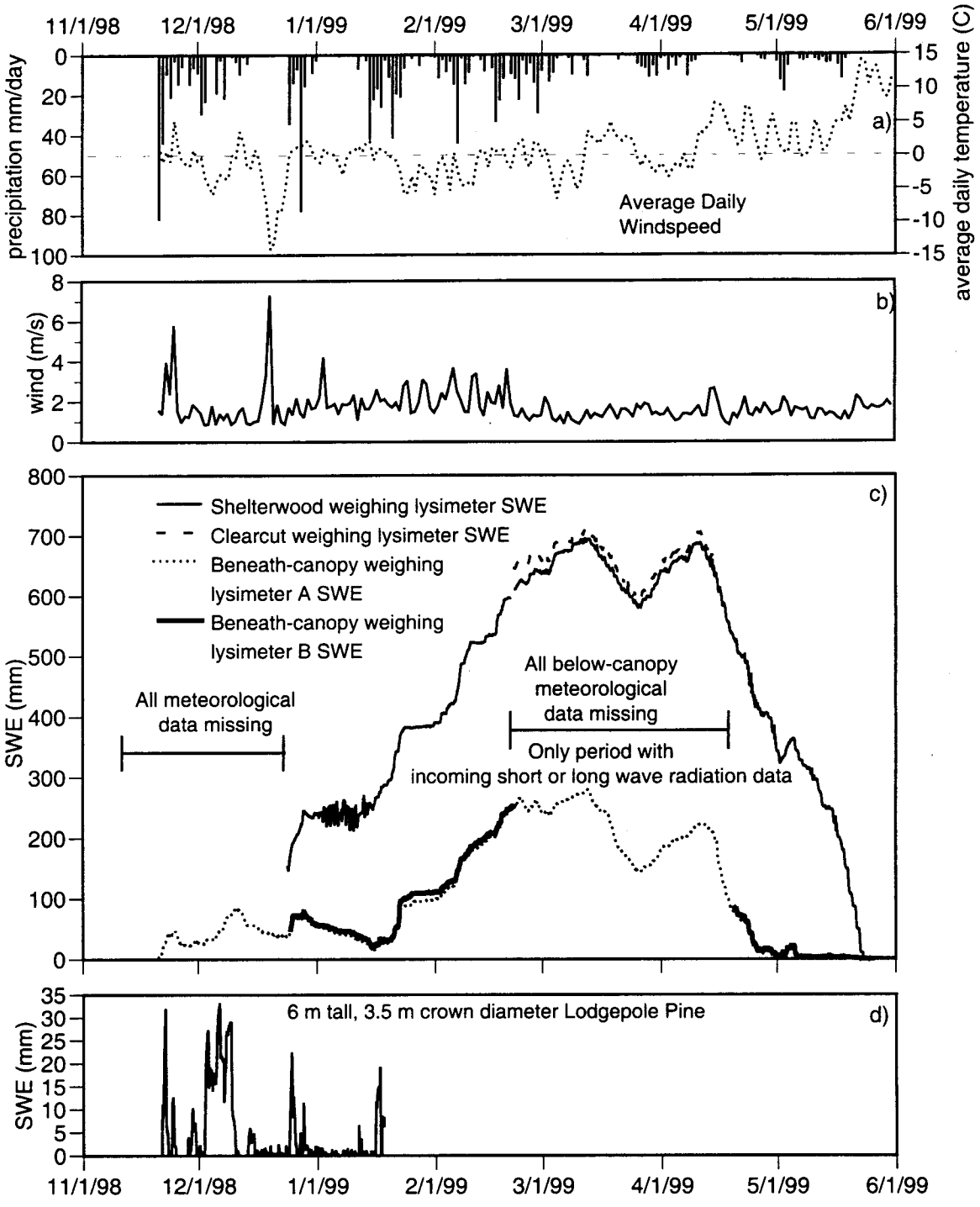

Figure 5.3. Summary results for 1998-99 snow season. a) daily average air temperature and total daily precipitation, b) daily average wind speed, c) shelterwood, clearcut and beneath-canopy SWE, and d) intercepted snow load on a cut lodgepole pine tree. Periods of missing data are shown. All precipitation data were reconstructed from a nearby site (see section 6.4.4).

lysimeters for the 1998/99 season. Similar agreement between the beneath-canopy lysimeters occurred during the 1996/97 and 1997/98 seasons.

While every attempt was made to provide continuous records of all measurements over the course of three winter seasons, there are significant gaps in the data records. These gaps occurred due to a combination of equipment failure, failure to instrument sites due to an early snow season, and, in some cases, bad luck (e.g. a herd of elk mistaking the clearcut and beneath canopy lysimeters for beds during the 1997/98 season). When equipment malfunction was suspected, these data were removed from presentation and discussion in this work. The only exception was reconstruction of some of the micrometeorological data for the 1998/99 seasons (Figure 5.3) from nearby sites (Figure 5.3). Details on the data reconstruction are given in Chapter 6 in the discussion of model testing against the 1998/99 winter season.

5.1.1. Climatic differences between seasons

Substantial differences in maximum snow accumulation occurred over the three years of measurements. Although the sample size is too small to be statistically significant, differences in seasonal maximum snow accumulation follow what would be expected as a consequence of the large scale climatic conditions during each period as determined from the ENSO (El Nino - Southern Oscillation) Index. The 1998/99 season was characterized by a strong La-Nina event in the Pacific, while the 1997/98 season occurred during a strong El-Nino event and 1996/97 was considered ENSO neutral. The large differences in snow accumulation between each of the three seasons provides an excellent range of conditions for building and testing the full canopy-snow model described in Chapter 6.

5.1.2. Weighing lysimeter data

Figures 5.1 through 5.3 show that the overall effect of the forest canopy on reducing ground snow accumulation is substantial, and is not well described by a simple relationship

between "beneath-canopy" and "open" snow accumulation. During the period through 1-Jan 1997, snow interception processes limited overall accumulation to approximately 50% of the shelterwood value. The ROS event of 29 Dec 1996 to 2-Jan 1997 is apparent on Figure 5.1 and resulted in significant loss of SWE by both the shelterwood and beneath-canopy weighing lysimeters. Loss of SWE was 60.4 mm and 86.9 mm at the beneath-canopy and shelterwood sites, respectively. This was the only major ROS event observed during the 3-year field campaign. During the period from 10 Jan 1997 to 1 Mar 1997, snow continued to accumulate at the shelterwood site but not beneath the canopy. By 1 Mar 1997, the below-canopy snowpack had almost completely melted while SWE in the shelterwood was 250 mm, close to the maximum for the year. Due to differences in accumulation patterns, the final snowmelt beneath the canopy occurred approximately one month before the final melt at the shelterwood site.

During the 1997/98 season the maximum SWE beneath the canopy was less than 50 mm while the maximum SWE in the shelterwood approached 250 mm. It was observed during frequent field visits in 1997/98 that denser forest stands adjacent to the beneath-canopy site remained snow free during the entire 1997/98 season.

Considerably greater snow accumulation occurred at all sites during the 1998/99 snow season. Even so, snow accumulation below the canopy was considerably less than that observed at the shelterwood site, especially before 15 Jan 1999. The accumulation and ablation of SWE in the clearcut and shelterwood sites were nearly identical during the period in which measurements of clearcut SWE were available (20 Feb 1999 to 15 Apr 1999).

5.1.3. Cut-tree experiments

Direct measurement of snow interception via the cut-tree experiments showed considerable differences in maximum observed interception loads between seasons. Intercepted snow load is expressed in mm of water equivalent as calculated from the total mass of snow held in the canopy (kg) divided by the plan area (vertical projection) of the cut-tree. Data on the

species and size of trees used in the cut-tree experiments over the three winter seasons are given in Table 5.1.

Heavy snow interception loads approaching 30 mm of SWE were observed during both the 1996/97 and 1998/99 seasons. Lighter snow loads, not exceeding 15 mm, were observed during 1997/98. During all seasons, remarkably similar behavior in the loading and unloading of intercepted snow was observed among trees of different species and different size.

Table 5.1. Species, height, and crown base diameter of trees used for the cut-tree experiment from 1996 to 1999.

Season	Species	Height to top whorl (m)	Crown base diameter (m)
1996/97	Douglas-Fir (*Pseudotsuga menziesii*)	11	3.25
1996/97	Douglas-Fir (*Pseudotsuga menziesii*)	8	2.5
1997/98	Douglas-Fir (*Pseudotsuga menziesii*)	7	4.2
1997/98	Ponderosa Pine (*Pinus ponderosa*)	7	4.2
1997/98	White Fir (*Abies concolor*)	6	2.0
1998/99	Lodgepole Pine (*Pinus contorta*)	6	3.5

5.2. Apparent snow interception by a mature Douglas-fir canopy

Figure 5.4 shows apparent maximum snow interception by the mature Douglas-Fir canopy above each of the beneath-canopy lysimeters. Data were obtained from 36 individual snowfall events from 1996 to 1999 and are presented individually for both below canopy weighing lysimeters (A and B in Figure 5.4). Some events were not observed by both beneath-canopy weighing lysimeters due to instrument malfunction. Total snowfall in the open during events was measured as the net change in weight of the shelterwood lysimeter. Events were assumed to begin after the air temperature fell below 1°C. Snow interception by the mature canopy was inferred as the difference between snowfall in the open and the net increase in weight

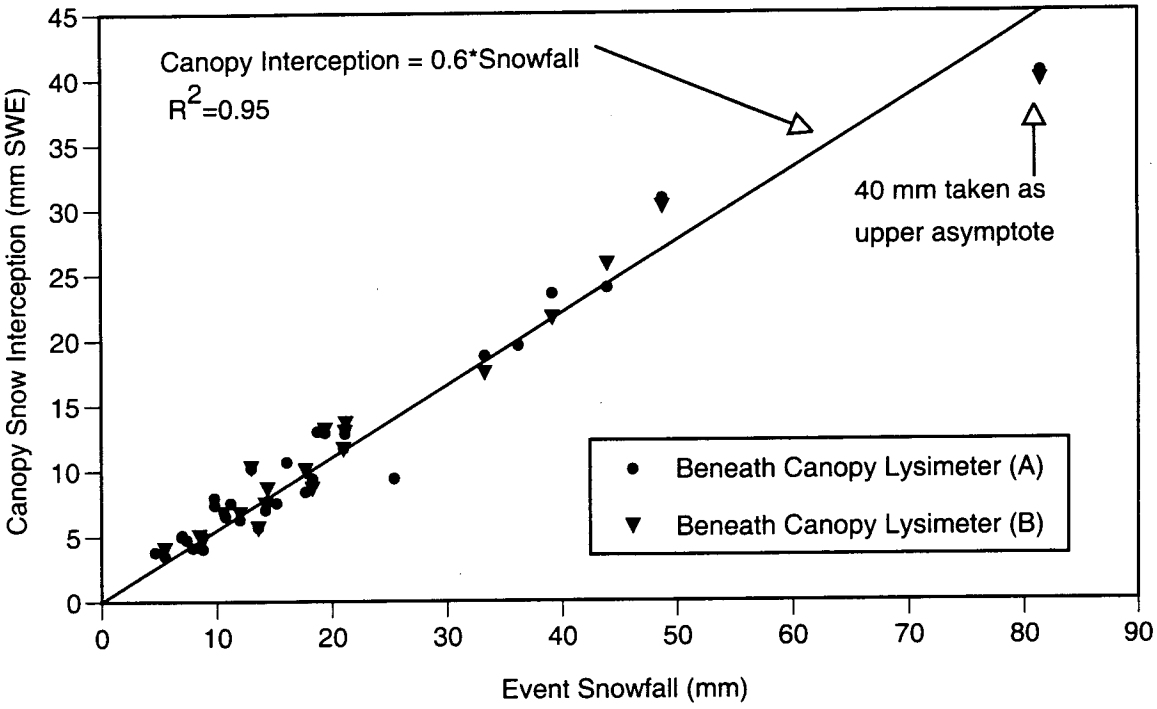

Figure 5.4. Estimated snow interception by a mature Douglas-fir canopy (residual of open and beneath-canopy snow accumulation) as measured by two beneath-canopy weighing lysimeters for 36 snowfall events.

of the beneath-canopy lysimeters. Events were taken to end either immediately after snowfall ceased or air temperature rose above freezing, whichever occurred first.

Canopy interception is remarkably well described as approximately 60% of total snowfall for all events with storm snowfall less than 50 mm of water equivalent. The 95 percent confidence interval for the slope of the regression shown in Figure 5.4 is +/- 4 percent. Although a clear upper asymptote on snow interception is not defined by these data, they suggest an upper asymptote of approximately 40 mm of water equivalent (Figure 5.4). The strongly linear relationship between apparent snow interception and snowfall also suggests that differences in air temperature and wind speed do not need to be considered for estimating snow interception by the mature canopy, at least over the range of micrometeorological conditions observed here. The large majority of these snowfall events occurred during periods of light wind (less than 2 m/s as observed at the shelterwood site) and relatively warm air temperatures (above -5°C).

A similar linear trend is seen governing the growth of intercepted snow during snowfall events (Figure 5.5a). Intercepted snow loads at 30 minute intervals during snowfall were calculated from the beneath-canopy and shelterwood lysimeter data as described above for the calculated maximum snow load. The growth of intercepted snow is well described as sixty percent of snowfall (for snowfalls less than 50 mm SWE) for seven of the eight example events shown. During the eighth, the February 1999 event, 40 mm of SWE was intercepted during a snowfall of 80 mm SWE. Data from all 36 events from Figure 5.4 are not shown on Figure 5.5a. However, for all 36 events, both total and incremental snow interception are well described by the same linear relationship for snowfalls less than 50 mm SWE. The February 1999 event was the only event measured during the three year period for a snowfall greater than 50 mm SWE.

Figure 5.5b shows the observed air temperature and windspeed plotted against accumulated snowfall (to facilitate comparison with Figure 5.5a) for the single largest observed interception event during the three year period. This event is of particular interest in that observed air temperature changed rapidly during the event. During the first part of the event, air

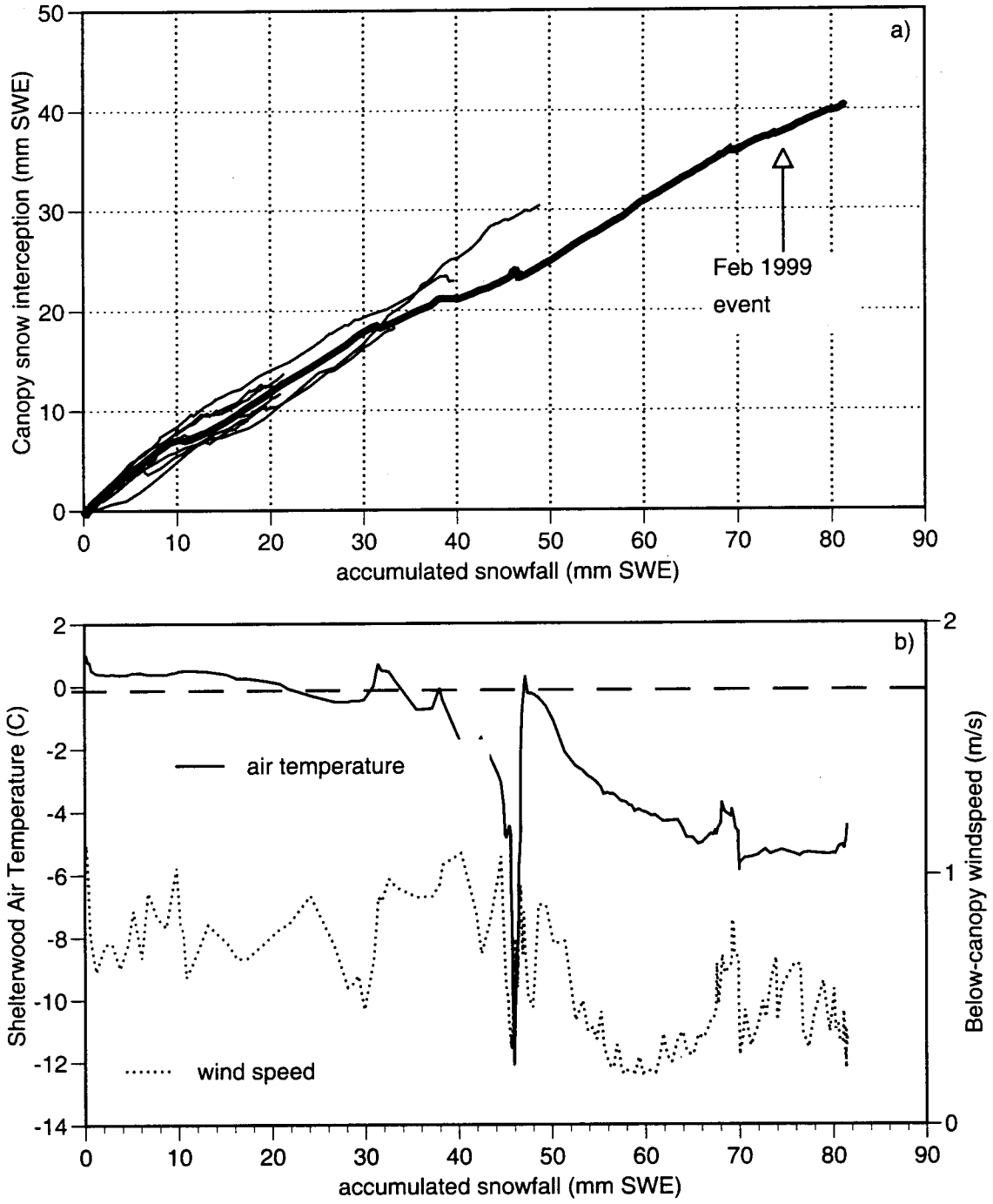

Figure 5.5. a) Calculated growth of intercepted snow on the mature canopy during eight major snowfall events. b) Air temperature and wind speed during February 1999 snow interception event plotted versus accumulated snowfall at the shelterwood site. Measurements of wind speed in the open were not available during this period.

temperature was slightly above freezing and growth of intercepted snow was sixty percent of snowfall. As the event progressed, air temperature fell abruptly to -12 °C, along with an increase in windspeed. These changes in meteorological conditions correspond to a reduction in the rate of snow interception. As the storm continued and conditions remained cold, snow interception proceeded at a rate close to sixty percent of snowfall up to 80 mm of total precipitation. Given the excellent agreement of a simple constant linear relationship to the majority of snow interception events on the mature canopy, it appears that micrometeorological effects on the rate of snow interception can be ignored for the range of conditions observed here.

5.3. Differences in snow interception between cut-trees

Over the course of three winter seasons, six cut trees of four different species were continuously weighed (see Table 5.1 and Figures 5.1 to 5.3) in an attempt to understand differences in the growth of intercepted snow and the maximum interception capacity between trees of identical species but different morphologies and trees of different species. Data from the cut trees were also used to provide an independent check on inferred snow interception by the mature canopy.

Figures 5.1 through 5.3 have already shown that overall patterns and magnitudes of snow interception between different trees are remarkably similar. To examine these differences more closely, the growth of intercepted snow during twelve snowfall events is shown in Figure 5.6. Snowfall during events was measured by the shelterwood weighing lysimeter. Each graph in Figure 5.6 was forced through the origin at the start of the event. For some events, intercepted water on the cut trees approached 5 mm before snowfall began. In many cases, this initial storage was due to rainfall interception prior to the onset of snowfall (these initial interception depths were typically observed to be 3 mm or less). In a few cases, the 5 mm initial storage was a residual from previous snowfall events. Observations from all simultaneously weighed cut trees during each event are shown.

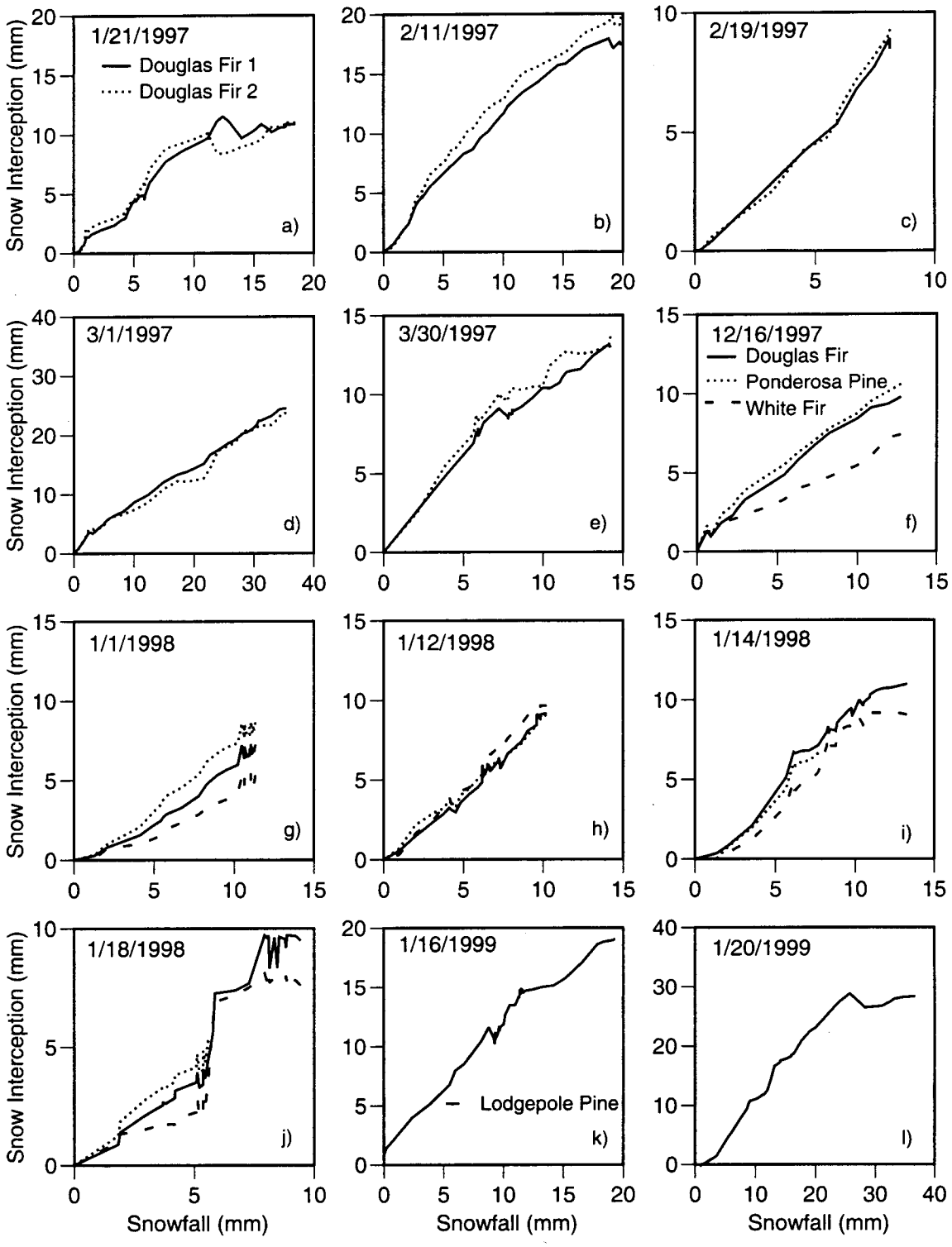

Figure 5.6. Snow Interception versus snowfall for 12 snowfall events over 3 snow seasons (1996/97 a-e, 1997/98 f-j, 1998/99 k-l) as observed on cut trees.

During 1996/97 only two cut tree devices were installed (Figure 5.6 a-e). During 1997/98 two additional devices were installed (for a total of four) but one device failed (Figure 5.6 f-j). During the winter of 1998/99 an early snowfall prevented the installation of all but one cut-tree experiment (Figure 5.6 k-l).

While snow interception by the mature canopy was well described for all events as a constant linear function of snowfall, no such clear relationship is seen from the cut-tree data. Individual snowfall events show considerable variability in the rate of growth of intercepted snow on cut trees, often initially exceeding the rate of snowfall.

Despite the variability between events, variability between individual cut trees (either of different species or size) during events is considerably less. Despite differences in size, both Douglas-fir trees behaved nearly identically during snow interception events during the 1996/97 observation season. Even more surprising, the Douglas-fir, ponderosa pine and white fir trees showed nearly identical patterns and magnitudes of snow interception during the 1997/98 season (Figure 5.6 f-j). Similar insensitivity to species type is also seen for white fir during the 1997/98 season. Lodgepole pine was not simultaneously compared against trees of other species, however, it too exhibited growth forms and interception capacities similar to the other species. This result is extremely important. Despite obvious differences in structure and branch flexibility between ponderosa pine, Douglas fir, white fir and lodgepole pine, these differences can apparently be ignored in determining the relative rate and maximum amount of snow interception, for the conditions that prevailed at the times and locations of the observations. Similar insensitivity to species type has been found in previous studies that have measured snow interception by weighing cut trees (Satterlund and Haupt 1970) and cut tree branches (Schmidt and Gluns 1991).

5.4. Seasonal estimate of intercepted snow sublimation - wet canopy evaporation

Comparisons between lysimeter data also provide estimates of losses from intercepted snow in the mature canopy. Figure 5.7 shows estimated losses from the mature canopy during the

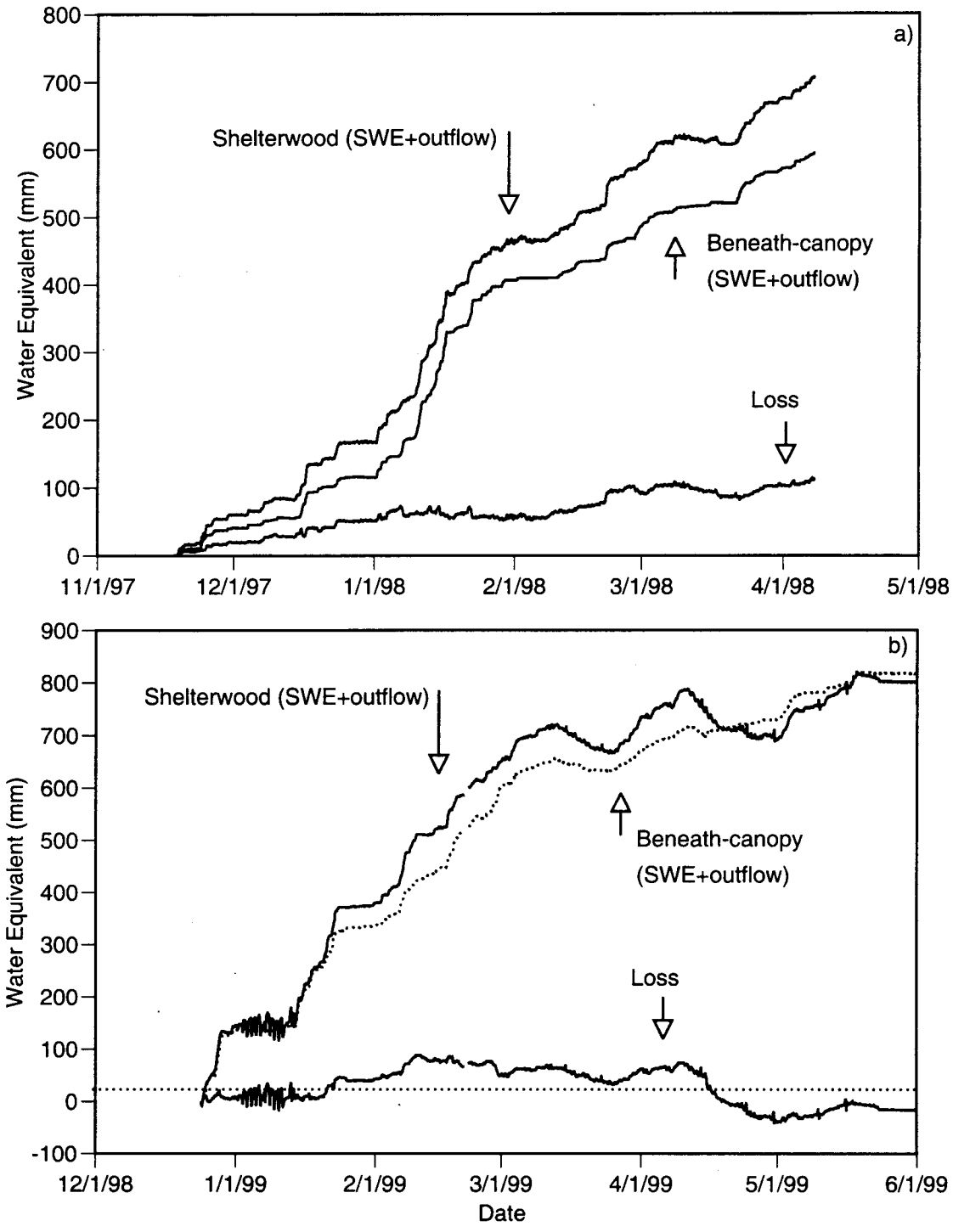

Figure 5.7. Estimated sublimation loss from intercepted snow (residual of shelterwood and beneath-canopy total water) over two winter seasons (1997/98 and 1998/99).

1997/98 and 1998/99 seasons. Data for the 1996/97 season are not shown due to the failure of the prototype lysimeter drain system during the ROS event of 1 Jan 1997. (The improved drain design, installed in November of 1997, is described in Chapter 4). Total accumulated water (SWE + accumulated outflow) is shown along with net loss. Net loss is the difference between total accumulated water as measured by the shelterwood and beneath-canopy weighing lysimeters.

The net loss term includes all possible processes which could remove water from the canopy and not deposit it in the below canopy lysimeter. These include sublimation of intercepted snow and evaporation of intercepted water. An additional factor which could be included in the loss term is melt water drip or mass release from intercepted snow that is not captured by the beneath-canopy weighing lysimeter. Great care was taken during the design and placement of the beneath canopy lysimeters to remove this source of error. During extended periods of time when snow interception, mass release, and meltwater drip occurred, estimated loss was near zero. This result suggests that the estimate of loss is not biased due to the size or placement of the lysimeters.

Estimated annual loss during 1997/98 is on the order of 100 mm and appears to be strongly dependent on local micrometeorology. During the relatively cold period from 1 Dec 1997 to 7 Jan 1998, during which air temperatures remained below freezing, estimated loss is 34 mm (~1 mm/day). During the warm, wet period from 7 Jan 1998 to 1 Feb 1998, estimated loss was limited to 4 mm.

Additional insight to these differences is given by the patterns of snow interception (as measured by the cut-tree experiment) shown on Figure 5.2. During both periods described above, significant snow interception occurred. However, during the period with high estimated loss, the snow remained on the canopy for significantly longer amounts of time than during the period when losses were negligible. A second period of large interception loss, centered around 1 Mar 1998, corresponds to another lengthy interception event.

Similar overall magnitudes and patterns of interception loss occurred during the 1998/99 season. During the relatively warm period just prior to 1 Jan 1999, significant snow interception occurred (as evidenced by the cut tree weight on Figure 5.3). Due to the rapid removal of snow from the canopy, total loss was negligible during this first event. Significant net loss of water due to canopy processes was observed during a later event, centered around 1 Feb 1999. The reduction in total water at the shelterwood site after 15 Mar 1999 is caused by routing of melt water out of the shelterwood lysimeter. Due to the depth of the snowpack during the latter part of the 1998/99 snow season (exceeding 2 meters) the observation of snowpack outflow at the shelterwood site after 15 Mar 1999 is biased by the variability in the flow paths of meltwater. After 1 May 1999 (and a considerable loss of snow depth), the shelterwood observation of outflow is correct. Net loss due to canopy processes during a two month period (24 Dec 1998 to 24 Feb 1998) was approximately one mm per day. If the outflow measurement at the shelterwood site is corrected for bias (by assuming that sublimation from the shelterwood lysimeter is negligible and closing the mass balance during precipitation free periods), the overall loss for the 1998/99 season is approximately 100 mm of water equivalent.

5.5. Evidence for high rates of intercepted snow sublimation

Occasional high rates of sublimation from intercepted snow were measured using the cut tree lysimeters. Although a number of periods with high sublimation rates are likely to have occurred (as described above), most periods could not be isolated as pure sublimation events from the cut trees due to either increases in the weight of the lysimeter below the cut-tree or the occurrence of lysimeter outflow during the event. Figure 5.8 shows observed micrometeorology, cut-tree snow interception, and ground SWE for a single sublimation event. Observed relative humidity often exceeded 100 percent due to the inaccuracy of the sensor at values above 95 percent. No outflow was measured during the event. Sublimation of 4.3 mm SWE over seven hours was observed from the canopy on 23 Feb 1998. While this rate is impressive, opportunities

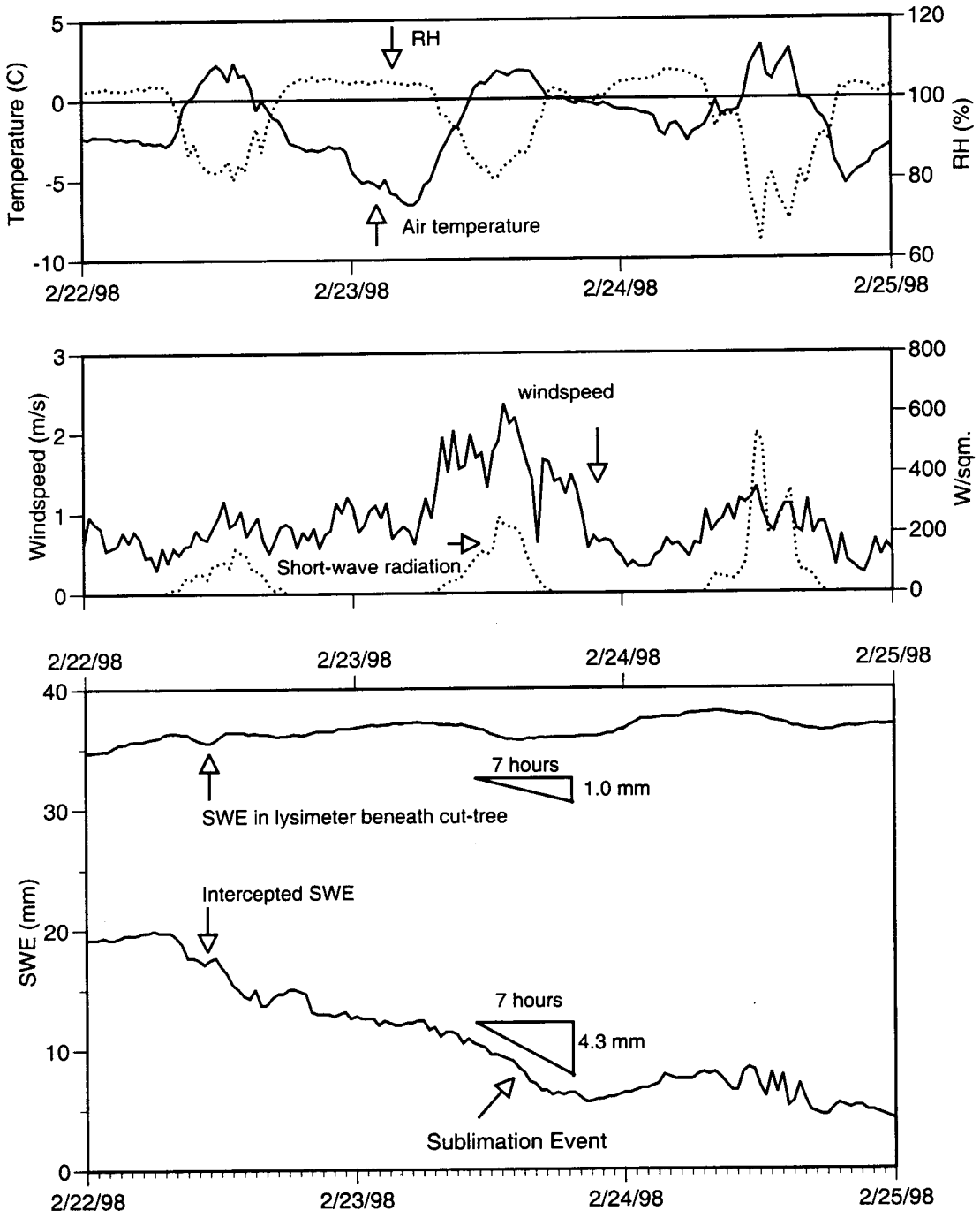

Figure 5.8. Loss of intercepted snow from a cut white fir tree during a rare precipitation free period during which intercepted snow remained on the canopy. No outflow was observed during this period from the lysimeter beneath the cut-tree or the lysimeter at the shelterwood site.

for these high sublimation rates are limited due to the rapid removal of snow from the canopy via meltwater drip or mass release. Sublimation from the weighing lysimeter beneath the cut-tree during this event was one mm over seven hours, only 25 percent of that observed from the intercepted snow on the canopy. The combination of increased temperature, reduced relative humidity, higher windspeed and radiation all contributed to the large sublimation loss.

5.6. Partitioning of meltwater drip and mass release

The two remaining mechanisms for removing intercepted snow from the canopy are meltwater drip and mass release. From the analysis above it is apparent that these two mechanisms must account for the majority of the difference in snow accumulation between forested and open sites in the transient snow zone of the Pacific Northwest. A sublimation loss of 100 mm per year can not account for the observed differences between sites. Unfortunately, the measurement of both of these processes is confounded by changes in the ground snowpack after interception events and that both mechanisms almost always occur simultaneously. For those periods in which the snow in the beneath-canopy lysimeter is actively melting or rain is occurring, the relative magnitudes of meltwater drip and mass release could not be determined.

An attempt was made to determine the partitioning of meltwater drip and mass release immediately after the 36 events shown in Figure 5.4. However, it soon became apparent that it was nearly impossible to distinguish meltwater drip from mass release over these short time frames. All snowfall events were accompanied by significant throughfall (both at the cut trees and below canopy weighing lysimeters), therefore the fresh snowfall in the lysimeters often stored meltwater drip until the pack became saturated. This problem became especially confounding when rainfall occurred before outflow was observed.

Despite these problems, evidence for the relative magnitudes of meltwater drip and mass was obtained from the period from 1-Dec 1996 to 14-Dec 1996 (Figure 5.1) during which melt of the ground snowpack did not occur (i.e. canopy processes controlled ground snow dynamics).

Snow accumulation in the shelterwood was 195 mm while 111 mm accumulated beneath the canopy. During this same time period, 84 mm of additional outflow was observed below the forest canopy. Assuming that 60 percent of all snowfall was intercepted by the canopy (117 mm total interception) and 40 percent was snow throughfall (78 mm direct throughfall), these data imply that 33 mm (28 percent) of the intercepted snow reached the ground as snow while 84 mm (72 percent) was removed as meltwater drip. These calculations suggest a ratio of mass release to meltwater drip of 0.4.

Similar results are seen from 7 Dec 1997 to 25 Dec 1997 (Figure 5.2). During this period, 67 mm of SWE accumulated in the shelterwood while only 31 mm accumulated below the canopy. Outflow beneath the forest canopy exceeded that in the shelterwood by 11 mm during this period. Assuming that 60 percent of snowfall was intercepted (40.2 mm) and 40 percent became direct snow throughfall (26.8 mm), these results suggest that an additional 4.2 mm of mass release occurred. Relative to the increase in outflow of 11 mm attributable to meltwater drip, these results again suggest a ratio of mass release to meltwater drip of 0.4.

While these results provide support for the dominance of meltwater drip over mass release of intercepted snow, they are by no means conclusive. These data suggest a hypothesis that the production of meltwater is the trigger for mass release of intercepted snow. This hypothesis is supported by the literature review of Chapter 3 and the observations that both mechanisms almost always seem to occur simultaneously. Adoption of a constant ratio between the two allows for a straightforward method of calculating mass release from meltwater drip for the climatic conditions and snow states of maritime regions. In colder climates, mass release is expected to occur in the absence of meltwater drip. In these cases, an explicit representation of wind removal of intercepted snow as well as meltwater drip and mass release will probably be necessary.

Chapter 6. A model of snow interception, ground snowpack accumulation and ablation

This chapter describes a model of snow interception and under-canopy snow accumulation and ablation for use in distributed hydrology models. Distributed hydrology models represent the landscape at a fine spatial resolution and typically simulate the energy and water balance of numerous elemental areas (pixels) simultaneously. Therefore, considerable emphasis was placed during model development on simplifying the formulation and reducing computational expense while maintaining model accuracy. The model presented here relies on an energy balance approach at the ground snowpack surface similar to that incorporated in previously developed models (e.g. Jordan 1991, Marks and Dozier 1992, Wigmosta et al. 1994, Tarboton et al.1995). The model formulation of interception processes draws heavily from the field data described in Chapter 5.

This chapter is organized as follows: the energy balance at the snowpack surface is presented first as it is the foundation of the canopy-snow model. Specific attention is given to the representation of turbulent heat fluxes under stable atmospheric conditions at the under-canopy snow surface. The model describing canopy interception and its effect on snowpack accumulation is then introduced. Results of the model calibration for the 1996/97 snow season and testing using the 1997/98 and 1998/99 snow season observations are presented followed by a sensitivity analysis of key model formulations and parameters. Lastly, the model is scaled from the plot (i.e. individual lysimeter) to the stand scale (~30 to 150 meters) via inclusion of a fractional canopy coverage parameter.

The main processes represented in the model are shown schematically in Figure 6.1. The model requires that the driving terms of the energy and mass balance (short- and long-wave radiation, temperature, wind, humidity, and precipitation) be specified at a reference height above the canopy. These values are adjusted to the canopy reference height and the ground snowpack

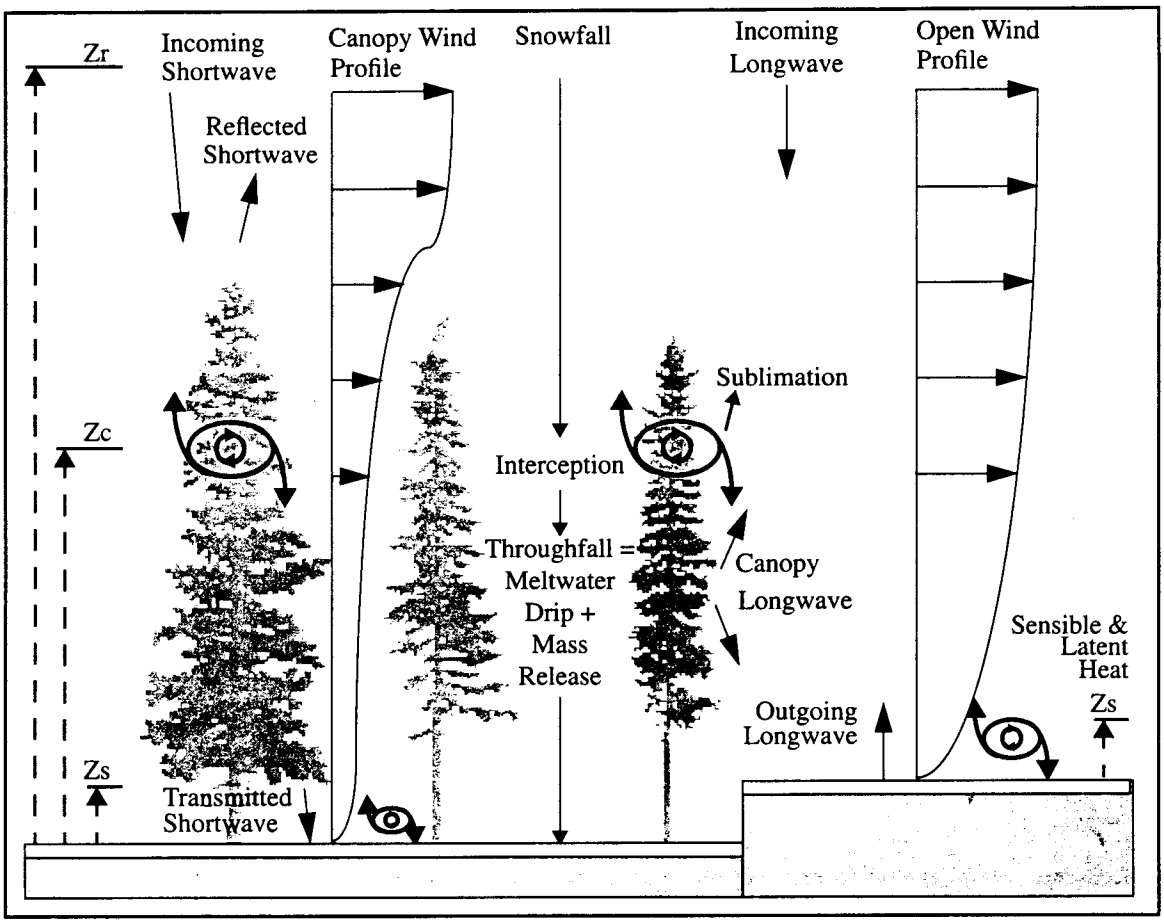

Figure 6.1. Schematic of full canopy - snow model. Meteorological forcings are specified at the above canopy reference height (Zr) and are adjusted to the canopy reference height (Zc) and the near surface reference height (Zs) as described in Appendix A.

reference height as described in Wigmosta et al. (1994) and modified by Nijssen et al. (1997) The full details are presented in Appendix A.

6.1. Ground snowpack accumulation and ablation

An energy balance approach is used to model snowmelt, similar to that developed by Anderson (1976). The snowpack is modeled as two layers: a thin surface layer and a pack layer. Except for changes to the atmospheric stability formulation (described in Section 6.2), the two-layer model described here is similar to that developed by Connelly et al. (1993) and described in Storck et al. (1995). Energy exchange between the atmosphere, forest canopy and snowpack occurs only with the surface layer. The energy balance of the surface layer is

$$\rho_w c_s \frac{dWT_s}{dt} = Q_r + Q_s + Q_e + Q_p + Q_m \tag{6.1}$$

where c_s is the specific heat of ice, ρ_w is the density of water, W is the water equivalent of the snowpack surface layer, T_s is the temperature of the surface layer, Q_r is the net radiation flux, Q_s is the sensible heat flux, Q_e is the latent heat flux, Q_p is the energy flux given to the snowpack via rain or snow, and Q_m is the energy flux given to the pack due to liquid water refreezing or taken from the pack during melt. Energy fluxes into the surface layer are defined as positive. If the flux terms are expressed in watts per square meter then W is given in meters. Solution of Eq. 6.1. is accomplished via a forward finite difference scheme over the model time step (Δt):

$$W^{t+\Delta t} T_s^{t+\Delta t} - W^t T_s^t = \frac{\Delta t}{\rho_w c_s}(Q_r + Q_s + Q_e + Q_p + Q_m) \tag{6.2}$$

Net radiation at the snow surface is either measured or calculated given incoming shortwave and longwave radiation as:

$$Q_r = L_i + S_i(1-\alpha) - \sigma T_s^4 \tag{6.3}$$

where L_i and S_i are incoming long- and short-wave radiation and α is the snow surface albedo. The snow surface albedo is assumed to decay with age. The decay functions are described in more detail in Section 6.4.

The flux of sensible heat to the snow surface is given by:

$$Q_s = \frac{\rho c_p (T_a - T_s)}{r_{a,s}} \tag{6.4a}$$

$$r_{a,s} = \frac{\ln\left[\frac{z - d_s}{z_o}\right]^2}{k^2 U_z} \tag{6.4b}$$

where ρ is air density, c_p is the specific heat of air, T_a is the air temperature and $r_{a,s}$ is the aerodynamic resistance between the snow surface and the near-surface reference height (z). In Eq. 6.4b, k is von Karman's constant (~0.4), z_o is the snow surface roughness, d_s is the snow depth, and U_z is wind speed at the near-surface reference height. Similarly, the flux of latent heat to the snow surface is given by:

$$Q_e = \frac{\lambda_i \rho \left[\frac{0.622}{P_a}\right]\left[e(T_a) - e_s(T_s)\right]}{r_{a,s}} \tag{6.5}$$

where λ_i is the latent heat of vaporization when liquid water is present in the surface layer and the latent heat of sublimation in the absence of liquid water, P_a is atmospheric pressure, and e and e_s are the vapor and saturation vapor pressure, respectively.

Advected energy to the snowpack via rain or snow is given by

$$Q_p = \frac{\rho_w c_w T_a P_r + \rho_w c_s T_a P_s}{\Delta t} \tag{6.6}$$

where c_w is the specific heat of water, P_r is depth of rainfall and P_s is the water equivalent of snowfall. Precipitation (P) is partitioned into snowfall and rainfall via:

$$\begin{aligned} P_s &= P, && T_a \le T_{\min} \\ P_s &= \frac{T_{\max} - T_a}{T_{\max} - T_{\min}} P, && T_{\min} < T_a < T_{\max} \\ P_s &= 0, && T_a \ge T_{\max} \\ P_r &= P - P_s \end{aligned} \tag{6.7}$$

The total energy available for refreezing liquid water or melting the snowpack over a given time step depends on the net energy exchange at the snow surface (Q_{net}):

$$Q_{net} = (Q_r + Q_s + Q_e + Q_p)\Delta t \tag{6.8}$$

If Q_{net} is negative, then energy is being lost by the pack. Liquid water (if present) is refrozen. If Q_{net} is sufficiently negative to refreeze all liquid water, then the pack may cool. If Q_{net} is positive, then the excess energy available after the cold content has been satisfied produces snowmelt.

$$\begin{aligned} Q_m\Delta t &= \min(-Q_{net}, \rho_w \lambda_f W_{liq}), \quad Q_{net} < 0 \\ Q_m\Delta t &= -(Qnet + c_s W_{ice} T_s^t), \qquad Q_{net} \geq 0 \end{aligned} \tag{6.9}$$

The mass balance of the surface layer is given by

$$\begin{aligned} \Delta W_{liq} &= P_r + \frac{Q_e}{\rho_w \lambda_v} - \frac{Q_m}{\rho_w \lambda_f} \\ \Delta W_{ice} &= P_s + \frac{Q_e}{\rho_w \lambda_s} + \frac{Q_m}{\rho_w \lambda_f} \end{aligned} \tag{6.10}$$

where Q_e exchanges water with the liquid phase if liquid water is present (i.e. $W_{liq} > 0$) and Q_e exchanges water with the ice phase in the absence of liquid water.

If W_{ice} exceeds the maximum thickness of the surface layer (typical taken as 0.10 m of SWE), then the excess, along with its cold content, is distributed to the pack layer. If W_{liq} exceeds the liquid water holding capacity of the surface layer, then excess is drained to the pack layer. If the temperature of the pack layer is below freezing then liquid water transferred from the surface layer can refreeze. Liquid water remaining in the pack above its liquid water holding capacity is immediately routed to the soil as snowpack outflow. The dynamics of liquid water routing through the snowpack matrix are not considered here due to the shallow depths of snowpacks in the transient snow zone of maritime climates and the relatively coarse time resolutions (1 to 3 hours) used by distributed hydrology models.

Eqs 6.1 through 6.10 are solved as follows: Given the initial snow surface temperature and water equivalent, additional snowfall is added to the mass of the surface layer and its initial temperature adjusted accordingly. The model first assumes that the final temperature of the snowpack surface layer is 0°C. The net energy exchange at the snow surface, Q_{net}, is calculated based on this assumption. If Q_{net} is positive, excess energy has been delivered to the pack from

the environment and the assumption regarding initial temperature was correct. Snowmelt is calculated directly from the energy excess via Eq. 6.9.

If Q_{net} is negative, then insufficient energy was provided to the surface layer to maintain it at 0°C. Liquid water may refreeze and the final temperature must be solved by iteration until the energy balance is satisfied.

6.2. Atmospheric stability

The calculation of turbulent energy exchange (Eq. 6.4, 6.5) is complicated by the stability of the atmospheric boundary layer. During snowmelt, the atmosphere immediately above the snow surface is typically warmer than the snow surface. As parcels of cooler air near the snow surface are transported upward by turbulent eddies they tend to sink back toward the surface and turbulent exchange is suppressed. In the presence of a snow cover, aerodynamic resistance is typically corrected for atmospheric stability according to the bulk Richardson's number (Ri_b). The Richardson's number is a dimensionless ratio relating the buoyant and mechanical forces (i.e. turbulent eddies) acting on a parcel of air (see e.g. Anderson 1976)

$$Ri_b = \frac{g z_a (T_a - T_s)}{\frac{(T_a + T_s)}{2} U(z_a)^2} \tag{6.11}$$

with the correction for stable conditions given as

$$r_{as} = \frac{r_{as}}{(1 - \frac{Ri_b}{Ri_{cr}})^2} \qquad 0 \le Ri_b < Ri_{cr} \tag{6.12}$$

and in unstable conditions as

$$r_{as} = \frac{r_{as}}{(1 - 16 Ri_b)^{0.5}} \qquad Ri_b < 0 \tag{6.13}$$

where Ri_{cr} is the critical value of the Richardson's number (commonly taken as 0.2). While the bulk Richardson's number correction has the advantage of being straightforward to calculate based on observations at only one level above the snow surface, previous investigators have noted that its use results in no turbulent exchange under common melt conditions and leads to an

underestimation of the latent and sensible heat fluxes to the snowpack (e.g. Jordan 1991, Tarboton et al. 1995).

An alternative formulation for the stability correction (adopted by Marks et al. 1998) is based on flux-profile relationships in which the vertical near-surface profiles of wind and potential temperature are assumed to be log-linear under stable conditions (see e.g. Webb 1970). In this case, the effect of atmospheric stability is described by the Monin-Obukhov mixing length (L):

$$L = \frac{u_*^3 \rho}{kg\left[\frac{H}{T_a c_p}\right]} \tag{6.14}$$

The friction velocity (u_*) and the sensible heat flux (H) are given by:

$$u_* = \frac{u_a k}{\ln(\frac{z_a}{z_0}) - \Psi(\frac{z_a}{L})} \tag{6.15}$$

$$H = \frac{(T_a - T_s) k u_* \rho c_p}{\ln(\frac{z_a}{z_0}) - \Psi(\frac{z_a}{L})} \tag{6.16}$$

The Ψ functions are given for stable conditions ($z_a/L > 0$) as

$$\Psi(\frac{z_a}{L}) = -5\frac{z_a}{L} \qquad 0 \le \frac{z_a}{L} \le 1 \tag{6.17}$$

$$\Psi(\frac{z_a}{L}) = -5 \qquad \frac{z_a}{L} > 1 \tag{6.18}$$

The stability correction of Eqs 6.14 - 6.18 does not force the sensible heat flux to zero. A lower limit on the Ψ function is imposed by Eq 6.18. Unfortunately, solution of these equations requires an iterative procedure which is computationally too burdensome for a spatially distributed model which may run over several hundred thousand pixels.

Therefore, a Ri_b formulation that does not entirely suppress turbulent exchange under stable conditions was developed. Similar to the restriction on Ψ in Eq. 6.18, an upper limit can be placed on Ri_b at the value of Ri_b at which z/L is equal to unity.

Combining Eqs 6.14 to 6.16 into one expression for L yields the following expression for the bulk Richardson's number when z/L is equal to 1.

$$Ri_u = \frac{1}{(\ln \frac{z_a}{z_0} + 5)} \tag{6.19}$$

where Ri_u is the upper limit on Ri_b.

Thus the stability correction with the bulk Richardson number becomes

$$r_{as} = \frac{1}{(1 - \frac{Ri_b}{Ri_{cr}})^2} r_a \qquad 0 \le Ri_b \le Ri_u \tag{6.20}$$

$$r_{as} = \frac{1}{(1 - \frac{Ri_u}{Ri_{cr}})^2} r_a \qquad Ri_b > Ri_u \tag{6.21}$$

A comparison of the formulation in Eq's 6.20 and 6.21 to the z/L formulation is shown in Figure 6.2. Over a snow surface with a roughness of 1 mm, turbulent exchange is not incrementally damped for $Ri_b > 0.08$. At a surface roughness of 1cm, Ri_u is 0.1. Experimental evidence for such a restriction is prevalent in the literature. In a review of experimental flux data, Webb (1970) suggested an upper value for the gradient Richardson's number (which differs slightly from Ri_b) of 0.17. Observations of sensible heat flux over snow under stable conditions by Ishikawa and Kodama (1994) suggest a steady decrease in the sensible heat flux to a bulk Richardson's number of 0.1 with little decrease (albeit high variability) from 0.1 to 1.0. Yague and Cano (1994) observed that the bulk transfer coefficient under stable conditions over the Antarctic ice sheet decreases rapidly from a gradient Richardson's number of 0 to 0.1 with no significant decrease thereafter. The Ri_b formulation is tested against three seasons of weighing lysimeter data in Section 6.5 (See Figures 6.8 and 6.9).

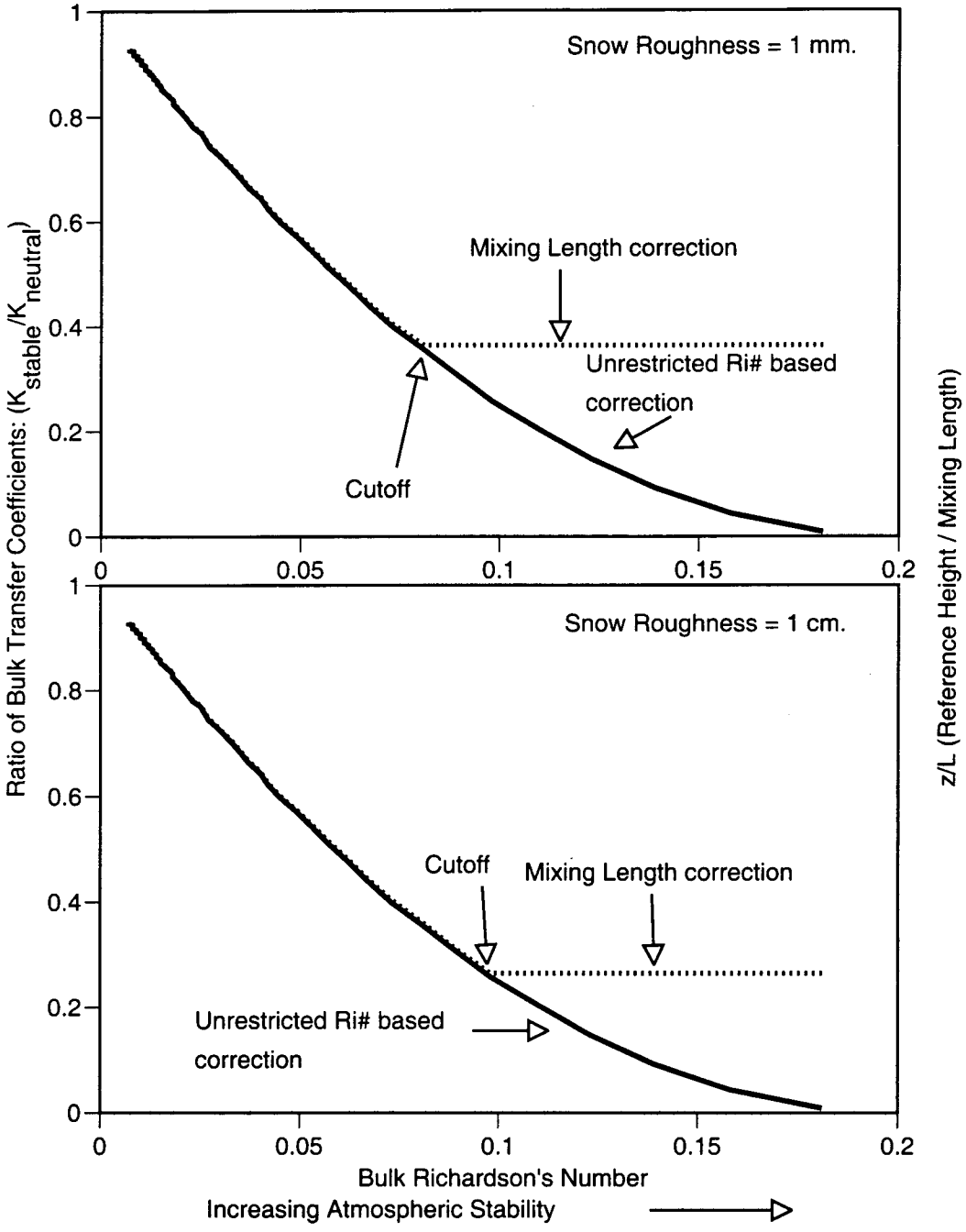

Figure 6.2. Comparison of the ratio of the stable to neutral bulk transfer coefficients (inverse of aerodynamic resistance) for the unrestricted Richardson's number formulation (heavy line) and a mixing length formulation (dotted line) for two values of snow surface roughness. As atmospheric stability increases, the restricted Richardson's number formulation follows the unrestricted formulation, until the cutoff, after which the ratio remains constant.

6.3. Snow interception model

Except for the stability formulation, the snowpack accumulation and melt model presented in Section 6.2 is similar to many previously developed models (e.g. Anderson 1976, Marks and Dozier 1992, Wigmosta et al. 1994, Tarboton et al. 1995). Prediction of snow accumulation and melt under a forest canopy is more complicated. While many of the models referenced above characterize the effect of the forest canopy on the micrometeorology above the forest snowpack, none attempt to model explicitly the combined canopy processes that govern snow interception, sublimation, mass release, and melt from the forest canopy. A simple snow interception algorithm is presented here that represents canopy interception, snowmelt, and mass release at the high spatial resolutions of distributed hydrology models.

6.3.1. Snow interception

During each time step, snowfall is intercepted by the overstory up to the maximum interception storage capacity according to

$$I = f\, P_s \tag{6.22}$$

where I is the water equivalent of snow intercepted during a time step, P_s is snowfall over the time step and f is the efficiency of snow interception (60 percent in Figure 5.4 and 5.5a). The maximum interception capacity (B) is given by

$$B = L_r(m * LAI) \tag{6.23}$$

where LAI is the single-sided leaf area index of the canopy and m is determined based on observations of maximum snow interception capacity (40 mm in Figure 5.4). The leaf area ratio (L_r) is a step function of temperature:

$$L_r = 0.004 \qquad T_a > -5^0 C \tag{6.24}$$

$$L_r = 0.001 \qquad T_a \leq -5^0 C \tag{6.25}$$

This step function is based on observations from previous studies of intercepted snow as well as data collected during the field campaign. Kobayashi (1987) observed that maximum snow

interception loads on narrow interception surfaces decreased rapidly as air temperature decreases below -3°C. Results from the field campaign presented in Chapter 5 suggest that intercepted load on the wide interception surfaces of conifer canopies is unaffected by decreases in air temperature to -5°C.

Newly intercepted rain is calculated with respect to the water holding capacity of the intercepted snow (W_c), which is given by the sum of the capacity of the snow and the bare branches:

$$W_c = hW_{ice} + 1e^{-4}(LAI_2) \tag{6.26}$$

where h is the water holding capacity of snow (taken as approximately 3.5 percent) and LAI_2 is the all sided leaf area index of the canopy. Excess rain becomes throughfall.

6.3.2. Removal of intercepted snow from the canopy

The intercepted snowpack can contain both ice and liquid water. The mass balance for each phase is:

$$\Delta W_{ice} = I - M + \left[\frac{Q_e}{\rho_w \lambda_s} + \frac{Q_m}{\rho_w \lambda_f}\right]\Delta t \tag{6.27}$$

$$\Delta W_{liq} = P_r + \left[\frac{Q_e}{\rho_w \lambda_v} - \frac{Q_m}{\rho_w \lambda_f}\right]\Delta t \tag{6.28}$$

where M is snow mass release from the canopy, and λ_s, λ_v, λ_f are the latent heat of sublimation, vaporization and fusion, respectively. Snowmelt is calculated directly from a modified energy balance, similar to that applied for the ground snowpack, in which

$$T_s = \min(T_a, 0) \tag{6.29}$$

Testing of a fully iterative (on T_s) intercepted snow energy balance revealed that the intercepted snow temperature closely followed that predicted by Eq 6.29.

Given the intercepted snow temperature and air temperature, snowmelt is calculated directly from Eqs 6.8 and 6.9. The individual terms of the energy balance are as described for the ground snowpack model. However, the aerodynamic resistance is calculated with respect to the

sum of the displacement and roughness heights of the canopy. Incoming shortwave radiation and longwave radiation are taken as their values at the canopy reference height (see Appendix A).

Snowmelt in excess of the liquid water holding capacity of the snow results in meltwater drip (D). Mass release of snow from the canopy occurs if sufficient snow is available and is related linearly to the production of meltwater drip:

$$M = 0 \qquad C \leq n \tag{6.30}$$

$$M = 0.4D \qquad C > n \tag{6.31}$$

where n is the residual intercepted snow that can only be melted (or sublimated) off the canopy (taken as 5 mm based on observations of residual intercepted load). The ratio of 0.4 in Eq. 6.31 is derived from observations of the ratio of mass release to meltwater drip as discussed in Section 5.6.

6.4. Model calibration and testing

6.4.1. Meteorological data

Hourly micro-meteorological observations from the shelterwood site were used to force the model during the calibration and testing periods. Observations of air temperature, humidity, precipitation, and incoming short- and long-wave radiation from the shelterwood were taken to be good approximations of above-canopy conditions. Wind speed at the 2-m (above soil) measurement height in the shelterwood was corrected for snow accumulation beneath the anemometer and then scaled to the 80-m height assuming a logarithmic profile and a surface roughness of 1 cm.

Below-canopy shortwave radiation was taken as 16% of the shelterwood value based on observations (Figure 6.3 d). Below-canopy windspeed was adjusted to match observations (i.e. 50% of shelterwood value, Figure 6.3 e). Below canopy longwave radiation (L_c) was calculated via:

$$L_c = (1 - F)L_o + (F) * \sigma(T_a)^4 \tag{6.32}$$

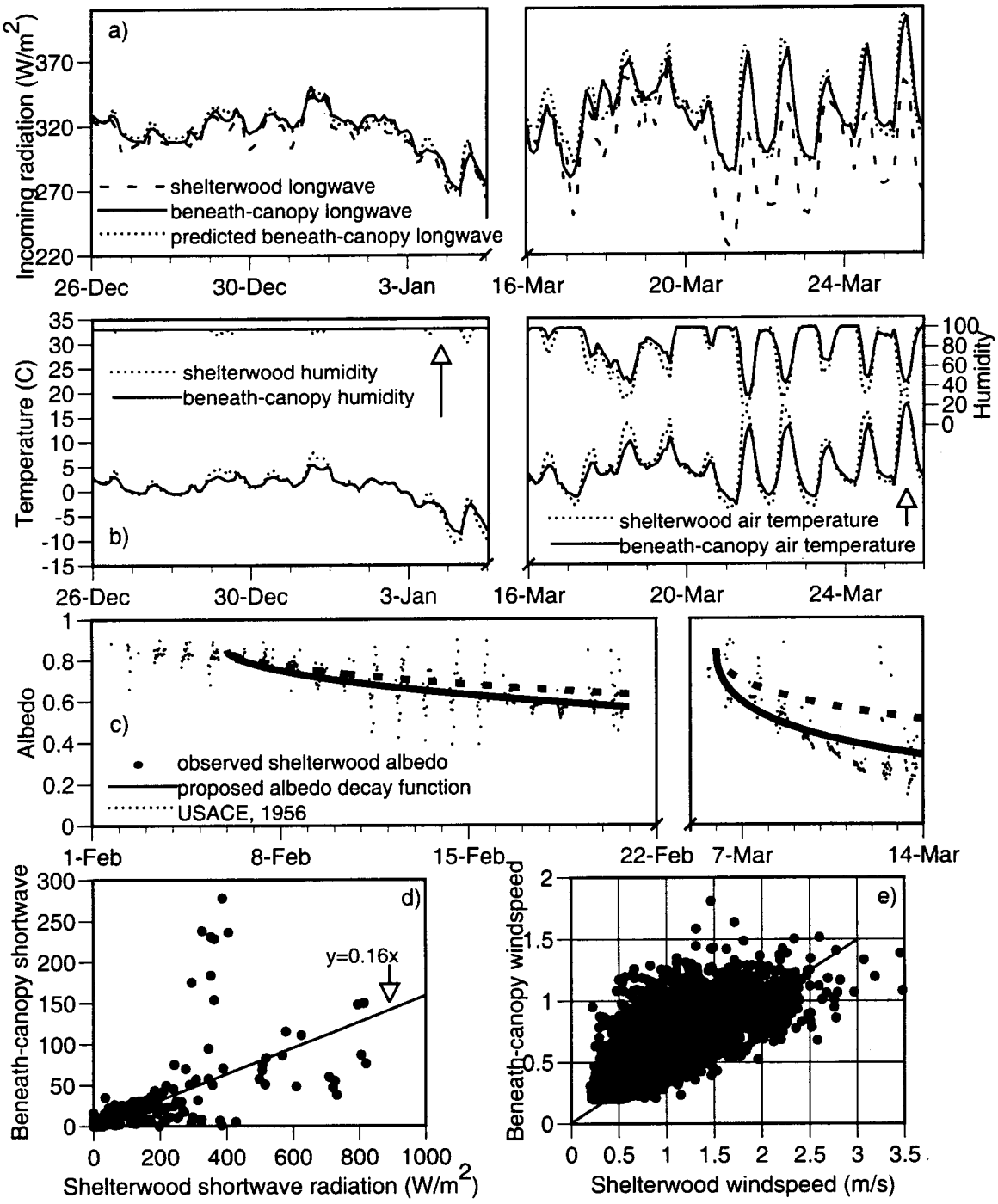

Figure 6.3. Observed beneath-canopy and shelterwood meteorology for a major ROS event (26 Dec 1996 to 5 Jan 1997) and a spring melt event (16 Mar to 26 Mar, 1996) a) observed longwave radiation at both sites vs. predicted beneath-canopy, b) observed air temperature and relative humidity at both sites, c) observed decay of snow albedo with age during two periods with no snowfall, d) hourly observed shelterwood and beneath canopy shortwave radiation (same period as a) and b)), and e) hourly observed shelterwood and beneath canopy windspeed (1997/98 season)

where L_o is above canopy longwave. The effective fractional canopy coverage (F) was determined as 80 percent by calibrating Eq 6.32 to observed longwave radiation beneath the forest canopy (Figure 6.3.a). Air temperature and humidity were assumed identical at the shelterwood and below-canopy sites. A comparison of the observed and predicted below-canopy meteorological data is shown in Figure 6.3 for a rain-on-snow and radiation-dominated event.

Snow albedo was assumed to decay with age. Based on observations in the shelterwood site (see Figure 6.3c):

$$\alpha_a = 0.85(\lambda_a)^{t^{0.58}} \tag{6.33}$$

$$\alpha_m = 0.85(\lambda_m)^{t^{0.46}} \tag{6.34}$$

where α_a and α_m are the albedo during the accumulation and melt seasons, t is the time in days since the last snow, λ_a is 0.92, and λ_m is 0.7. Accumulation and melt seasons are defined based on the absence and presence of liquid water in the snow surface layer, respectively. These simple exponential decay functions were chosen over more complex formulations that calculate snow albedo based on snow microphysics and metamorphosis because of the importance of litter (needles and moss) accumulation on the snow surface and the computational simplicity of Eq's 6.33 to 6.34.

Identical transformations of the observed shelterwood micrometeorology were used for the 1997/98 test period. Immediately before the 1998/99 season, most of the forest canopy to the southwest of the beneath-canopy weighing lysimeters was harvested. Observations of below-canopy windspeed showed an overall increase to approximately 60% of the shelterwood value.

Data logger failure during the 1998/99 season resulted in the loss of most of the shelterwood short- and long-wave radiation data and all precipitation data. Missing shortwave radiation data were filled in directly with hourly observations of global (direct and diffuse) shortwave radiation from Eugene, OR. Missing longwave radiation data were estimated from the observed air temperature and relative humidity according to Van Heesjwick et al. (1996). Hourly precipitation was estimated from daily totals observed at the nearby Lemolo Lake National

Weather Service Cooperative site (located approximately 10 km east of the field site at an elevation of 1500 m). Daily values of precipitation were disaggregated based on hourly observations at the Toketee Falls, OR Remote Automatic Weather Station (RAWS) (located approximately 15 km west of the field site at an elevation of 600 m). Based on the 1996/97 and 1997/98 data, precipitation in the shelterwood site is approximately 80 percent of that observed at Lemolo Lake.

6.4.2. Calibration (1996/97)

The model was calibrated using the shelterwood and beneath-canopy weighing lysimeter data for the 1996/97 snow year (Figure 6.4). The model was calibrated first against the shelterwood data. The values for T_{min} and T_{max} (minimum air temperature for rain and maximum air temperature for snow) were adjusted to match the observed snow accumulation in the shelterwood during the periods from 1-Dec 1996 to 25-Dec 1996 and from 25-Feb 1997 to 5-Mar 1997. Snow surface roughness was adjusted to match the observed snow ablation during the ROS event of 1-Jan 1997.

Calibration using the beneath-canopy data applied the same values for T_{min} and T_{max} as the shelterwood site. The value of m, which controls the maximum snow interception capacity, was estimated as 1.0 based on a single sided LAI of 10 and an inferred maximum interception capacity of 40 mm SWE (from Figure 5.4). Good agreement with observed beneath-canopy snow accumulation was obtained during the initial snowfall events (1-Dec 1996 to 1-Jan 1997). During the secondary snow accumulation event (just after 1-Mar 1997), snow accumulation beneath the forest canopy is underestimated. Figure 6.4b reveals that predicted snow interception reached its upper limit during this event. The beneath-canopy snow surface roughness was adjusted to match the observed ablation during the 1-Jan 1997 ROS event. Table 1 lists the final parameter values obtained during calibration.

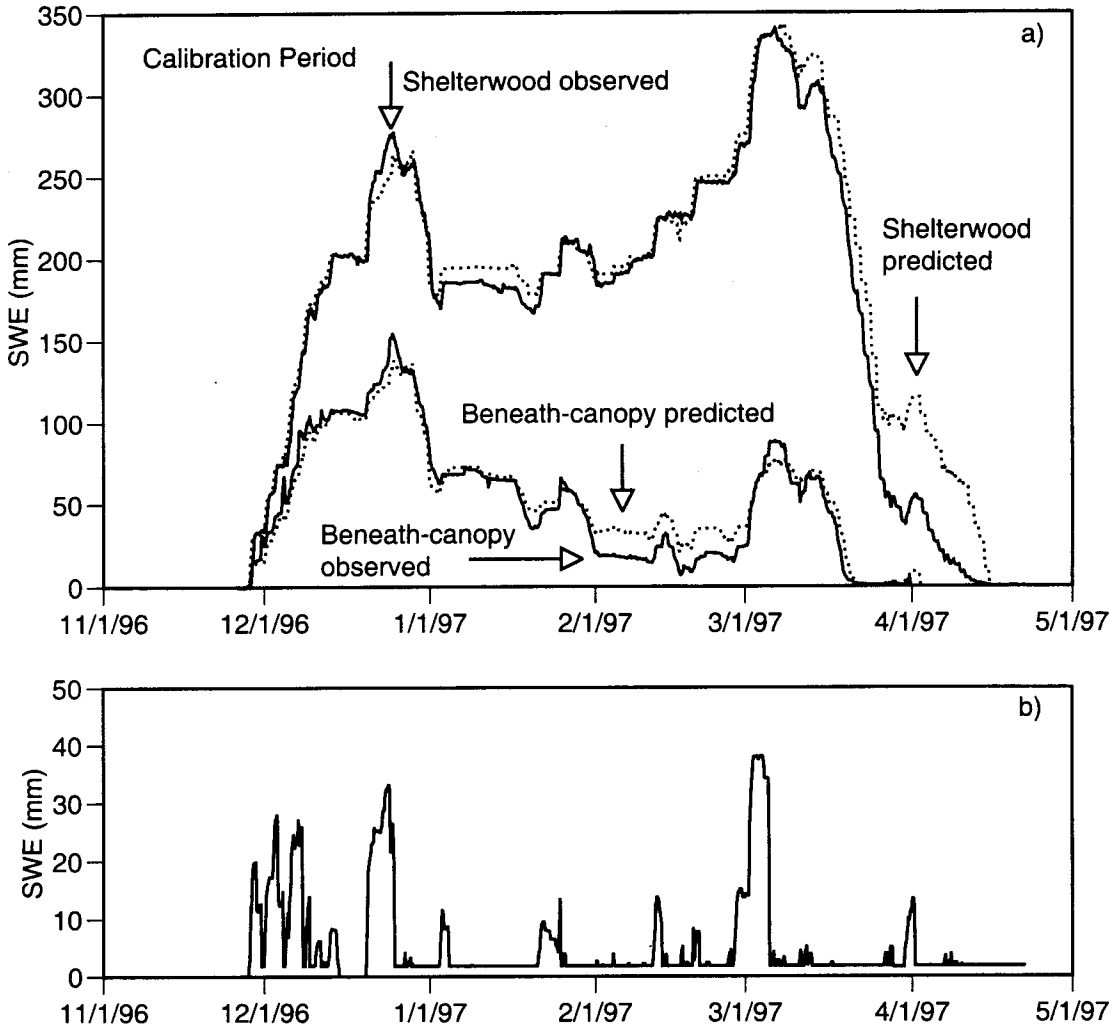

Figure 6.4. a) Results of full canopy snow model calibration to 1996/97 weighing lysimeter data, b) Predicted intercepted snow water equivalent. Final model parameters are given in Table 6.1.

Table 6.1. Parameter values from snow model calibration using 1996/97 data.

Site	Parameter	Value
Shelterwood	T_{min} (for rain)	0.4 °C
Shelterwood	T_{max} (for snow)	0.5 °C
Shelterwood	z_0	0.007 (m)
Beneath-canopy	$m*LAI$	10
Beneath-canopy	z_0	0.20 (m)

6.4.3. Testing (1997/98)

The results of model testing using the 1997/98 shelterwood and beneath-canopy weighing lysimeter data are shown in Figure 6.5. Given the same rain-snow threshold temperatures and snow surface roughness used in the calibration period, SWE was well predicted at the shelterwood site, especially during the initial accumulation phase. Late season SWE was overestimated due to an underestimation of melt from 1-Feb 1998 to 20-Feb 1998 during mid-winter radiation dominated events.

Beneath-canopy SWE accumulation and melt were well predicted during the entire 1997/98 season. This result is encouraging considering the differences in snow accumulation between the 1997/98 and calibration seasons. While maximum beneath canopy snow accumulations during calibration exceeded 150 mm, maximum observed accumulations of SWE during the 1997/98 season were less than 50 mm. Predicted intercepted loads remained below 20 mm of SWE during the 1997/98 season; considerably less than during the calibration season. The predicted differences in intercepted loads between seasons follows the observations of intercepted load on the cut-tree experiments (See Figure 5.1 and Figure 5.2). Observed intercepted loads exceeded 30 mm SWE during the calibration season. During the 1997/98 season, observed intercepted loads remained below 15 mm SWE.

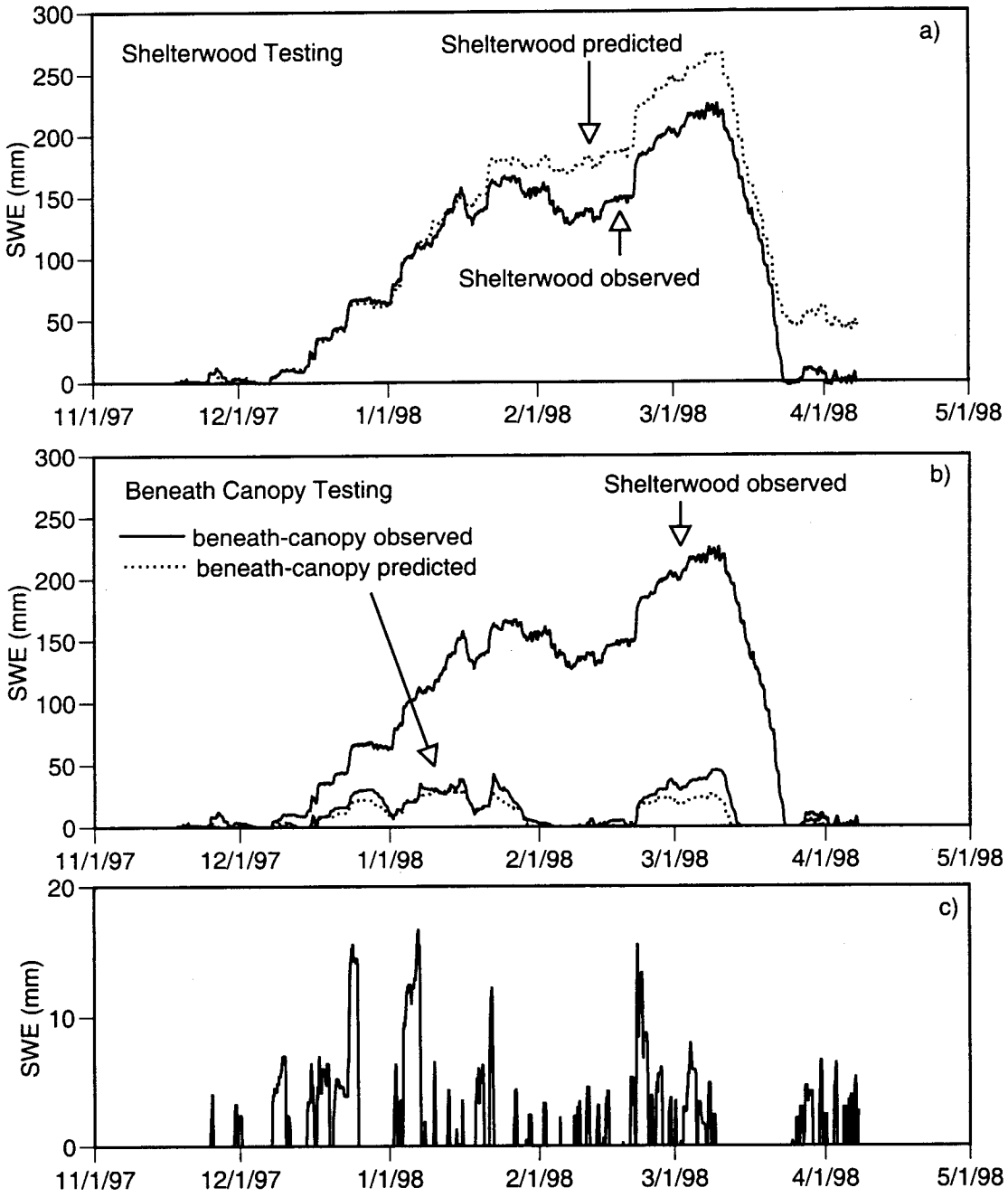

Figure 6.5. Testing using 1997/98 data: a) shelterwood, b) beneath-canopy data, c) predicted intercepted snow water equivalent.

6.4.4. Testing (1998/99)

The testing of the canopy-snow model using the observed data from the winter of 1998/1999 is shown in Figure 6.6. This winter season was characterized by record breaking snowfall totals over the Washington and Oregon Cascades. Maximum snow accumulation observed at the shelterwood site approached 700 mm of water equivalent (approximately double that observed during the 1996/97 season). Unfortunately, much of the meteorological data required for forcing the canopy snow model were lost due to a combination of heavy snow accumulation and data logger failure. Observations of temperature, humidity and wind speed were available at all or some of the field sites throughout the winter. Observations of incoming shortwave and longwave radiation were mostly absent and all precipitation data were lost. The missing data were estimated as described above.

Figure 6.6a shows the results of model testing against the 1998/99 weighing lysimeter data from the shelterwood site. Overall snow accumulation was well predicted as was the snowmelt during the spring melt season (15-Apr 1999 to 25-May 1999). This result is noteworthy because the spring melt period during model calibration was completed before the 1998/99 spring melt period began. During all seasons, the energy balance formulation of the ground snowpack combined with the simple exponential albedo decay formulation yielded close agreement with observations.

The 1998/99 season was also characterized by significant snow accumulation beneath the forest canopy (approaching the maximum observed snow accumulation at the shelterwood site during model calibration). Overall snow accumulation and ablation were well predicted through 15-Feb 1999. Observed snow accumulation immediately after 15-Feb 1999 was underestimated due largely to an underestimation of shelterwood snowfall during the same period. The melt event in the later part of March 1999 was underestimated while the final melt of the beneath-canopy snowpack was well predicted. Unfortunately, all beneath-canopy observations of meteorology are missing during the March 1999 melt event.

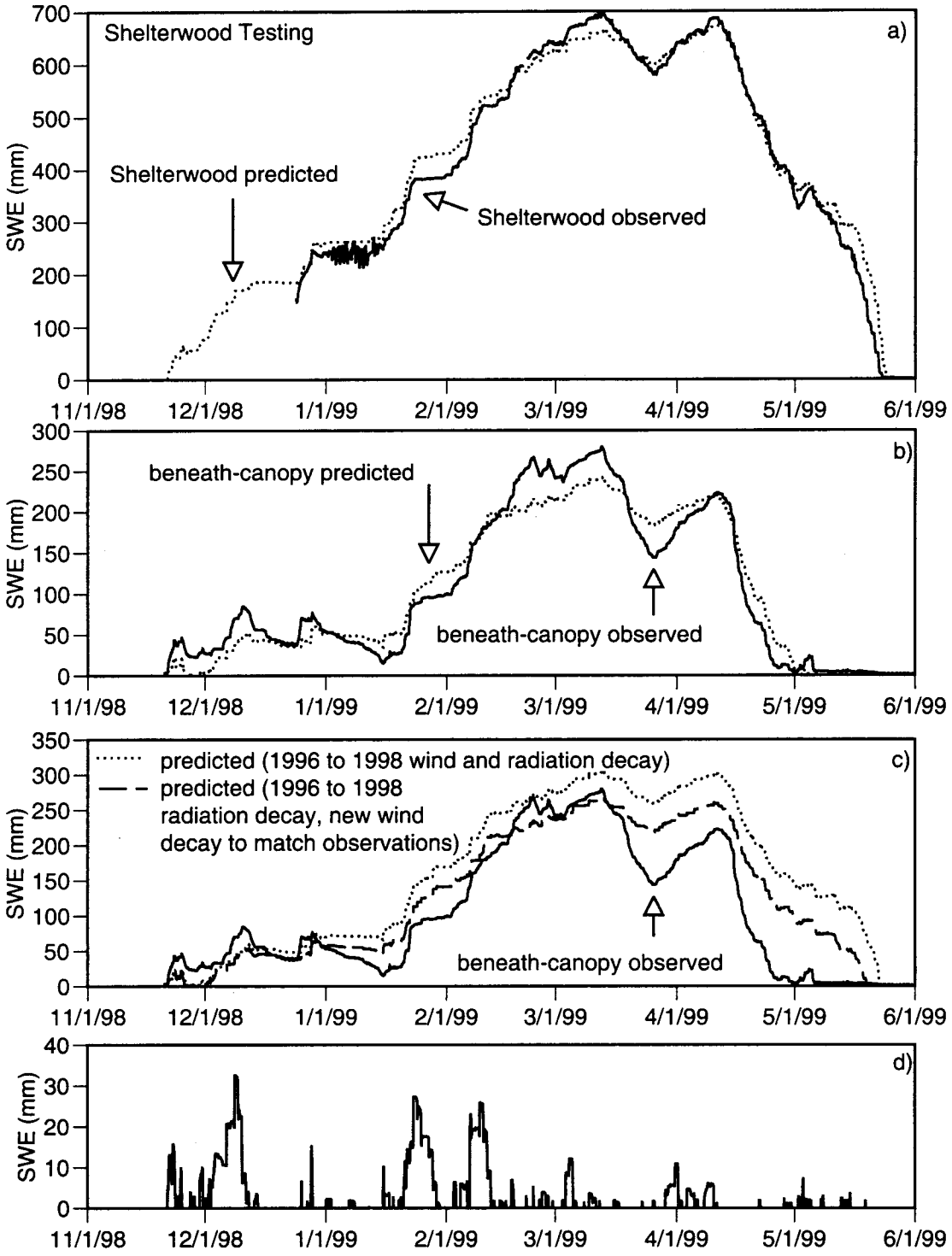

Figure 6.6. Testing using 1998/99 data: a) shelterwood, b) beneath-canopy (with new wind and radiation decay parameters), c) beneath canopy data (with previous season's wind and radiation decay parameters), and d) predicted intercepted snow water equivalent.

Figure 6.6c shows the below canopy testing for the 1998/99 season with the same wind speed and radiation exponential decay coefficients applied during model calibration and the1997/98 testing season (dotted line) as compared to observations (solid line). Use of the previous season's decay coefficients resulted in considerable over-prediction of beneath-canopy SWE as well as underestimation of spring melt rate. As was noted above, immediately before the 1998/99 season, a large fraction of the forest canopy was harvested to the south-east of the beneath-canopy weighing lysimeters. This harvest resulted in an observed increase of average windspeed from 50 to 60 percent of the shelterwood wind speed. Incorporating this increase into the model parameters (dashed line) resulted in closer agreement with observations, however, the spring melt rate was still underestimated. Re-calibration of the exponential decay coefficient governing the transmission of shortwave radiation through the canopy was necessary to match the observed final spring melt rate (dashed line in Figure 6.6b). This re-calibration resulted in an increase in shortwave radiation transmission from 16 to 25 percent of the shelterwood value. Direct observations of the increase in radiation are not available. However, due to the extent and proximity of canopy removal to the beneath-canopy weighing lysimeters, this increase is justified. These results underscore the importance of characterizing correctly the transfer of wind and radiation through the forest canopy and suggest that edge effects (from nearby forest harvest) can alter the dynamics of snowmelt beneath the canopy. While no data were collected during this field campaign on the extent of edge influence on snowmelt, Chen (1991) found that the distance of edge influence is between 30 to 90 m for solar radiation and greater than 240 m for wind.

6.5. Sensitivity analysis

This section presents a sensitivity analysis of the major parameters of the canopy-snow model as well as its albedo and atmospheric stability formulations. The parameters and formulations pertaining to the ground snowpack model are presented first followed by an analysis of the snow interception model parameters. The sensitivity of each parameter is shown over all three seasons for each analysis.

6.5.1. Albedo formulation.

The effect of the albedo formulation on the predictions of ground SWE for both the shelterwood and beneath-canopy sites is shown in Figure 6.7 for all three seasons. Model predictions from the albedo decay formulation, given in Eq's 6.33 and 6.34, are shown compared to an alternative formulation based on the data of the USACE (1956).

The formulation based on local measurements of albedo results in better predictions of late season melt rate than the formulation based on the measurements of USACE (1956). Predictions of maximum snow accumulation in the shelterwood site are less sensitive to the albedo formulation. The sensitivity of late season melt predictions to the albedo formulation is considerably less beneath the forest canopy, where the exchange of shortwave radiation with the snow surface is not as important in the overall energy balance as in the shelterwood site.

6.5.2. Atmospheric stability formulation

The effect of the atmospheric stability formulation on predictions of beneath-canopy SWE is shown in Figure 6.8 for all three seasons. Each panel shows three stability formulations: the restricted Richardson's number formulation (Ri_b), an unrestricted Richardson's number formulation, and no stability correction. Because the importance of the stability formulation increases as wind speed decreases (i.e. as conditions become more stable), comparisons between formulations are shown only for the predictions of beneath-canopy SWE. All predictions in Figure 6.8 are based on a below-canopy snow surface roughness of 20 cm.

The overall effect of the stability formulation is dramatic and underscores the importance for correct representation of the turbulent heat fluxes in the transient snow zone of maritime climates. Large over-predictions of below canopy SWE are expected if the stability correction is allowed to suppress turbulent heat exchange completely (shown as the unrestricted case in Figure 6.8). Dramatic over-predictions of snowmelt are seen for all seasons if the effect of atmospheric stability is ignored.

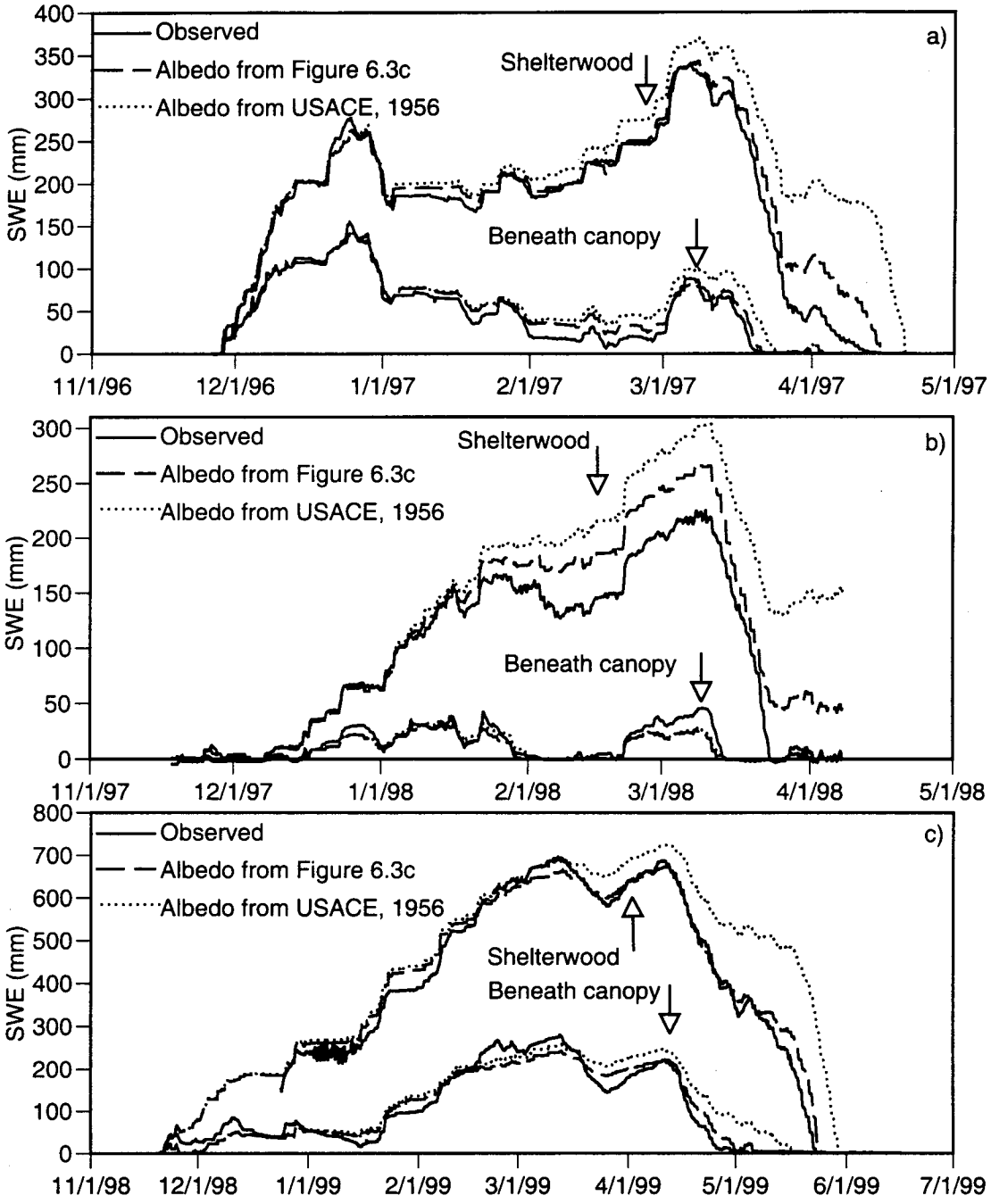

Figure 6.7. Effect of snow surface albedo formulation on model predictions as compared against observations for three seasons of weighing lysimeter data: a) 1996/97, b) 1997/98 and c) 1998/99.

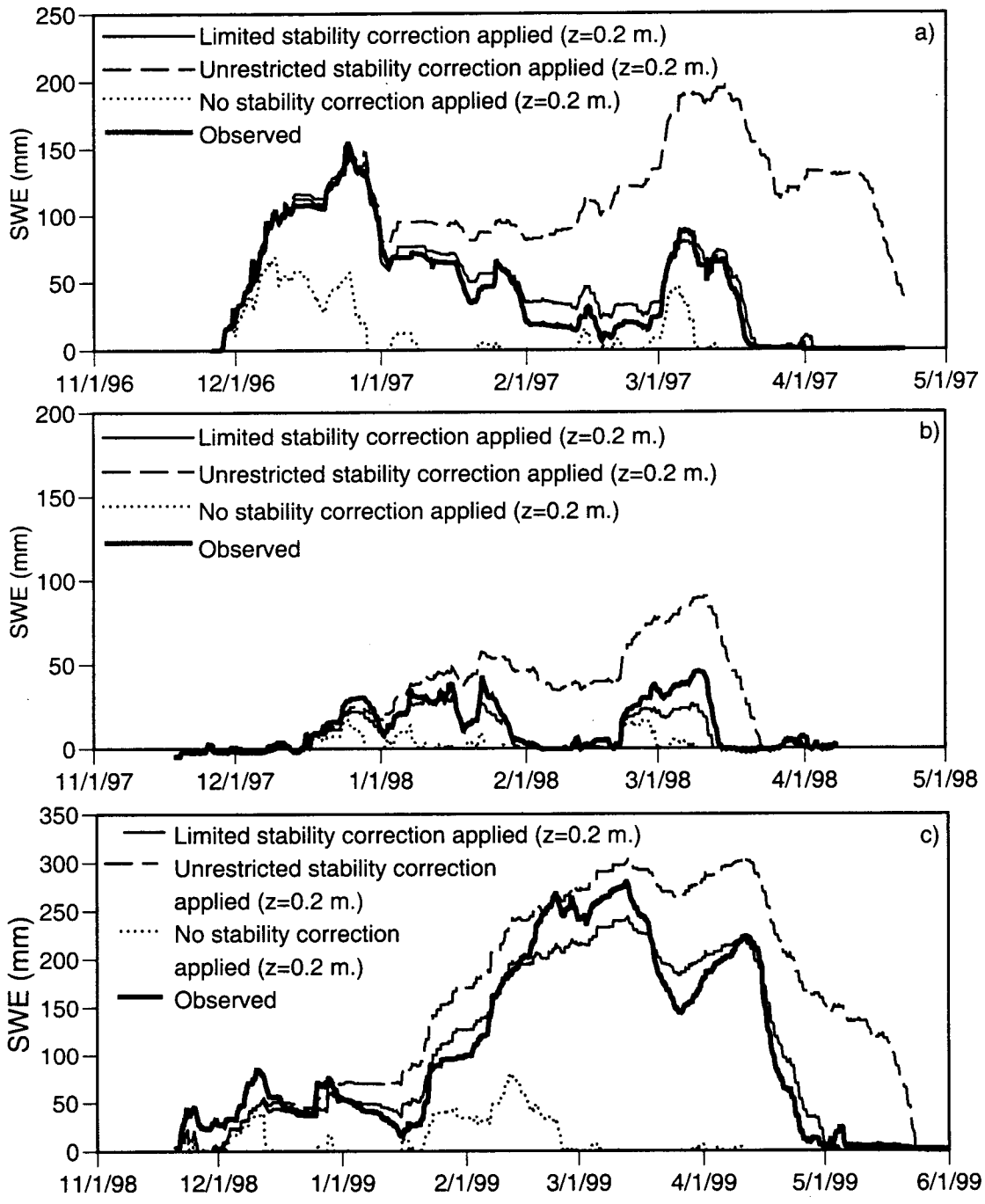

Figure 6.8. Effect of atmospheric stability formulation on model predictions for three seasons of beneath-canopy weighing lysimeter data: a) 1996/97, b) 1997/98 and c) 1998/99.

Because an unrestricted stability correction and a surface roughness of 20 cm results in insufficient melt, an attempt was made to recalibrate the snow surface roughness for the unrestricted formulation (Figure 6.9a). As snow surface roughness is increased from 20 cm to 40 cm, the model overestimates snowmelt during the New Year's ROS event. However, it underestimates subsequent melt events (most notably on Feb. 1 and Feb. 15). Increasing snow surface roughness further results in unacceptable over-prediction of melt during the New Year's ROS event.

A similar attempt to recalibrate the "no correction" model was also made (Figure 6.9b). With a snow surface roughness of 20 cm and no stability correction, melt was significantly overestimated. If the snow surface roughness was reduced to 5 mm, melt rates under the canopy were still overestimated. Further reduction of snow surface roughness beneath the canopy resulted in insufficient melt during the New Year's ROS event. Based on these results, the restricted Richardson's number formulation (Ri_b) is suggested for model application.

6.5.3. Snow surface layer thickness

The energy balance formulation for the ground snowpack divides the snowpack into two layers. The top surface layer exchanges energy with the atmosphere and the canopy. The bottom layer receives meltwater and excess cold content from the surface layer. Melt from the surface layer is transmitted to the pack layer only after the surface layer becomes isothermal at 0°C and the liquid water holding capacity of the surface layer is exceeded. Satisfying both of these conditions depends on the thickness of the surface layer. The cold content and liquid water holding capacity of a thin surface layer will be quickly satisfied during all melt events. A thick surface layer will delay melt and meltwater transfer to the pack layer.

The sensitivity of model predictions to the maximum thickness of the snow surface layer is shown in Figure 6.10. No sensitivity to this parameter is seen if the total thickness of the snowpack does not exceed the maximum thickness of the surface layer (e.g. beneath-canopy predictions of Figure 6.10b). The thickness of the surface layer does not affect predictions during

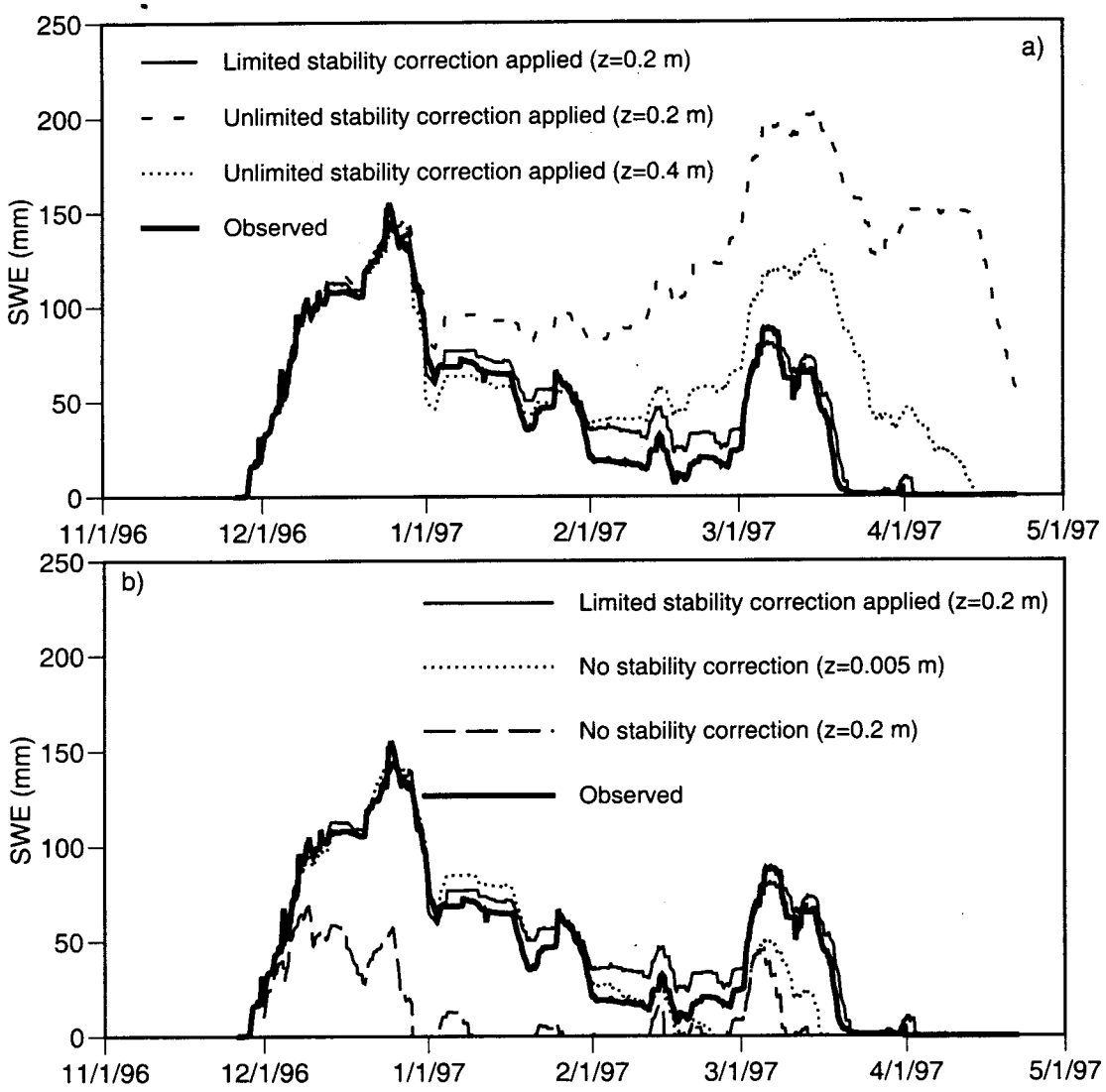

Figure 6.9. Combined sensitivity of atmospheric stability formulation and snow surface roughness on model predictions for three seasons of beneath canopy weighing lysimeter data. a) comparison of limited stability formulation to unlimited formulation with alternate roughness, and b) comparison of limited stability formulation to assumption of constant neutral stability with alternate roughness.

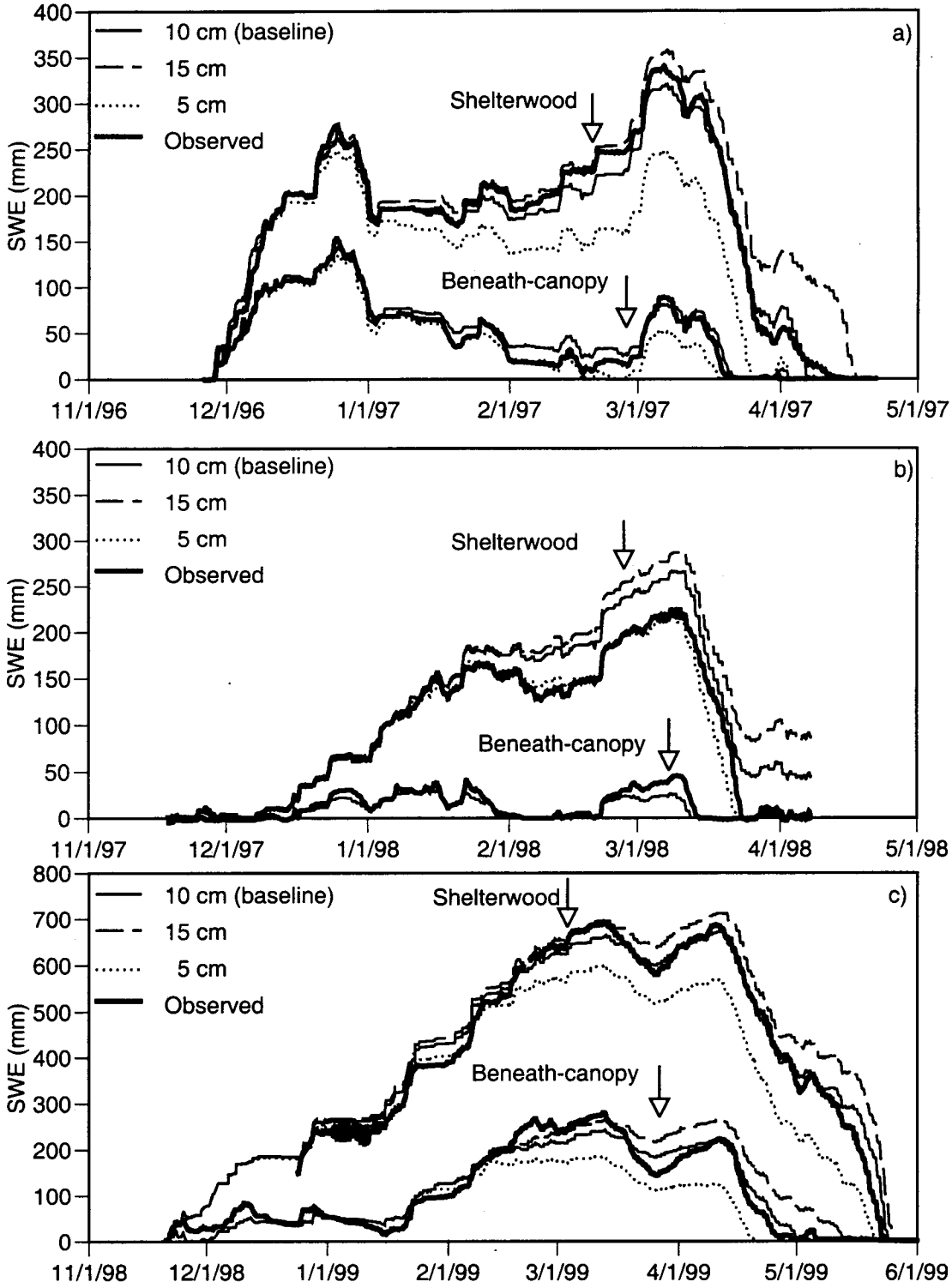

Figure 6.10. Effect of snow surface layer thickness on model predictions for three seasons of weighing lysimeter data: a) 1996/97, b) 1997/98 and c) 1998/99. Predictions for the shelterwood and beneath-canopy sites are shown for all seasons.

accumulation phases. A thinner surface layer can lead to overestimation of snowmelt during mid winter melt events. For example, during the period from 1-Feb 1997 to 1-Mar 1997, model predictions based on a surface thickness of 5 cm show almost no increase in SWE at the shelterwood site while observations show a continuous gain of SWE. A thinner surface layer also results in accelerated melt during spring melt events. An overall suppression of mid-winter and spring melt rates is seen when the model predictions based on a 15 cm surface layer are compared to those obtained with a 10 cm surface layer.

Based on a comparison of model predictions to observed spring snowmelt, a snow surface layer thickness of 10 cm was adopted as the baseline value. While it can be argued that uncertainty in the representation of turbulent heat fluxes (which control mid winter melt) can be offset by uncertainty in the surface layer thickness, the energy balance during spring melt is dominated by shortwave radiation and the snow surface albedo, both of which are directly measured. A surface layer thickness of between10 and 20 cm was suggested by Marks et al. (1998), based on observations of snowpack temperature profiles during spring melt in the Sierra Nevada. A surface layer thickness of 10 cm was used by van Heesjwick et al. (1998) for prediction of snowmelt in the Pacific Northwest.

6.5.4. Efficiency of snow interception

In the model presented here, snow interception efficiency (f) is a constant percentage of snowfall at all times until the maximum snow interception capacity is reached. After this point, snow interception no longer occurs. The sensitivity of model predictions to the efficiency of snow interception is shown in Figure 6.11. As f is decreased from the baseline value of 60 percent, total snow accumulation beneath the canopy increases dramatically. Exactly the opposite effect is seen as f is increased. Since the efficiency parameter directly controls the partitioning of snowfall into interception storage and throughfall, it is expected to be an extremely sensitive parameter. Fortunately, it is one of the parameters which is known with the most certainty in this application. Based on Figure 5.4, a value of 60 percent seems most appropriate for estimating interception

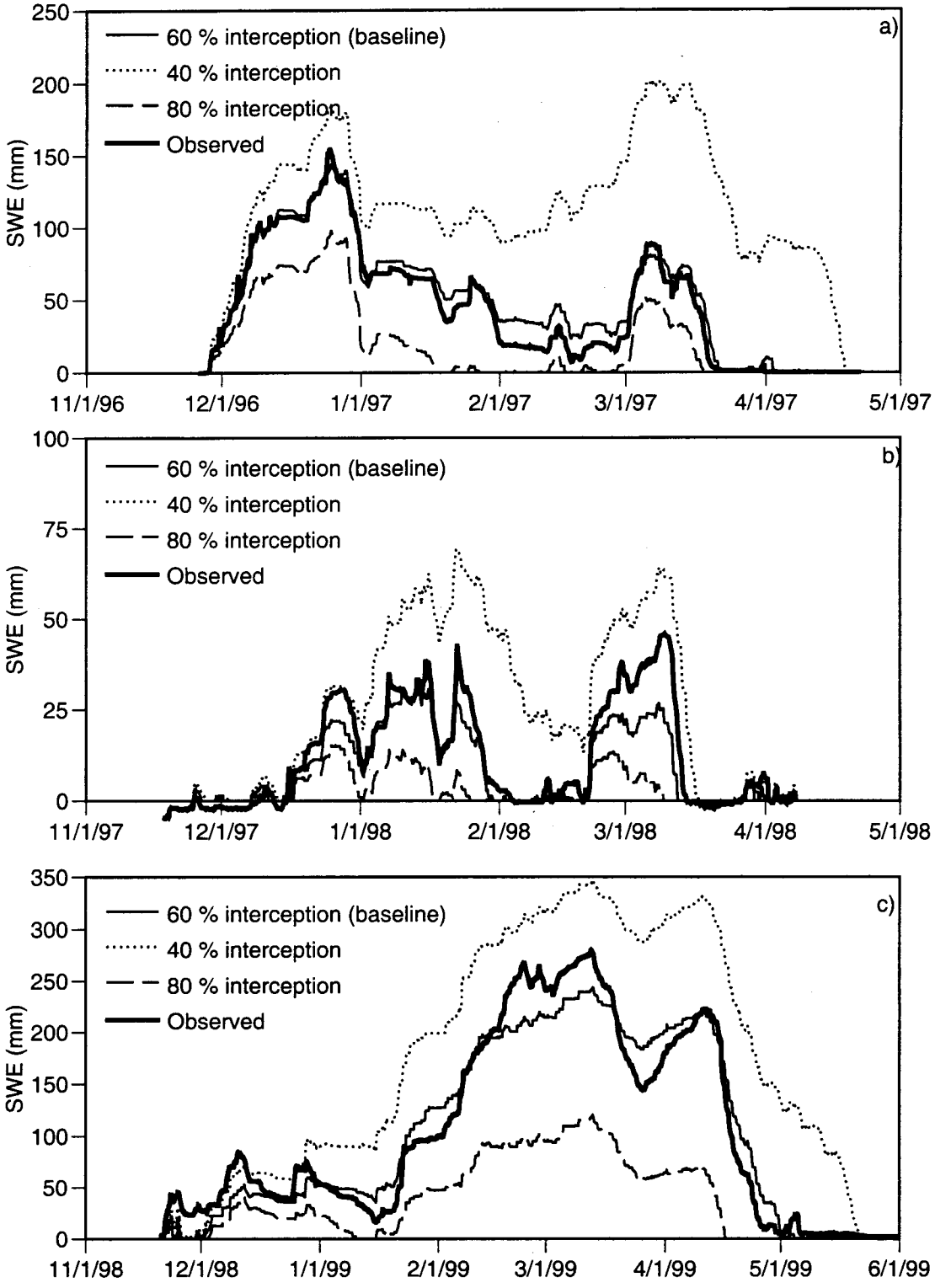

Figure 6.11. Effect of fractional snow interception parameter on model predictions over three seasons of beneath-canopy weighing lysimeter data. a) 1996/97, b) 1997/98, and c) 1998/99.

loads in a mature Douglas-Fir canopy. Given the similarity in growth forms observed by the cut-tree experiments for all the species studied (see Figure 5.6 and Table 5.1), the value of 60 percent is also recommended for those species.

6.5.5. Maximum snow interception capacity

Maximum snow interception capacity is the maximum load (expressed as mm of water equivalent) that the tree can intercept. The results from the cut-tree experiments suggest strongly that this capacity is greater than 30 mm and does not vary between the species studied here. An upper maximum load of 40 mm on the mature Douglas-Fir canopy is suggested by Figure 5.4a. The sensitivity of model predictions to the maximum snow interception capacity is shown in Figure 6.12. Model predictions are not sensitive to snow interception capacity above a value of 30 mm SWE. Below 30 mm SWE, model predictions are sensitive to the value chosen. These results are further explained by the predicted intercepted snow loads over each season shown on Figures 6.3 - 6.5. The maximum snow interception capacity (40 mm) was reached during only one event (1 Mar 1997). During the 1997/98 season, which has the least sensitivity to the maximum snow interception capacity, predicted intercepted snow load never exceeded 20 mm SWE.

6.5.6. Ratio of mass release to meltwater drip

The partitioning of intercepted snow into mass release and meltwater drip is controlled by a single parameter (M/D), which fixes the fraction of mass release that occurs relative to the amount of meltwater production. For model calibration and testing, a baseline value of 0.4 was adopted based on continuous observations from the weighing lysimeters over a period of several days (see section 5.6). This value implies that for every 10 mm of meltwater that drips from the forest canopy, 4 mm of mass release occurs. If meltwater drip is absent then mass release does not occur and the snow remains on the canopy where it can sublimate.

The sensitivity of model predictions to M/D is shown in Figure 6.13. Model predictions are largely insensitive to values of M/D ranging from 0.3 to 1.0 for the 1997/98 and 1998/99

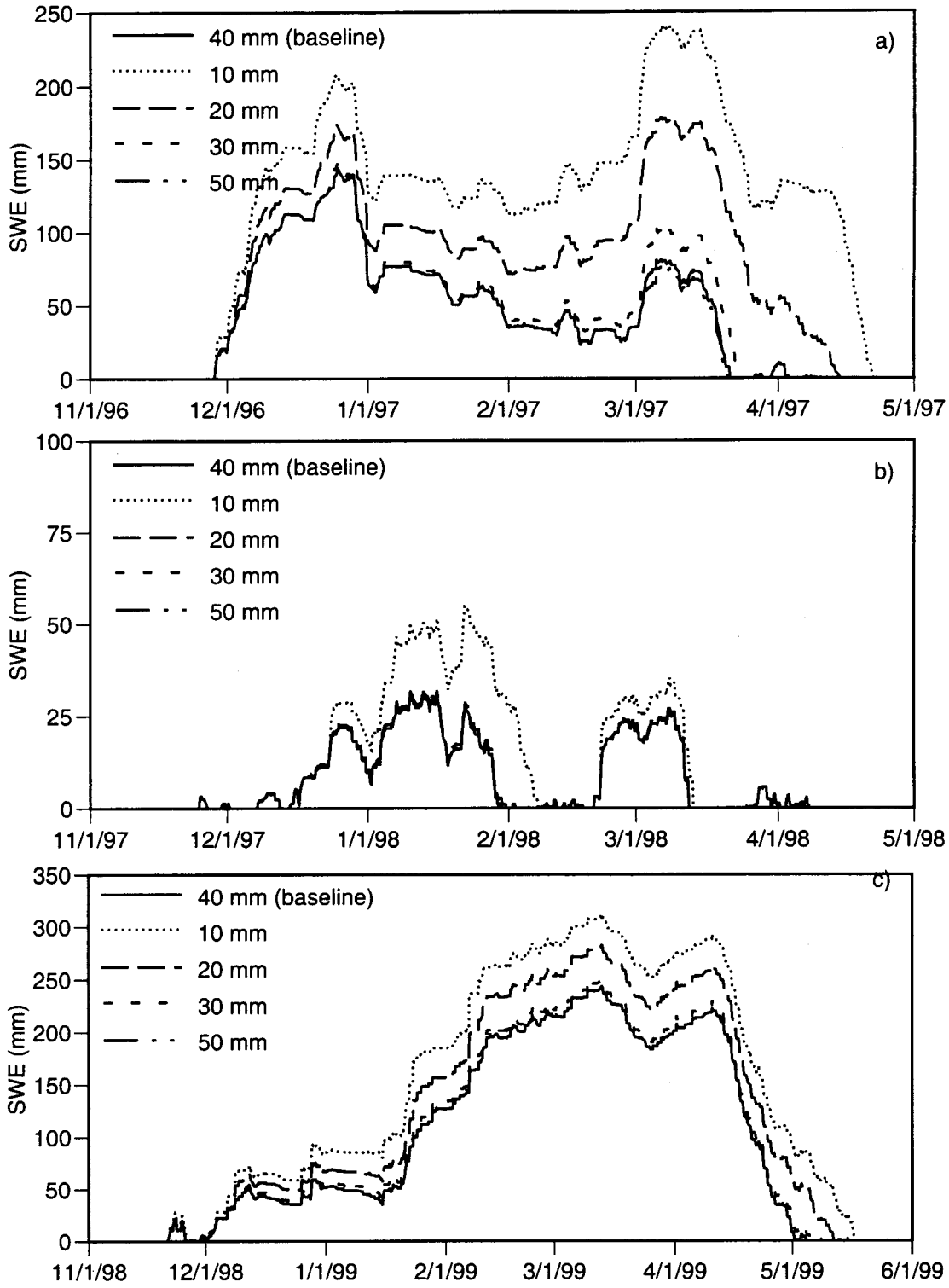

Figure 6.12. Effect of maximum snow interception capacity on model predictions over three seasons of beneath-canopy weighing lysimeter data. a) 1996/97, b) 1997/98, and c) 1998/99.

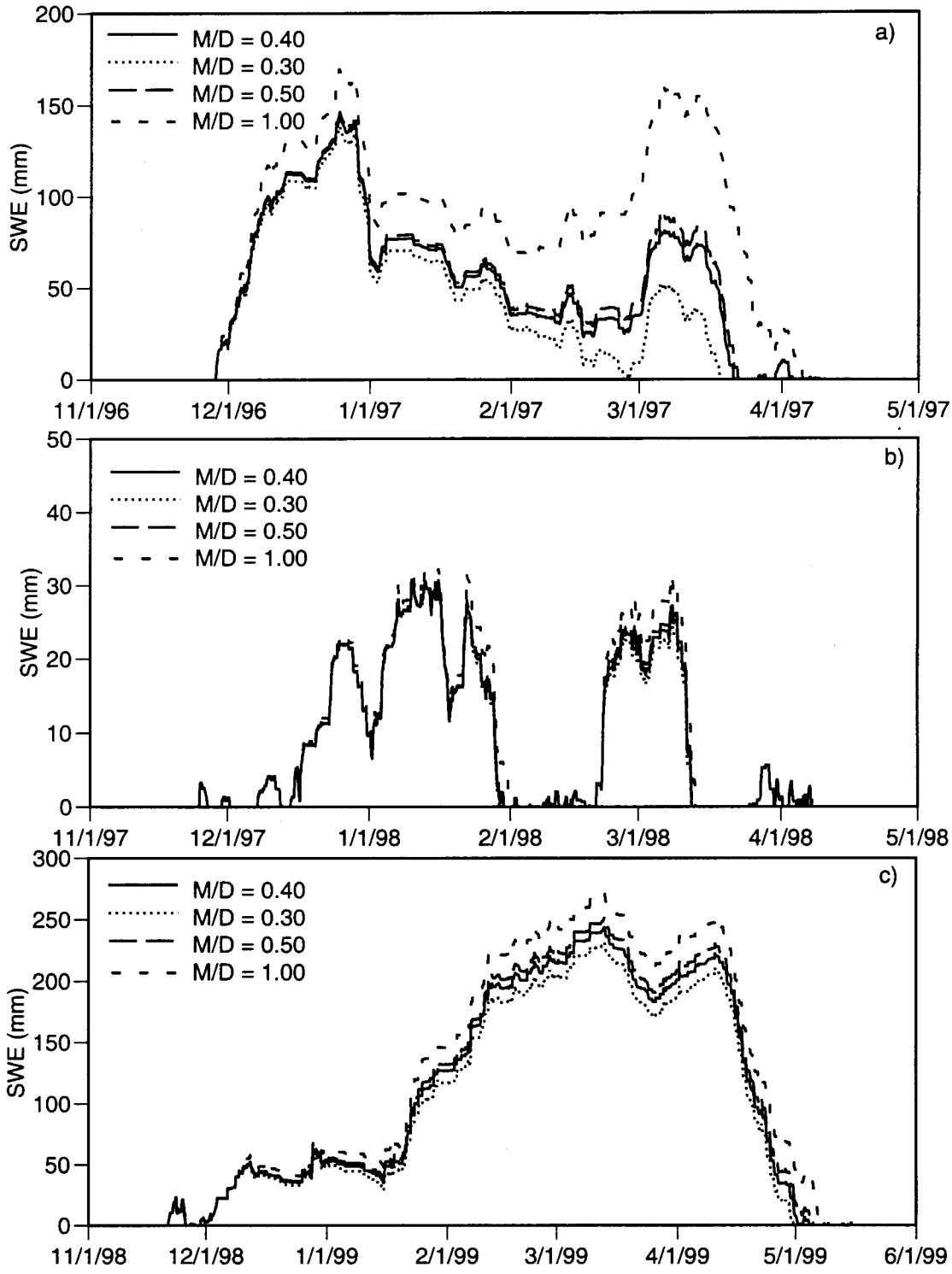

Figure 6.13. Effect of the ratio of mass release to meltwater drip production on model predictions over three seasons of beneath-canopy weighing lysimeter data. a) 1996/97, b) 1997/98, and c) 1998/99.

seasons. Sensitivity to this parameter is much greater for the 1996/97 season. Increasing the ratio of mass release to meltwater drip allows more snow to be released from the canopy and results in greater accumulations of SWE beneath the canopy for all seasons. The strong sensitivity during the 1996/97 period is largely due to differences in melt rates that occur due to the thickness of the snowpack. During the period immediately after 1 Jan 1997 through 1 Mar 1997, air temperatures remained near freezing and gradual melt of the beneath-canopy snowpack was observed. Because energy influxes to the beneath canopy snowpack were small, the depth of the snowpack largely determined the melt rate. By decreasing M/D, snowpack thickness was decreased, thereby increasing the amount of melt given the same energy influx. This leads to an even shallower snowpack, which further accelerates melt. The cumulative effect of these processes (decreased snow accumulation and accelerated melt) over two months resulted in a divergence of model predictions. During the 1997/98 season, beneath canopy accumulations were minimal and melt was rapid for all M/D values, therefore divergence was minimal. During the 1998/99 seasons, snow accumulations exceeded the maximum thickness of the surface layer for the majority of the season and divergence was minimal.

To test the hypothesis that the combination of snow thickness and accelerated melt rates caused the divergence in model predictions during the 1996/97 seasons, the sensitivity analysis was performed again with an additional 100 mm of SWE added to the below canopy snowpack on 1 Dec 1996. With the additional 100 mm of SWE, the sensitivity to M/D for the 1996/97 season was reduced and was found to be similar to that observed during the 1998/99 season.

6.5.7. Minimum intercepted SWE available for mass release

During frequent field visits, residual intercepted snow was often observed on the forest canopy, even after repeated mass release events. This snow was only removed via meltwater drip or sublimation and often remained in the canopy for a period of several days after snowfall. This phenomena was observed more often on the stout branches of the mature canopy than on the cut tree experiments. However, based on a few observations of the cut tree experiments (e.g. Figure

6.8), a value of 5 mm SWE (12.5 percent of the maximum interception capacity) was adopted as a baseline value for this parameter.

The sensitivity of model predictions to this parameter is shown in Figure 6.14. As the amount of residual interception storage is increased from 2.5 mm to 7.5 mm, the total accumulation of snow beneath the canopy is decreased. Once again, this parameter is most sensitive during those periods when snow interception loads are lowest. As intercepted load decreases, the percentage of intercepted load available for mass release increases as the residual interception storage parameter decreases. An example of this sensitivity is seen during the period from 1 Feb 1997 to 1 Mar 1997. Predicted intercepted loads during this period were light (less than 7 mm SWE for all events except the large snowfall event of 15 Feb 1997). Increasing the residual interception snow storage to 7.5 mm has the overall effect of eliminating the mass release mechanism for these events and underestimating snow accumulation beneath the canopy.

6.6. Scaling from a point to forest stands

The above discussion has calibrated and tested the canopy-snow model at the point scale beneath a mature Douglas-Fir canopy (i.e. under essentially 100 % canopy cover). Natural canopies have a wide range of average fractional coverages. Therefore, the snow accumulation and ablation model must be able to account for the fractional coverage of the overstory at the pixel scale of a distributed hydrology model (typically 30 to 100 m).

6.6.1. Scaling methodology

This section presents and tests two methods of incorporating a fractional canopy coverage parameter into the point model described above. Both of these methods are shown schematically in Figure 6.15. The distributed method maintains the differences in snowpack between open and covered areas. The aggregated method redistributes the snowpack evenly over the entire forest stand at the end of each time step. In both methods, snow accumulation and ablation over that fraction of the forest stand covered by the canopy are calculated as described above. The

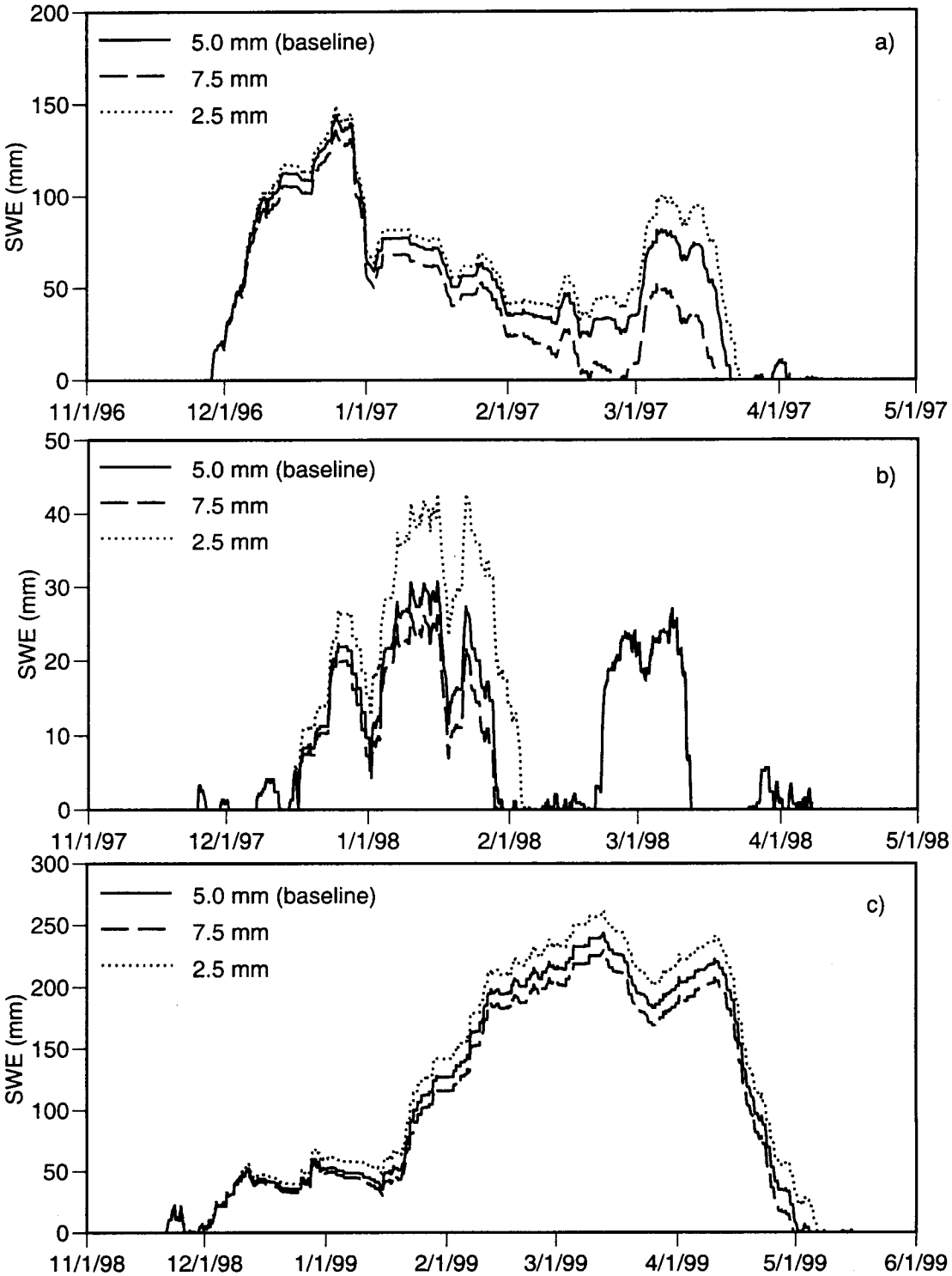

Figure 6.14. Effect of minimum interception storage available for mass release on model predictions over three seasons of beneath-canopy weighing lysimeter data. a) 1996/97, b) 1997/98, and c) 1998/99.

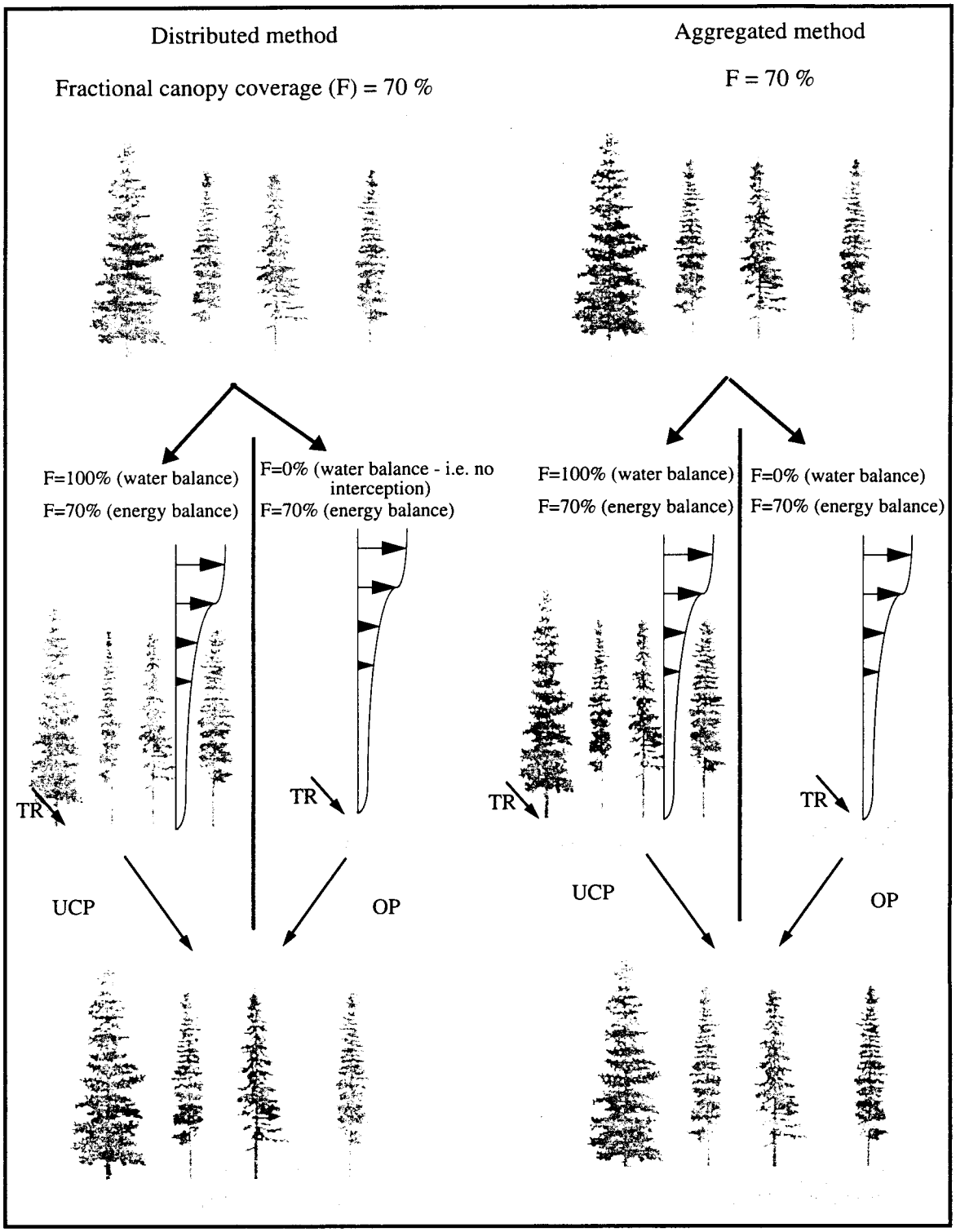

Figure 6.15. Comparison of two methods for implementing fractional canopy coverage. TR is transmitted radiation through the canopy. Arrow lengths indicate magnitude of radiation flux. Wind profiles are shown. UCP is under-canopy snowfall, OP is open snowfall.

parameters that control the amount of wind and radiation reaching the snow surface beneath the canopy are set to values that are representative of the entire forest stand. An identical energy balance is then applied over the ground snowpack irrespective of canopy cover. Snow interception is only considered on that portion of the pixel covered by a forest canopy (i.e. 100% forest cover over that fraction of the pixel covered by a canopy, 0 % forest cover over the uncovered fraction). Because the initial snowpack state can differ between open and covered areas, snowmelt must be calculated separately for each area in the distributed method and computational expense is increased.

6.6.2. Testing

Each method of scaling the snow-canopy model to the scale of an entire forest stand was tested against the snow course data collected over three winter seasons from 1996 to 1999 (see Section 4.7). To review, for the 1996/97 and 1997/98 seasons, forty observations of SWE were taken over a 26 ha forest stand adjacent to the beneath-canopy weighing lysimeters. During the 1998/99 season, only twenty observations over a 13 ha forest stand were available for testing of the scaling methods.

Meteorological data to drive the canopy-snow model at the stand scale were taken from the shelterwood site (as described above for the calibration-testing of the point model). The parameters used to attenuate wind and radiation through the canopy for the calibration of the point model were applied to drive the energy balance over the entire forest stand. This is equivalent to assuming that below-canopy meteorology measured at one point beneath the forest canopy (i.e. at the weighing lysimeter site) is representative of the average near surface conditions over the entire forest stand, irrespective of small scale differences in canopy cover. The assumption might be justified here given that these forest stands were selected to be as homogenous as possible (Halpern et al, 1999). Observations with a Moosehorn densiometer (which measures overhead canopy coverage with a field of view of five degrees) suggest that the

average fractional overhead canopy coverage of the forest stand (F) is approximately 70 percent. Therefore, 30 percent of the forest stand was modeled as open.

A significant fraction of the forest canopy to the southeast of the weighing lysimeters was removed during the summer of 1998. Although this harvest altered the attenuation of wind and radiation at the weighing lysimeters, the snow course points used for testing the scaling model during the 1998/99 season are located in the interior of an adjacent forest stand and are not thought to have been affected by the harvest.

6.6.3. Results

The stand level model predictions against the snow course data for all three winter seasons are shown in Figure 6.16. For the distributed model, the individual predictions for the beneath-canopy and open areas are shown. Observations shown on each figure include all measurements of SWE along with the stand average SWE.

The two models are nearly identical in their prediction of average stand SWE during accumulation phases and closely match observations. This similarity continues through most of each simulation and is apparent over all three seasons. Differences are evident during the later portion of the snow season, especially during 1996/97 and 1997/98. This difference is due entirely to the redistribution of snow over the entire stand combined with the sensitivity of snowmelt to the total depth of snow (described in Section 6.5.3). Redistributing snow from the canopy gaps to those areas beneath the forest canopy has the tendency to increase the average thickness of the snowpack below the forest canopy (which accounts for 70 % of the forest stand) and thus reduce the overall melt. In the distributed model, snowmelt below the forest canopy can be more rapid, due to the shallower depths, while snowmelt in the canopy gaps is slow. When snow depths below the canopy and in the canopy gaps exceed the minimum SWE of the surface layer, model predictions are nearly identical for both formulations (e.g. 1998/99 season).

The distributed formulation also shows differences at the end of each snow season. After the snow has melted over the entire unit with the aggregated formulation, snow remains in the

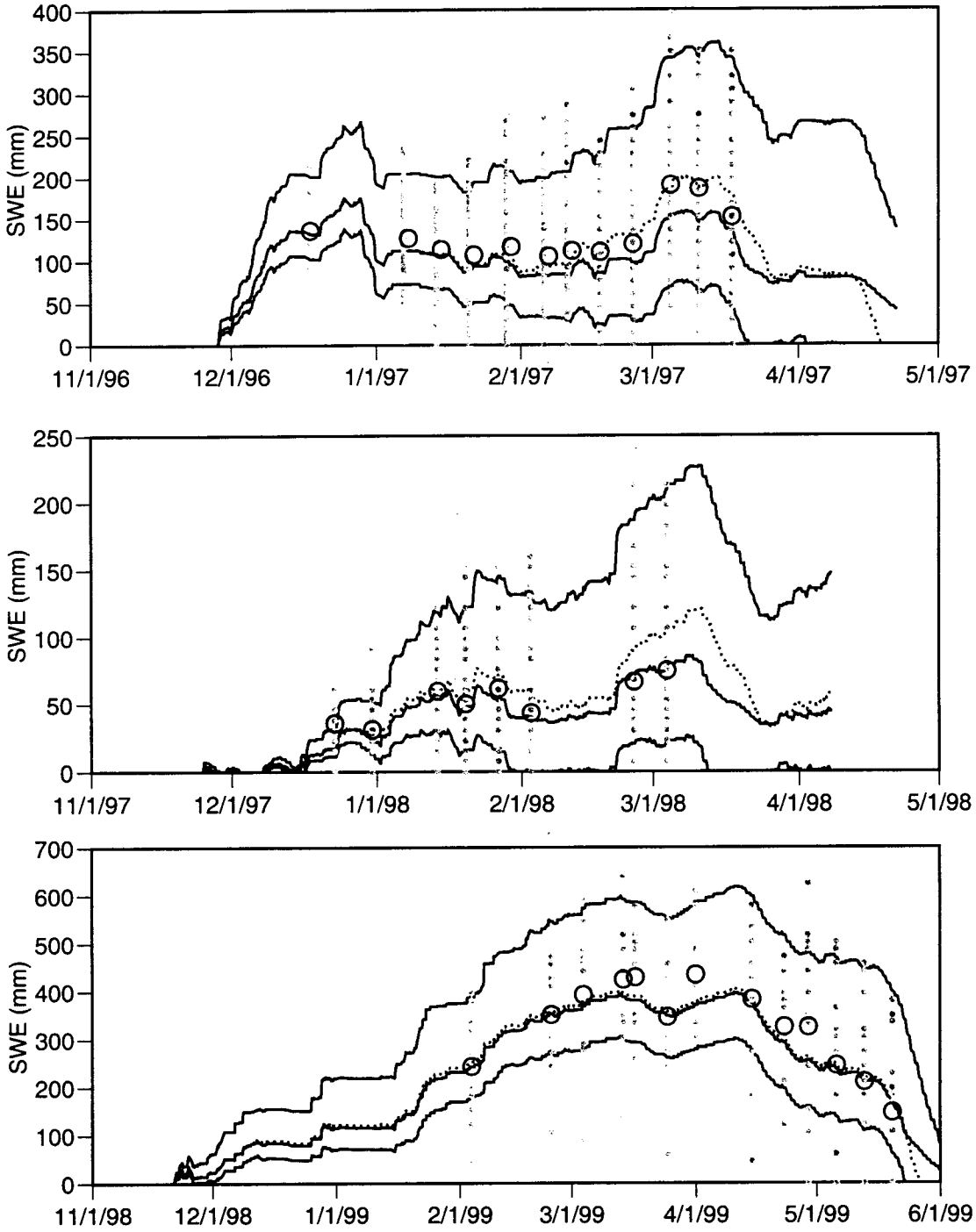

Figure 6.16. Results from incorporation of fractional canopy coverage parameter for scaling of canopy-snow model from point to stand scales. Predictions are shown for 100 % canopy coverage (lower solid line on each panel), in canopy gaps (upper solid line on each panel), 70 % aggregated canopy coverage (dashed line) and 70 % distributed canopy coverage (middle solid line on each panel). Available snow course data are shown as dots with the average SWE for each snow course shown as an open circle.

canopy gaps of the distributed formulation. These snow deposits have the tendency to lengthen the duration of the final melt phase. Although both model formulations appear to predict stand average SWE equally well, the distributed formulation can better represent the actual distribution of SWE over a forest stand and is more appropriate for modeling late season melt.

Chapter 7. Catchment-scale testing and assessment.

The previous chapters of this dissertation have shown the strong influence of a forest canopy on snow accumulation and melt. Although these effects can be modeled readily at the plot and stand scales, evaluation of the catchment-scale effects of vegetation change is more complicated. The magnitude of the enhanced rain-on-snow effect at the catchment scale depends on the freezing level during any particular storm, the spatial distribution of antecedent snow accumulation, and the specific meteorological conditions occurring during the storm. Therefore, simple extrapolations of the plot scale results can not describe the effect of canopy removal at the watershed scale directly.

This chapter presents an application of the canopy-snow model developed in Chapter 6 implemented in the distributed hydrology model of Wigmosta et al. (1994) to explore the effects of forest canopy removal on peak streamflows in the Pacific Northwest. Specific attention is given to ten floods that occurred from 1988 to 1996 in the Snohomish River Basin (4000 km^2), which drains from the Cascade Mountains to the Puget lowland in western Washington State.

This chapter is organized as follows. First, the Distributed Hydrology Soil Vegetation Model (DHSVM) is described along with its input data requirements. The Snohomish River Basin is then described briefly with an emphasis on the data available for implementing DHSVM. Next, the calibration and testing of DHSVM to the observed streamflow and snow records of the Snohomish basin are presented. The chapter concludes with an analysis of changes in peak streamflow due to various forest harvest scenarios and the relative contribution of increased antecedent snow accumulation and increased snow melt rates to these changes.

7.1. The Distributed Hydrology-Soil-Vegetation Model (DHSVM)

DHSVM (Wigmosta et al. 1994) provides a dynamic (one day or shorter time step) representation of the spatial distribution of soil moisture, snow cover, evapo-transpiration, and

runoff production. It consists of a two-layer canopy representation for evapotranspiration, a multi-layer unsaturated soil model, and a saturated subsurface flow model. Model inputs are near-surface meteorology (precipitation, temperature, wind, and humidity) and incoming short- and longwave radiation. Digital elevation data are used to represent topographic influences on incoming shortwave radiation, precipitation, air temperature, and downslope water movement. Surface land cover and soil properties are assigned to each digital elevation model (DEM) grid cell or pixel. The DEM resolution is arbitrary, but the land surface is usually represented with pixels of dimension on the order of 100 m.

In each model pixel, the land surface may be comprised of overstory vegetation, understory vegetation, and soil. The overstory may cover all or a prescribed fraction of the land surface. The understory, if present, covers the entire ground surface. The model allows land surface representations ranging from a closed two-story forest, to sparse low-lying natural vegetation or crops, to bare soil. Meteorological conditions (precipitation, air temperature, solar radiation, wind speed, and vapor pressure) are prescribed at a specified reference height well above the overstory.

Solar radiation and wind speed are attenuated through the two canopies. If snow is present, it is assumed to cover the understory and thus affects radiation transfer and the wind profiles via increased albedo and decreased surface roughness. Temperature and relative humidity are not adjusted through the canopy.

An independent one-dimensional (vertical) water balance is calculated for each pixel. Evaporation of intercepted water from the surfaces of wet vegetation is assumed to occur at the potential rate. Transpiration from dry vegetative surfaces is calculated using a Penman-Monteith approach. The model follows Entekhabi and Eagleson (1989) in using a soil physics-based approach to estimate point soil evaporation.

Precipitation occurring below a threshold temperature is assumed to be snow. For the assessment presented here, the model describing snow interception, ground snow accumulation, and melt is the same as that described in Chapter 6.

Vertical unsaturated moisture movement through each soil layer is calculated assuming a unit hydraulic gradient and a constant vertical saturated hydraulic conductivity in each layer. Different layers may have different saturated hydraulic conductivity. Percolation from the lowest rooting zone recharges the grid cell water table. Each DEM grid cell exchanges saturated subsurface flow with its eight adjacent neighbors according to the local hydraulic gradient. This method allows a transient, three-dimensional representation of saturated subsurface flow. Return flow and saturation overland flow are generated in locations where the grid cell water tables intersect the ground surface.

Water is transported toward the basin outlet using an explicit surface runoff and channel routing scheme that uses information about the location of stream channels and road networks (Wigmosta and Perkins 2000, Bowling and Lettenmaier 2000). These two networks are imposed on the digital elevation model of the watershed topography as Geographic Information System (GIS) coverages of vectors mapped to specific pixels. The fraction of each pixel covered by a road or stream is prescribed along with the depth of the road cut and / or channel incision. These networks directly intercept precipitation and subsurface flow. Once in the road or channel networks, flow movement is approximated using a linear reservoir scheme, details of which are presented in Appendix B. Surface water not in the channel or road networks is modeled with a simplified overland flow scheme (Wigmosta and Perkins 2000) and may reinfiltrate into neighboring model pixels or be intercepted by the road or stream networks.

To simulate a given watershed, DHSVM requires detailed information about the meteorology and land surface. DHSVM input files fall into two general categories: time series data and land surface characterization. The majority of the meteorological data are represented by time series data at the model's computational time step (typically in the range of one hour to one day). Land surface data are represented by constant grid or pixel-based maps of elevation, dominant soil type, dominant overstory vegetation type, and stream channel and road locations.

Figure 7.1 shows a schematic representation of DHSVM, its inputs and outputs. Raw data describing the basin's topography and land surface are preprocessed with GIS software to

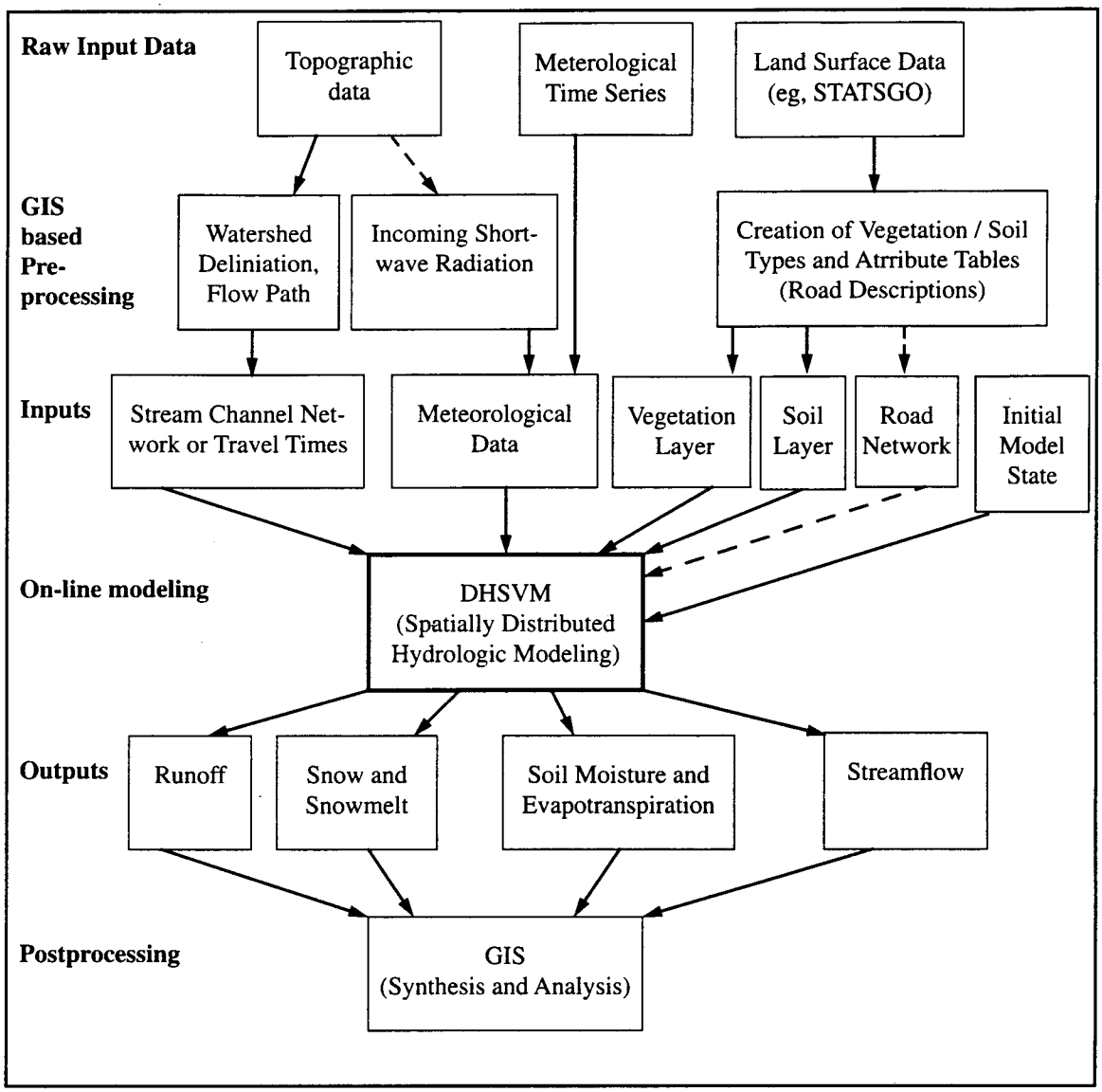

Figure 7.1. Schematic representation of DHSVM inputs, preprocessing requirements, outputs and interaction with GIS software. DHSVM options are indicated with dashed arrows.

produce the required DHSVM input files. Data from the meteorological time series are used to force the model during the hydrologic simulation. Output data are stored for later post-analysis. A more in-depth discussion of input data requirements for DHSVM is presented in Storck et al. (1998).

7.2. Snohomish River Basin

The Snohomish River basin (Figure 7.2) is located on the western slopes of the Cascade Mountains in Washington State. As delineated at the confluence of the Snoqualmie and Skykomish Rivers (USGS Gauge # 12150800, Snohomish River near Monroe, WA) it drains an area of approximately 4,000 km^2. The basin ranges in elevation from 30 to 2300 meters. Annual average precipitation is approximately 3 meters with significantly more precipitation falling at high elevations. The majority of precipitation falls during the winter months. The flood of record (4,250 cms) occurred during a rain-on-snow event on Nov 25, 1990. Annual average discharge from the basin is approximately 2000 mm which corresponds to an average annual flow of 270 cms. Flood stage occurs at 920 cms at Monroe. Flow diversions for power generation and irrigation are minimal. Two reservoirs exist in the basin, the Tolt Seattle water supply reservoir and Spada Lake reservoir, but they control only a small fraction of the catchment drainage area.

7.2.1. Topography, soils and vegetation

Figure 7.2 shows the elevation, dominant overstory vegetation type, and dominant soil class for the Snohomish basin. These data layers were obtained from the Puget Sound Regional Synthesis Model (PRISM) database (Westrick et al. 2000, http://www.prism.washington.edu).

For this application of DHSVM to the Snohomish basin, topography was represented by a digital elevation model (DEM) with a horizontal resolution of 150 m. The 150 m DEM was generated from a high resolution (10 meter) DEM as a part of the PRISM database. The 10 meter DEM was obtained from the U.S. Geological Survey as part of its National Elevation Dataset (USGS, 1999). The stream network was derived based on the 10 meter DEM with a contributing

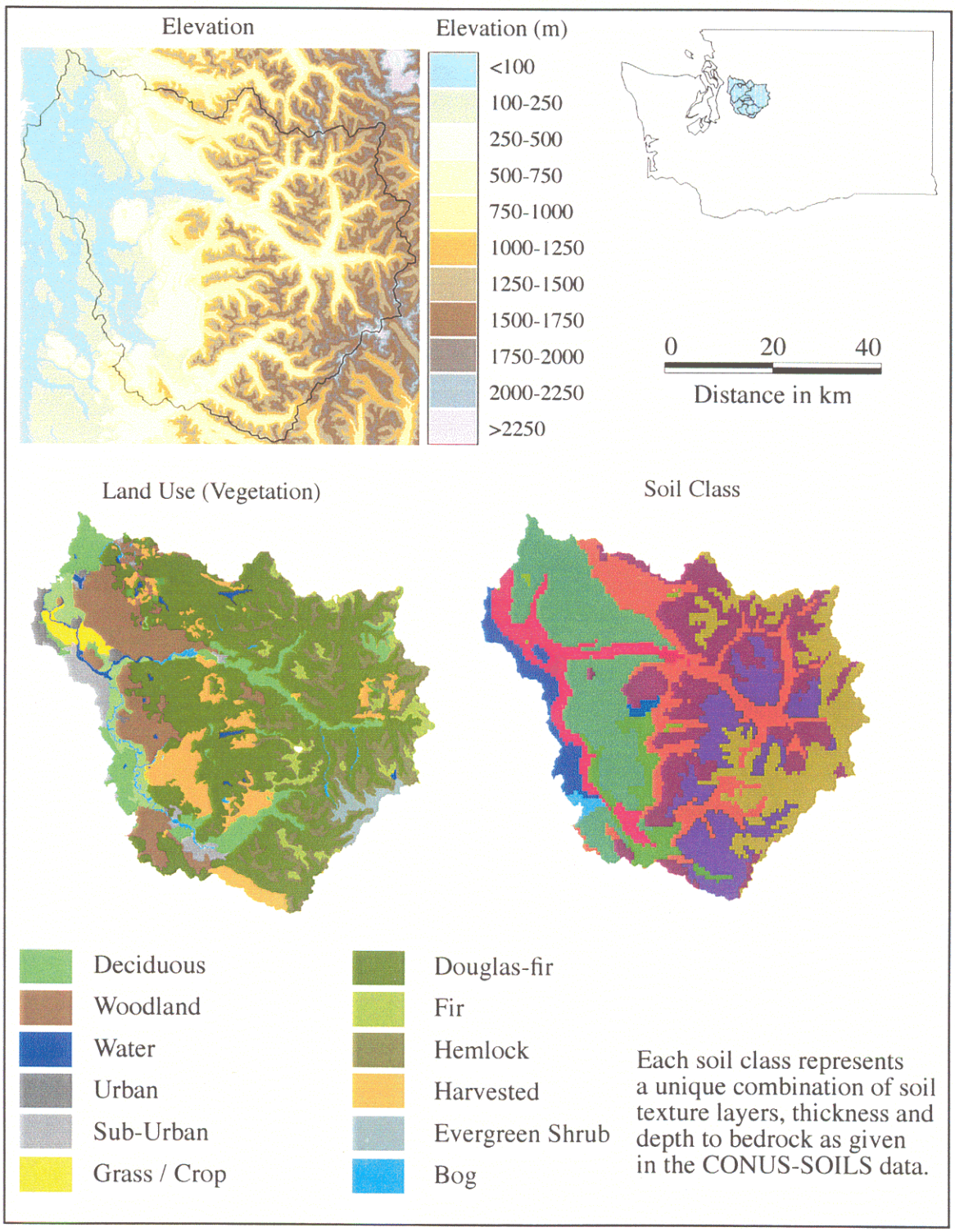

Figure 7.2. Overview of Snohomish River basin showing its location, topography, dominant overstory vegetation and soil classifcation.

source area of 0.25 km^2. The high resolution stream network was used to correct the 150 m DEM to force the streams to flow downhill at all points in the DEM.

The vegetation cover was taken from Gap Analysis Program (GAP) data (Scott and Jennings, 1998), which maps the major vegetation classes over the basin. The GAP data were based on LandSat TM imagery from 1991, which had a maximum resolution of 30 meters. The GAP data were aggregated into polygonal mapping units of similar coverage with a minimum area of 10 ha.

Soils data were taken from the Conterminous United States soil data set (CONUS) (Miller and White 1998) based on the USDA State Soil Geographic Database (STATSGO). The CONUS data were at a horizontal resolution of 1 km. These data were aggregated into 33 soil classes based on the dominant texture class as part of the PRISM data base development. Soil depth over the basin was based roughly on the depth to bedrock data contained in the CONUS data.

7.2.2. Meteorological data

DHSVM requires observations of incoming short- and long-wave radiation, windspeed, temperature, humidity and precipitation at every pixel over the model domain. The twenty three meteorological stations shown in Figure 7.3 were used to satisfy these input data requirements. These include the National Weather Service Cooperative observer network (COOP) (which typically observe precipitation and temperature) and the National Resource Conservation Service SNOTEL data network (which typically observe precipitation, SWE and temperature). In addition, three NOAA primary reporting stations are located outside the Snohomish Basin at Seattle-Tacoma International Airport, Stampede Pass and Paine Field. These first order stations typically observe temperature, humidity, windspeed, precipitation and cloud cover.

These observations were used to provide the forcings for the full energy balance at all twenty three observation points for the period from 1-Oct 1987 to 31 Dec 1996 as part of the PRISM database development. Details are provided in Westrick et al. (2000). Briefly, air

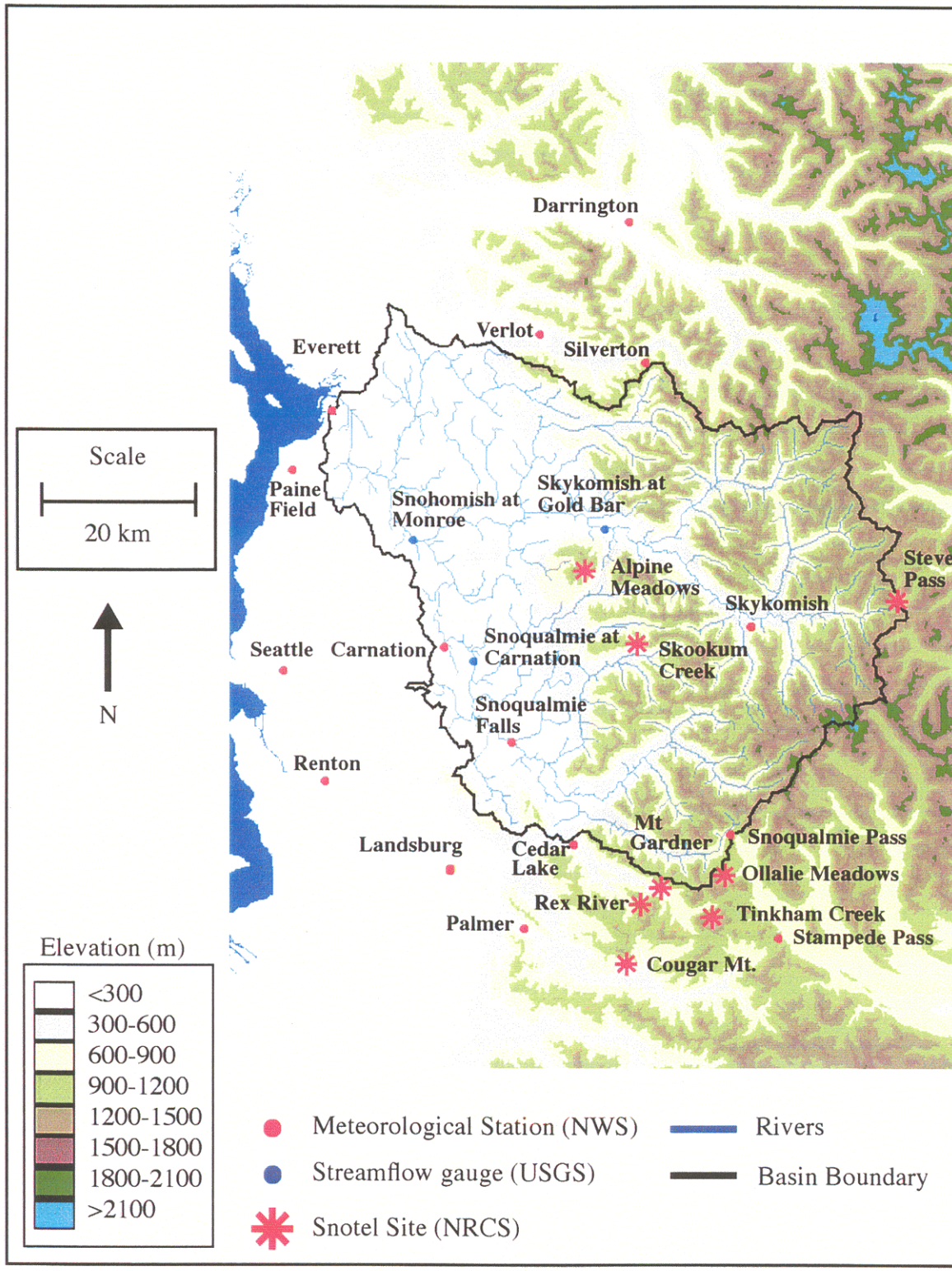

Figure 7.3. Location of meteorological stations used as DHSVM model forcings for the Snohomish River application.

temperature, humidity and windspeed were interpolated to all meteorological sites based on available observations for a given time step. Incoming shortwave radiation was based on calculations of clear-sky radiation, adjusted for observed cloud cover and interpolated to sites with a distance elevation weighted scheme (Dingman 1994). Incoming longwave radiation was calculated based on site air temperature, humidity and cloud cover (Dingman 1994). Interpolation between sites was accomplished with an inverse distance weighting scheme.

7.2.3. Road network

The effect of forest roads on basin hydrology was included in this application of DHSVM to the Snohomish River basin. Although the assessment of forest roads on basin hydrology is not an explicit part of this work, previous investigations using DHSVM (Bowling and Lettenmaier 2000, Lamarche and Lettenmaier 1998) have shown predicted increases in flood peaks attributed to roads that are similar to the effects of vegetation removal. The methodology for incorporating a road network into DHSVM is described by Wigmosta and Perkins (2000) and Bowling and Lettenmaier (2000) and has been applied over a large basin by Lamarche and Lettenmaier (1998).

The road network in the Snohomish basin is shown in Figure 7.4. Data describing the locations of the roads in the Snohomish basins are available from the U.S. Census Bureau's TIGER (Topologically Integrated Geographic Encoding and Referencing) data-base of geographic information. The data-base contains the location of every public road segment in the United States completed prior to 1990. Information on private road networks in the TIGER database was obtained from USGS 1:100,000 topographic maps derived from aerial photos. Due to the number of road segments and road-stream intersections in the more populated areas of the basin (which are generally lowland areas and therefore not active areas of forest harvest), the incorporation of roads in this thesis focuses only on the subbasins shown in Figure 7.4. A list of these subbasins and their respective road densities is given in Table 7.1.

The data input requirements to represent the road network can be extensive. These include: precise road locations, culvert locations, road cut-bank height, and connectivity of ditch-

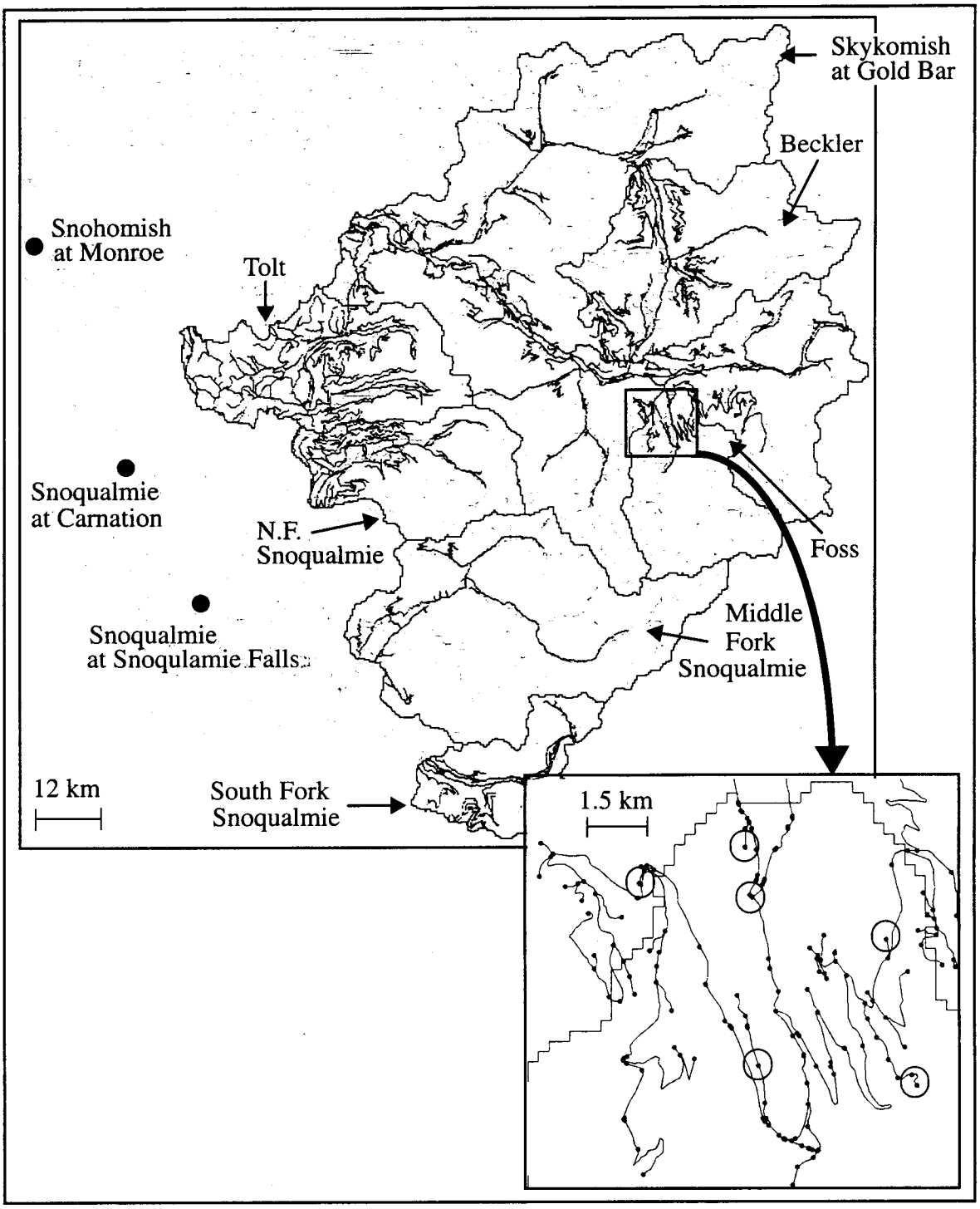

Figure 7.4. Headwater road network (black segments) over the Snohomish Basin with respect to the stream network (gray segments). Detail shows all road segments and nodes (dots) over the lower Foss River. Circled nodes are examples of non-stream crossing nodes that are in the same model pixel (150 m) as a stream channel.

relief culverts to the natural stream channel. While these data can be collected via hand held GPS (Global Positioning System) (Bowling and Lettenmaier 1997, Lamarche and Lettenmaier 1998), such an approach is infeasible over a 4000 km^2 basin.

To incorporate the road network into DHSVM for this application, a series of Arc/Info AML (Arc Macro Language) scripts were used to divide the observed road network into individual segments based on the location of road intersections, road-stream intersections and divides (Wigmosta and Perkins 2000). Data on road intersections were available from the TIGER data base. Stream-road intersections were based on the observed road locations and the predicted stream network. Divides were placed at all points at which flow direction changed along a road segment. These processing steps resulted in a road network which contained 4403 individual road segments representing 1519 km of roads. An example of the locations of nodes with respect to the road and stream networks is shown in the detail of Figure 7.4. The final road density for each of the basins shown in Figure 7.4 is given in Table 7.1.

Table 7.1. Road density for select sub-basins of the Snohomish River. Road location were obtained from US Census Bureau TIGER data.

Basin Name	Basin Area (km^2)	Road Density (km/km^2)
Skykomish at Gold Bar	1385	0.61
Beckler River	258	0.86
Foss River	142	0.32
Tolt River	211	1.44
N.F. Snoqualmie	165	1.0
M.F. Snoqualmie	399	0.23
S.F. Snoqualmie	108	1.06

Based on the locations of the road segments and its nodes, AML scripts (Perkins et al. 1996) were used to further process the road network according to the location of culverts. Because actual data on culvert locations were not available for the road networks, three

hypothetical scenarios were considered for culvert locations. The first scenario placed culverts only at road-stream intersections. The second scenario placed culverts at all road stream intersections and all nodes that were within the same model pixel (150 meters) as a stream channel. The third scenario placed culverts at all road segments. In all three scenarios, only those culverts that are in the same model pixel (150 m) as a stream channel are assumed to be directly connected to the stream channel. Table 7.2 provides additional data for each of the three scenarios. If culverts are limited to stream crossings, the average distance between culverts is 1 km. Incorporating additional culverts at all near stream segments reduces culvert spacing to 470 m. Allowing ditch relief culverts at all segments decreases the average spacing to 350 m.

Table 7.2. Number of road segments containing culverts compared to those draining to other segments for each culvert location scenario considered. In each scenario, those culverts that are in the same model pixel as a stream (near-stream) are assumed to be directly connected to the stream channel.

Culvert location scenario	Road Segments that contain culverts	Culverts that drain directly to the stream network	Road segments that drain to other segments	Average distance between culverts
Stream crossing only	1494	1494	2909	1000 m
Near stream	3231	3231	1172	470 m
All segments	4403	3231	0	350 m

In the absence of a more detailed field investigation (which is beyond the scope of this work), it is difficult to determine which of the proposed culvert location scenarios is most realistic for the Snohomish Basin. Piehl et al (1988) found the following spacing between ditch-relief culverts: USFS roads ~ 1.3 km, Bureau of Land Management (BLM) roads ~2.1 km, private roads ~ 2.7 km. Bowling and Lettenmaier (1997) found an average between culvert spacing of 0.2 km during a survey of 22.1 km of roads owned by the Weyerhaeuser Co. Lamarche and Lettenmaier (1998) found an average between culvert spacing of 0.24 km during a survey of 530 km of roads in the headwaters of the Deschutes River Watershed in Washington State.

Additional AML scripts were used to determine calculation order and the geometry of the road segments with respect to the individual model pixels (e.g. length, slope, aspect). All road segments were assumed to cut through the entire soil thickness. A sensitivity analysis of peak streamflow to the road network formulation is presented in Section 7.3.5.

7.3. DHSVM Calibration / Testing

7.3.1. Streamflow Calibration and Testing

DHSVM was calibrated to the daily observed streamflow record from 1 Oct 1987 through 30 Sep 1991, which includes the flood of record on 25 Nov 1990 (daily average observed flow of 3738 cms in the Snohomish River at Monroe). A model time step of 3 hours was used in all simulations. Calibration focused on adjusting the basin average soil parameters to obtain the observed streamflow on the Snohomish at Monroe. These parameters were limited to the lateral saturated hydraulic conductivity (final value 0.01 m/s) and the exponential decay of hydraulic conductivity (final value 4.0). Precipitation was not adjusted during the calibration period. Station observations of precipitation were interpolated over the basin using the PRISM (not related to the Puget Sound Regional Synthesis Model) monthly precipitation maps (Daly 1994). DHSVM was tested against the daily flow record from 1 Oct 1993 to 31 Dec 1996. This includes the two major floods of 30 Nov 1995 (3200 cms daily average flow) and 9 Feb 1996 (2600 cms daily average flow).

Figure 7.5 shows the results of the calibration to the November 1990 flood and testing against the February 1996 flood for the Snohomish at Monroe and five of its headwater tributaries. During model calibration, streamflow during the Nov 1990 event was well predicted over the basin. Although the initial flood event in early November is overestimated in the smaller headwater catchments, the total volume of runoff and the timing of the peak during the 25 Nov event is well predicted. The model performs equally well during testing and is able to capture both the timing and magnitude of the February 1996 flood peak.

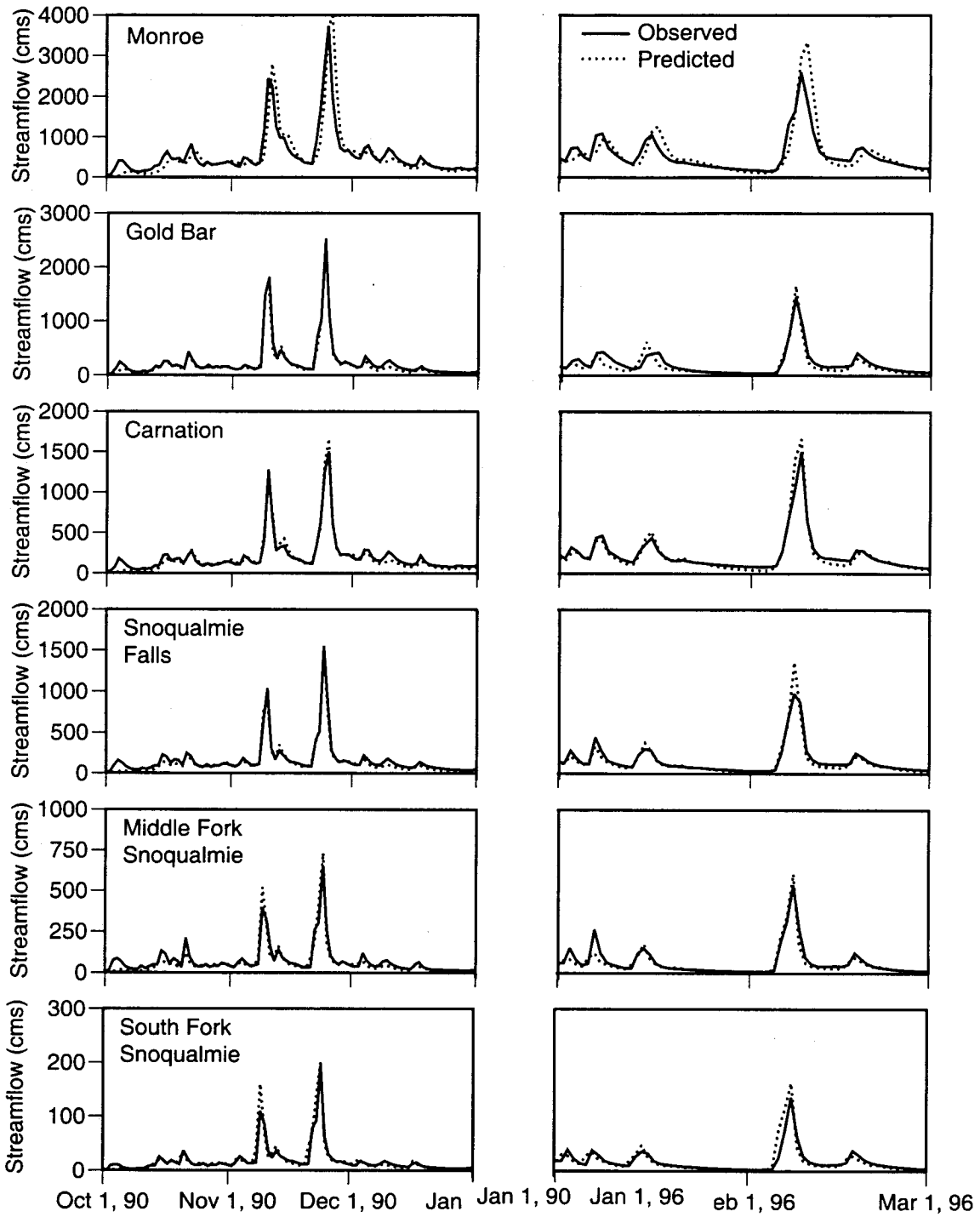

Figure 7.5. Sample results from calibration-testing of DHSVM to Snohomish River Basin daily streamflows Calibration results are shown for the November 1990 event. Testing is shown for the February 1996 event.

7.3.2. Channel routing model calibration and testing

DHSVM represents the channel network (both streams and roads) as a series of interconnected linear storage reservoirs (described in Appendix B). The following parameters are required for each channel segment to implement the linear routing model: Length (L), slope (S_o), Manning's n and flow depth (D). For this application, length and slope were calculated by overlaying the stream network on the digital elevation model. Flow Depth and Manning's n were determined by calibration. Before the routing model was calibrated to the Snohomish Basin, the overall channel lengths based on the predicted stream network were adjusted to match observed channel lengths (USGS 1985). Results of this process are shown in Table 7.3. Errors in predicted flow length are due to insufficient representation of channel sinuosity over specific reaches.

Table 7.3. Predicted versus observed stream channel lengths between points of reference in the Snohomish Basin. Correction factor is uniformly applied to all predicted channel lengths if total reach error is greater than 2km. (Snoq = Snoqualmie, Sky = Skykomish)

Reach	Predicted length (km)	Observed length (km)	Correction factor applied.
Sky at Gold Bar to confluence (Snoq)	36.6	36.2	1
Snoq at Carnation to confluence (Sky)	28.6	37.0	1.3
Confluence (Tolt,Snoq) to Snoq at Carnation	2.6	3.1	1
Tolt (below Reservoir) to confluence(Tolt, Snoq)	12.5	14.0	1
Confluence(Raging, Snoq) to confluence(Tolt, Snoq)	9.4	18.2	1.9
Raging River to confluence (Raging, Snoq)	4.8	4.2	1
Snoq Falls to confluence (Raging, Snoq)	7.5	6.1	1
Confluence (SF Snoq, Snoq) to Falls	4.7	7.1	1.5
SF Snoq to confluence (SF Snoq, Snoq)	25.5	27.9	1.1
NF Snoq to confluence (NF Snoq, Snoq)	15.2	14.8	1
MF Snoq to confluence (NF Snoq, Snoq)	16.2	17.2	1

For the purpose of calibration, all channel segments were grouped into 18 classes based on Strahler order and average segment slope. These classes are shown in Table 7.4. The distinction between classes is arbitrary as the specific thresholds were adopted more to allow a manageable number of classes on which to calibrate than any physical guidelines. Even so, the parameters are qualitatively plausible; flow depth increases with channel order and Manning's n increases with slope.

Table 7.4. Final parameters obtained from channel routing calibration. Stream channel classes are derived based on Strahler order and slope. The total number of predicted channel segments for the Snohomish Basin is 19348.

Class	Data from stream network		Assigned by Class		# of
	Order	Slope	Flow Depth (m)	Manning n	segments
1	<10	<0.002	0.5	0.03	1328
2	10-50	<0.002	1.0	0.03	481
3	50-100	<0.002	1.5	0.03	227
4	100-150	<0.002	2.0	0.03	172
5	150-200	<0.002	3.0	0.03	152
6	>200	<0.002	3.5	0.03	113
7	<10	0.002-0.01	0.5	0.05	1201
8	10-50	0.002-0.01	1.0	0.05	426
9	50-100	0.002-0.01	1.5	0.05	269
10	100-150	0.002-0.01	2.0	0.05	171
11	150-200	0.002-0.01	3.0	0.05	86
12	>200	0.002-0.01	3.5	0.05	21
13	<10	>0.01	0.5	0.1	12725
14	10-50	>0.01	1.0	0.1	1703
15	50-100	>0.01	1.5	0.1	243
16	100-150	>0.01	2.0	0.1	58
17	150-200	>0.01	3.0	0.1	22
18	>200	>0.01	3.5	0.1	0

To allow for rapid iteration on the parameters of the routing model, it was extracted from DHSVM so that it could be run independently. Given the observed upstream hydrographs at five locations in the Snohomish Basin (North, Middle and South Forks of the Snoqualmie River, the Skykomish at Gold Bar and the Tolt River), flow depth and Manning's n were calibrated to the observed hydrographs at three downstream locations (Snoqualmie Falls, Snoqualmie at Carnation, and the Snohomish at Monroe). For the purpose of routing model calibration, all lateral inflows to the channel network were ignored. The assumption of no lateral inflow is reasonable for spring dominated hydrographs for which the headwater portions of the basin contribute the majority of the streamflow and all flows are contained within the channel. This assumption is less realistic for the winter periods, however, for major ROS events, the headwaters of the Snohomish Basin (i.e. above the inflow hydrographs) receive considerably more precipitation than lower elevations (Daly 1994) and are expected to have the strongest snowmelt signature.

The routing model was calibrated to a spring snowmelt dominated period and was tested against the observed flow series from 1 Oct 1995 to 31 Dec 1996. Results are shown in Figure 7.6. Given the simplicity of the routing model, the results are encouraging. Both the timing of the peaks and the overall attenuation of the hydrograph are well predicted during the calibration and testing periods. Initial attempts at routing model calibration revealed that it was impossible to match the peak timing at all three downstream gauges simultaneously without first correcting the predicted stream channel lengths to match observations.

7.3.3. Snow water equivalent testing

Observations of Snow Water Equivalent (SWE) at two SNOTEL sites in and near the Snohomish basin were used to test DHSVM during the period from 1-Oct 1989 to 1-Oct 1996. The Cougar Mountain Snotel site is located just south of the Snohomish Basin at an elevation of 975 meters. The Stevens Pass Snotel site is located at an elevation of 1240 meters. The location of both sites is shown on Figure 7.3. During the testing period, both sites recorded daily values of

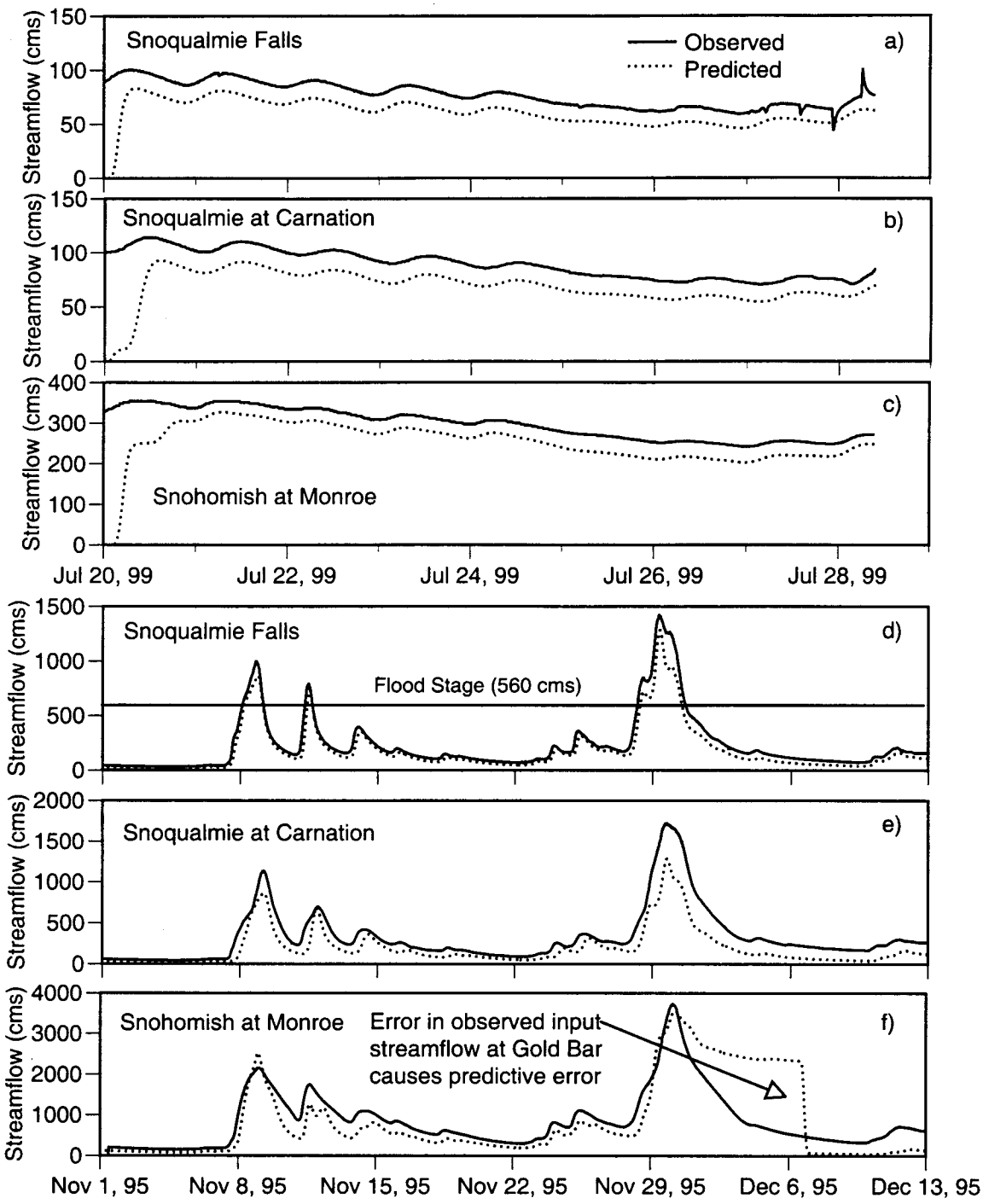

Figure 7.6. Calibration - testing of DHSVM routing model to Snohomish River Basin streamflows. The model was calibrated to a spring snow melt dominated event (a, b and c) and tested against an early winter flood series (d, e and f). The abrupt initial increase in predicted streamflow (a, b, c) is due to dry initial channel state.

precipitation and minimum and maximum air temperature. Observations of wind, humidity and radiation were interpolated from nearby meteorological sites as described above in Section 7.2.2. Both sites were modeled as clearings with parameters identical to those used to model the shelterwood site in Chapter 6 (minimum temperature for rain of 0.4°C, maximum temperature for snow of 0.5 °C, snow surface roughness of 0.007 m). No parameters were adjusted.

Figure 7.7 shows DHSVM model-predicted SWE and observations at both Snotel sites. There is a tendency to overestimate total SWE accumulation during the winter at Stevens Pass. For those years when maximum predicted and observed SWE agree, the predicted final melt season agrees well with observations. Predictions of SWE at the lower Cougar Mountain site do not agree as well with observations. There is a bias toward over-prediction of maximum SWE accumulation and over-prediction of final season melt rate during some years. However, there are clear examples when snow accumulation is significantly underestimated and the late season melt rate is underestimated. Given the absence of local observations of wind or radiation and the uncertainty of SNOTEL observations of precipitation, these results are encouraging as they suggest that good predictions may be possible even in the absence of detailed local data..

7.3.4. Comparison of predicted and observed areal extent of snow cover

Estimates of Snow Covered Area (SCA) from DHSVM were compared against estimates of Snow Covered Area obtained from AVHRR (Advanced-Very-High-Resolution-Radiometer) data. AVHRR is a passive multi-spectral satellite with an effective resolution of 1.1 km. The AVHRR data product segregates each scene into regions that are cloud covered, snow covered or bare ground (Maxson et al. 1996). Daily maps of SCA are available from the National Operational Hydrologic Remote Sensing Center (NOHRSC) at a 1 km resolution (Hartman et al. 1996). Given the persistence of cloud cover in the winter months over the Pacific Northwest, usable maps are available approximately weekly.

Estimates of SCA from AVHRR can be significantly underestimated due to the presence of a forest canopy (Hartman et al, 1996). Nevertheless, given a cloud free image, snow detection

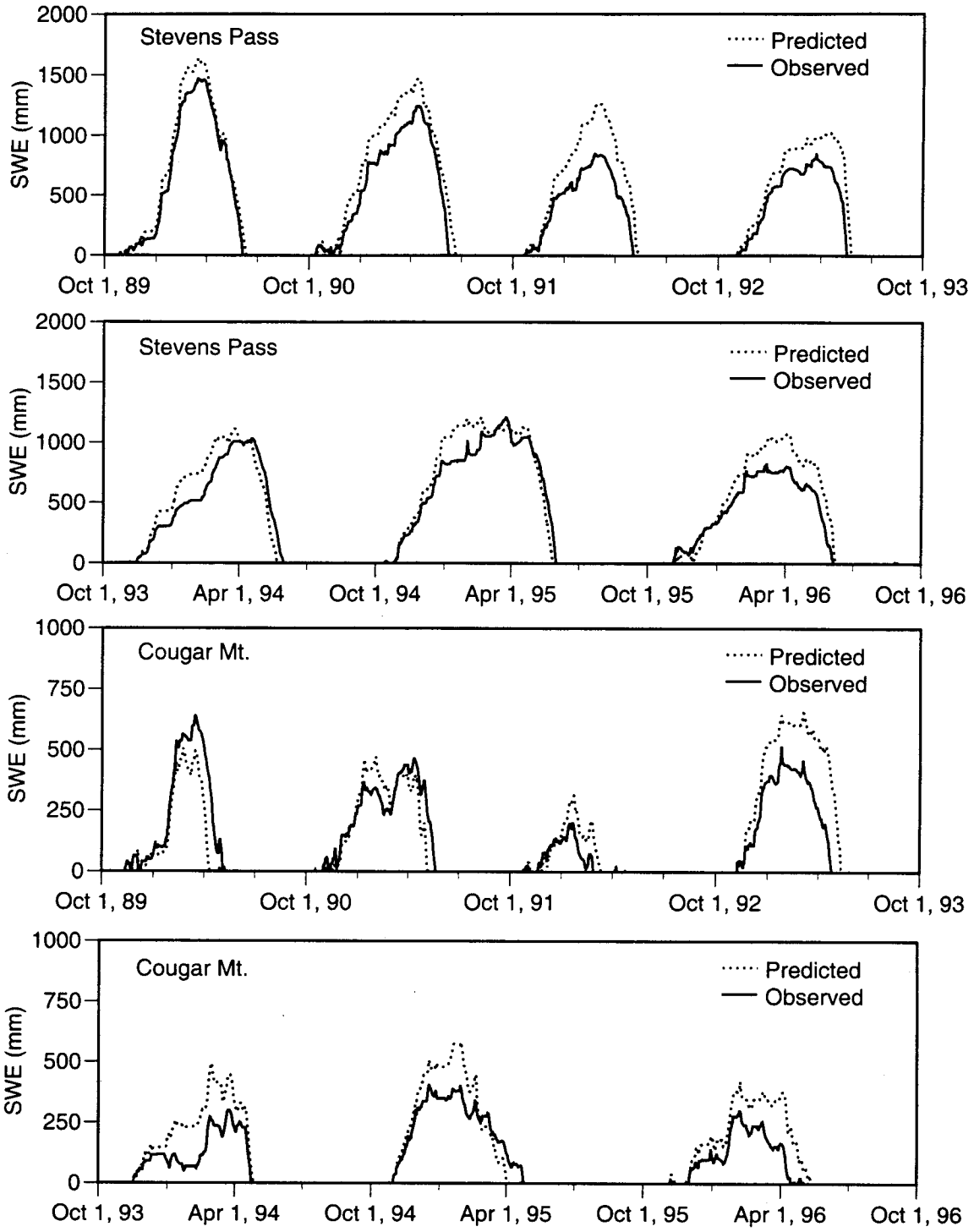

Figure 7.7. Comparison of DHSVM predicted SWE against SNOTEL observations. Snow model parameters are identical to those used for the shelterwood calibration and testing Only observations of air temperature and precipitation were available at each site, all other forcings were estimated from indirect observations as described in Section 7.2.2.

by AVHRR should be conservative. If AVHRR detects snow over a given 1-km pixel, then DHSVM should be expected to predict snow cover in at least one corresponding high resolution pixel. Conversely, the failure of AVHRR to detect snow may be attributable to the presence of a forest canopy or the lack of continuous snow cover and does not necessarily imply that snow is absent.

Figure 7.8 shows a comparison of DHSVM predictions of SCA to AVHRR observations of SCA. Model performance is evaluated with respect to four categories. 1) DHSVM predicts SCA and it is observed, 2) DHSVM does not predict SCA and it is not observed, 3) DHSVM predicts SCA but it is not observed, and 4) DHSVM does not predicted SCA but it is observed. The first two categories indicate agreement, the last two indicate disagreement. Given the limitations of AVHRR, errors that fall under category 3 are expected to occur often; errors that fall under category four are expected to be infrequent. DHSVM and AVHRR output were compared by aggregating DHSVM output (150 m) to the coarser AVHRR resolution (1 km). If SWE was present on a single DHSVM pixel corresponding to the AVHRR pixel, then that pixel was assumed to be positive for the prediction of SCA. Results were found to be insensitive to a limited sensitivity analysis on the number of pixels required for positive prediction (between 1 and 10) and the SWE required for positive prediction (between 0 and 1 cm).

Agreement between DHSVM and AVHRR estimates of SCA is approximately 80 percent during the period from 1 Jan 1996 to 7 Jul 1996. Agreement is nearly 100 percent during the widespread snowfall event of 31 Jan 1996. On average, type 3 error is the major source of disagreement and type 4 error is minimal. The widespread occurrence of type 4 error on 6 Feb, 8 Feb, and 9 Apr apparently corresponds to misclassification of low level clouds as snow in the AVHRR scenes. For example, in the scene from 9 Apr, both DHSVM and AVHRR indicate snow in the high-elevation portions of the basin and do not indicate snow in the mid-elevation portions of the basin. However, AVHRR detects snow in the low-elevation portions of the basin that are immediately adjacent to those pixels categorized as cloud covered. Similar cloud contamination can be seen in the 6 Feb and 8 Feb images. In cloud free images, type 4 error is nearly absent.

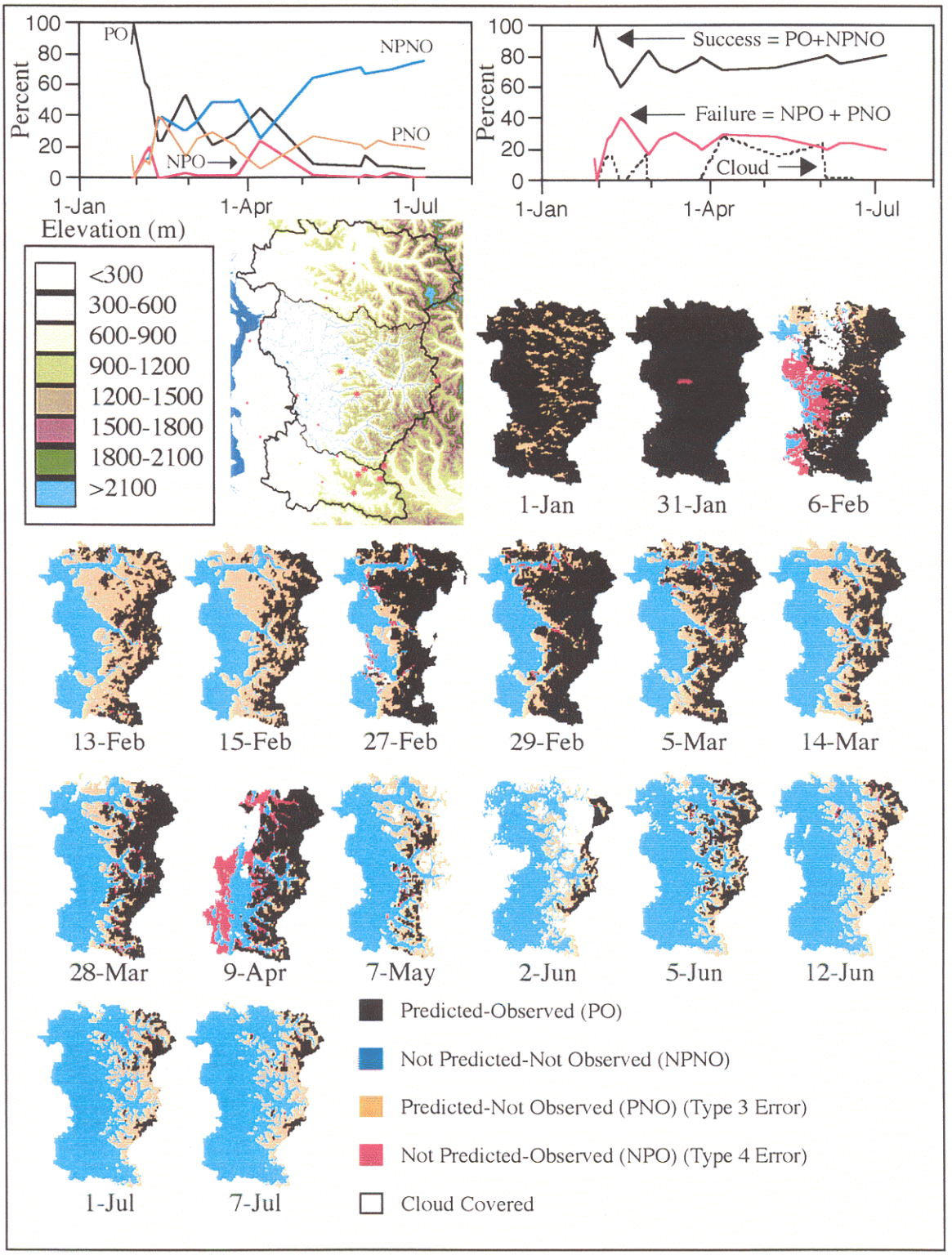

Figure 7.8. Comparison of DHSVM model predicted snow covered area to observations from AVHRR for 1996. Percent detection is calculated relative to cloud free portion of each image.

These results suggest that DHSVM model predictions of snow melt rate over the Snohomish basin are conservative. If the predicted melt rate over the basin were too rapid then type 4 error would be prevalent.

7.3.5. Effect of the forest road network on peak streamflow

The sensitivity of the streamflow hydrograph for the November 1990 flood event to the method for incorporating the road network is shown in Figure 7.9. The percent change in the hydrograph is shown with respect to a simulation without roads. In general, larger increases during the ascending limb of the hydrograph (and decreases during the descending limb) are predicted as culvert spacing is increased (see Table 7.2).

The results are consistent across all watersheds for the options that place culverts near the stream channels and at all road segments. The predicted increase in streamflow on the ascending limb of the hydrograph is approximately 5 to 10 percent, with a corresponding decrease in streamflow on the descending limb. For those basins with the highest road density (see Table 7.1) (Tolt River, North and South Fork of the Snoqualmie) the predicted increase in streamflow due to roads at the time of the flood peak is approximately 5 percent for both of these options.

For some of the watersheds, the option that places culverts only at stream crossings results in a greater than 10 percent predicted increases in streamflow during the peak without any evidence of a corresponding decrease. These results are due to changes in the drainage area of the individual watersheds resulting from road segments that cross watershed boundaries. The addition of near-stream culverts removes this bias. Based on the similarity of the predicted increase in peak streamflow obtained with the near-stream culvert locations to those obtained by previous investigations of forest road effects with DHSVM (Lamarche and Lettenmaier 1998), the near stream option was chosen to represent the road network in this application (Table 7.2).

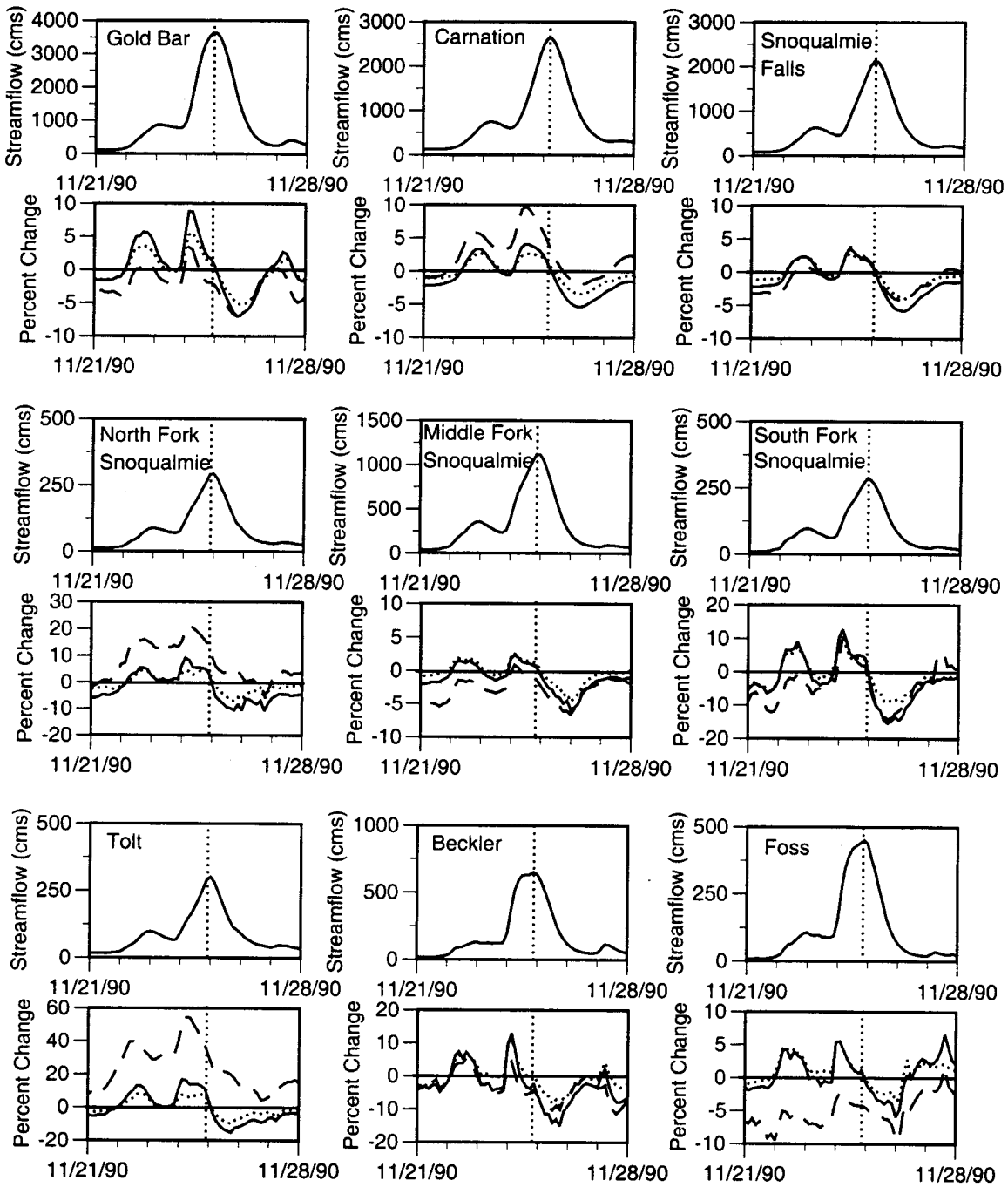

Figure 7.9. Predicted effect of forest road network during November 1990 flood event on 9 tributaries of the Snohomish River. Predicted streamflow without roads is shown in top panel for each tributary. Bottom panel shows the percent change in streamflow for three specifications of culverts locations over the road network: stream crossings only (long dashed), near stream (solid), all road segments (short dashed). Horizontal line in each panel is time of peak.

7.4. Catchment scale assessment

7.4.1. Selection of flood events for analysis

Ten flood events were selected for a sensitivity analysis of forest harvest effects on peak streamflow. These events correspond to the ten largest streamflow events that exceeded flood stage on the Skykomish River at Gold Bar and the Snoqualmie River at Carnation during the period for which micrometeorological data were available (1 Oct 1987 to 31 Dec 1996). Daily average streamflow at both stream gauges, the model forcings at Stevens Pass and the SWE at three Snotel sites during each event is shown in Figure 7.10. In addition, the observed total precipitation and average air temperature and wind speed at Stampede Pass along with change in SWE at the Cougar Mountain Snotel site over the duration of each event is shown in Table 7.5.

For the analysis of increases in peak streamflow and snowmelt considered here, each event was assumed to begin at the onset of rainfall or snowmelt over the basin and was assumed to end when the Snohomish River peaked at Monroe. The onset of rainfall and the time of peak streamflow were taken from observations. The onset of snowmelt was determined from model predictions.

Based on observations at Stampede Pass (elevation 1209 m), total event precipitation exceeded 100 mm, maximum air temperature exceeded 5°C and maximum hourly wind speed at 10 m elevation exceeded 10 m/s during all ten events. In eight of these events, snow was present at the Cougar Mountain Snotel Site (elevation 975 m). These events include the flood of record of November 25, 1990, during which approximately 300 mm of precipitation fell over an 84 hour period with a loss of 92 mm of SWE at Cougar Mountain. Also included is the event of February 9, 1996. Prior to this flood event, a significant low elevation snow pack developed (see Figure 7.8). During the storm event, 313 mm of precipitation fell at Stampede Pass and the entire snow pack melted below an elevation of 300 meters.

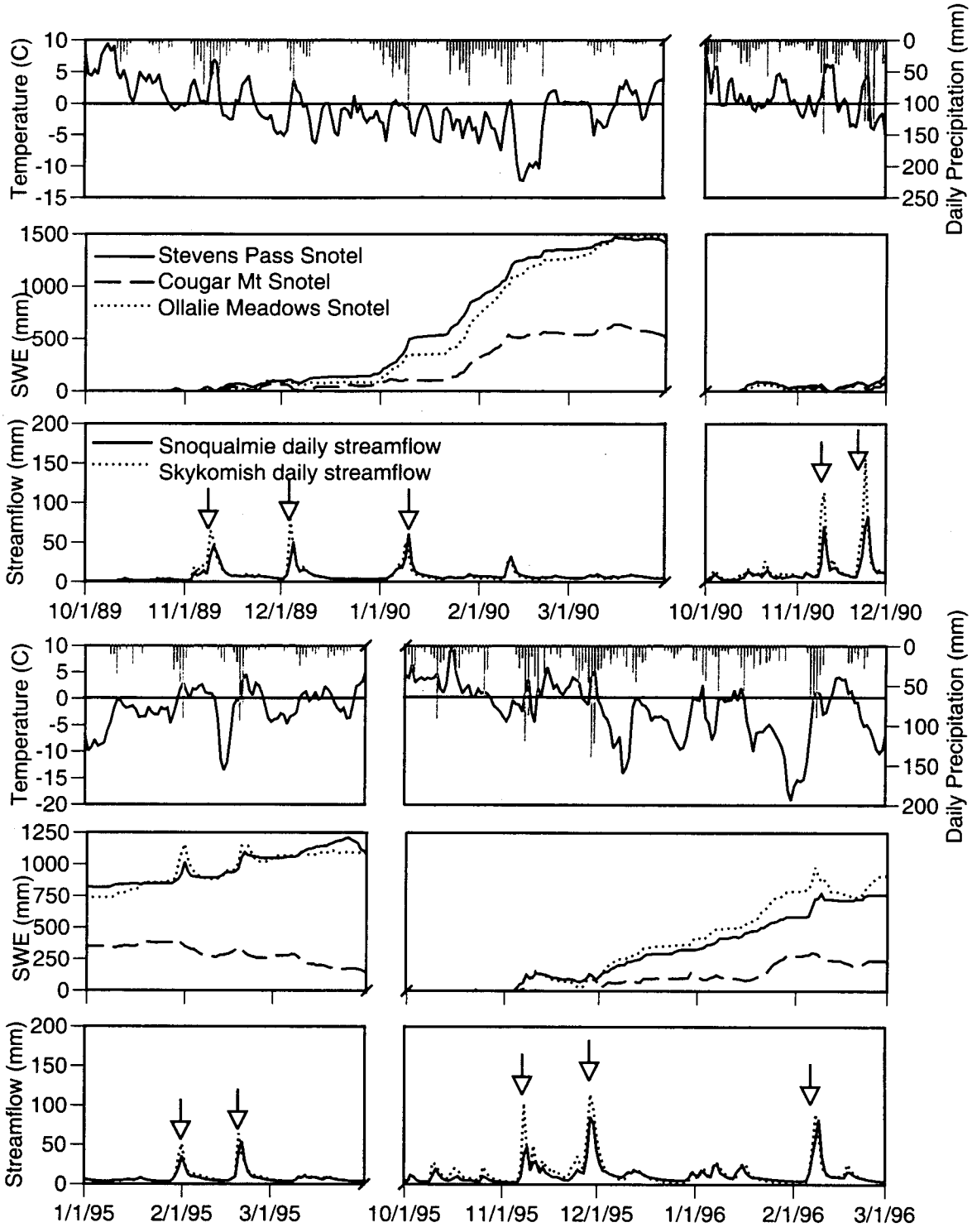

Figure 7.10. Ten major flood events in the Snohomish basin as observed at the Snoqualmie River at Carnation and the Skykomish River at Gold Bar from 1987 to 1996. Observations of SWE are shown for three Snotel sites: Stevens Pass (elevation 1240 m), Cougar Mt. (elevation 975 m), and Ollalie Meadows (elevation 1128 m). Daily average precipitation and air temperature are shown for Stevens Pass.

Table 7.5. Flood events for which the sensitivity of various forest harvest scenarios is explored. Micrometeorological observations are from Stampede Pass. SWE data are from the Cougar Mountain Snotel site (see Figure 7.3).

Event	Duration (hours)	Precipitation at Stampede Pass (mm)	Average (Maximum) Air Temperature (deg C)	Average (Maximum) 10 m. height Windspeed (m/s)	Observed SWE (mm) (begin/end)
11/10/89	69	112	4.8 (8.4)	9.9 (12.8)	0/0
12/6/89	75	163	2.5 (6.9)	4.5 (9.6)	61/7
1/10/90	75	256	0.6 (2.6)	5.4 (12.9)	96/100
11/10/90	75	166	4.1 (8.2)	10.0 (15.7)	56/7
11/25/90	84	296	4.5 (7.8)	9.5 (14.1)	97/5
2/1/95	87	138	3.0 (7.0)	6.4 (14.1)	400/340
2/20/95	84	100	2.8 (7.0)	5.6/ (13.1)	345/281
11/9/95	42	170	5.0 (8.5)	8.7 (12.9)	18/0
11/30/95	48	264	5.6 (7.6)	9.3 (13.8)	0/0
2/9/96	105	313	-1.7 (5.6)	6.0 (11.7)	300/254

7.4.2. Identification of basins and harvest scenarios

The ten sub-basins of the Snohomish River for which the sensitivity analysis of forest harvest effects was conducted is shown in Figure 7.11 a. The basins range in size from 100 to 4000 km^2 (Table 7.6). The area elevation curve for each basin is shown in Figure 7.12 based on the 150 meter DEM.

Four simulations of streamflow were conducted for each of the ten basins and 10 flood events. The distribution of vegetation for each of the various forest harvest simulations is shown in Figures 7.11 b - d. The first simulation was based on the GAP 1991 land cover (Figure 7.11 b) which was assumed to represent current land use conditions. The second simulation was based on an un-harvested scenario (Figure 7.11 c) in which all harvested areas were replaced with a mature Douglas-fir canopy. This non-harvested scenario is referred to as the historic scenario for the remainder of this discussion. The third simulation is based on a completely clear-cut scenario in which the entire 4000 km^2 basin was clear-cut. The final simulation is based on an elevation

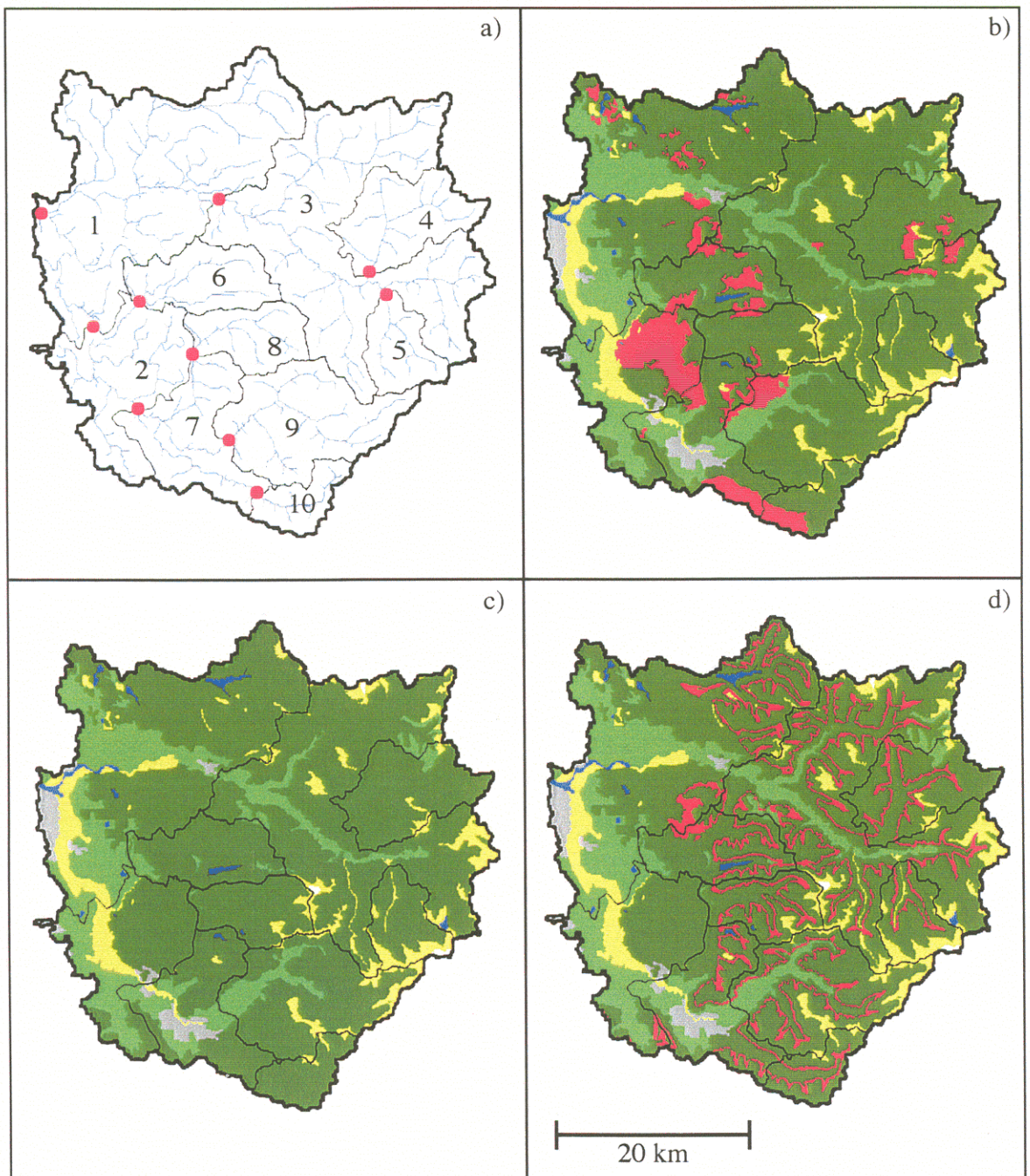

Figure 7.11. Distribution of vegetation type for each forest harvest scenario. a) Locations of the ten test basins with respect to the stream network (blue lines) and the stream-flow gauge locations (red circles), b) 1991 land cover based on GAP data, c) historic vegetation (no harvest), and d) complete clearcutting of the historic vegetation between 700 and 900 meters elevation.

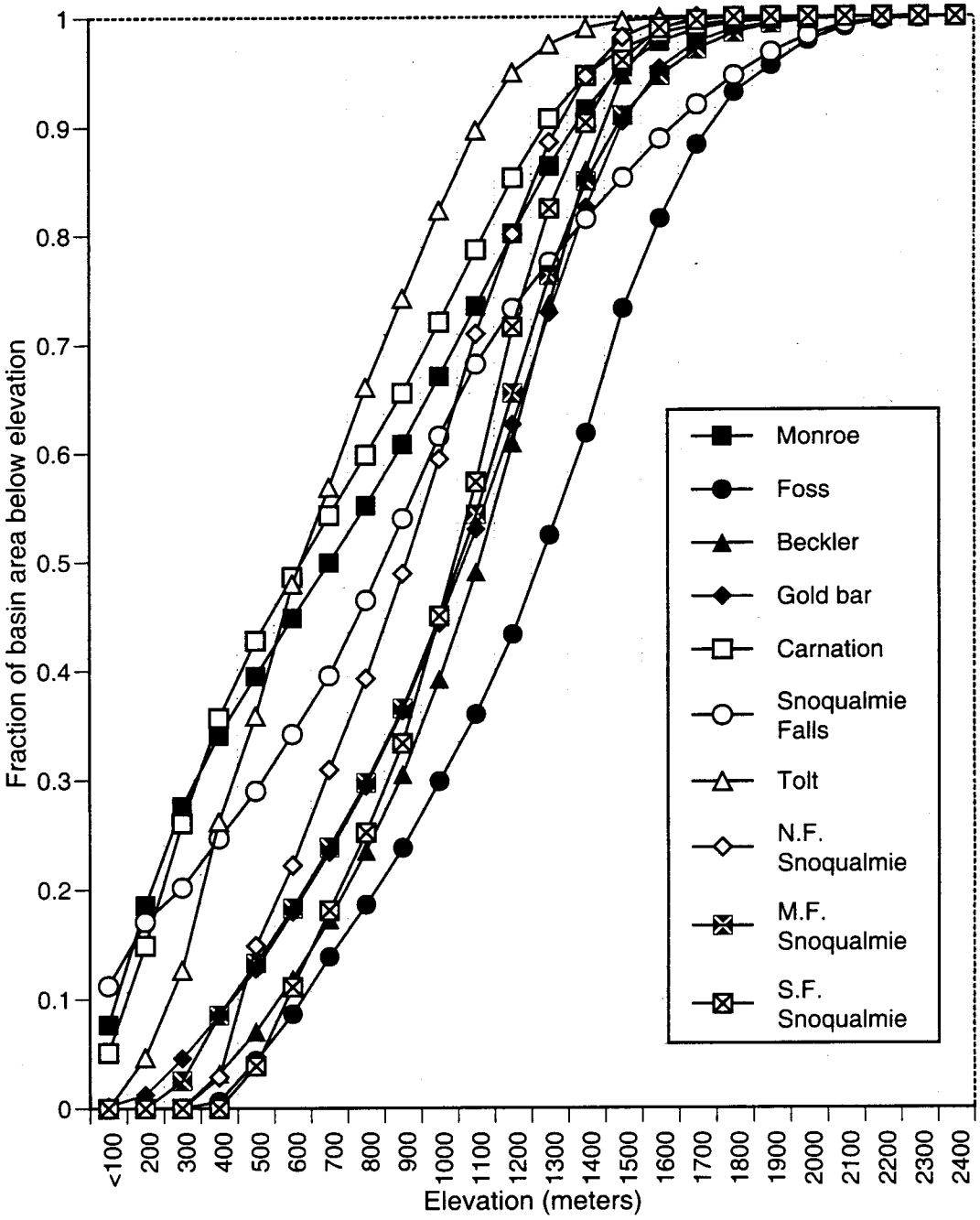

Figure 7.12. Area vs. elevation for each of the ten test basins in the Snohomish Watershed.

dependent harvest (Figure 7.11 d) in which the entire basin was clear-cut between an elevation of 700 and 900 meters. The 700 to 900 meter elevation band was chosen because it is in the transient snow zone (300 to 1200 m) of the central Washington Cascades (WFPA 1994). The percent of forest canopy removal over each of the sub-basins for each of the forest harvest scenarios is summarized in Table 7.6.

Table 7.6. Drainage basins for which the effect of alternative forest harvest scenarios are investigated.

Basin Name	Drainage Area (km^2)	Index on Figure 7.11a.	Percent harvested (GAP 1991)	Percent harvested (clearcut 700-900m)
Snohomish at Monroe	3985	1	8.3	10.9
Snoqualmie at Carnation	1562	2	16.1	11.2
Skykomish at Gold Bar	1386	3	2.5	12.9
Beckler River	258	4	6.5	13.2
Foss Fiver	142	5	0.0	9.9
Tolt River	212	6	18.6	17.3
Snoqualmie at Snoqualmie Falls	977	7	11.4	14.4
N.F. Snoqualmie	165	8	5.3	18.0
M.F. Snoqualmie	399	9	6.6	12.7
S.F. Snoqualmie	108	10	22.0	15.2

Streamflow for each forest harvest scenario was based on a simulation of the period from 1 Oct 1987 through 1 Mar 1996 with a three hour time step. For each simulation, initial conditions on 1 Oct 1987 were obtained from the model state on 1 Oct 1995 with the 1991 land cover. The period from 1 Oct 1987 to 1 Oct 1988 was used as a spin-up period so that the streamflow predictions for the first flood event would be relatively uninfluenced by the specified initial state. All simulations included the forest road network described in Section 7.2.3 and 7.3.5

with culverts specified in all road segments that are in the same model pixel (150 m x 150 m) as a stream channel.

For each simulation, canopy coverage on those pixels containing an overstory was taken as 95 percent. The snow surface roughness below an overstory was set to 20 cm. All other pixels were given a snow surface roughness of 1 cm. These snow surface roughness values are similar to those that yielded the best agreement with observations during calibration of the canopy-snow model to the weighing lysimeter data (Chapter 5).

7.4.3. Results

7.4.3.1. Predicted increase in peak streamflow during floods due to forest canopy removal

In all cases peak streamflows increased due to forest harvesting (Tables 7.7 and 7.8 and Appendix C). Clearcutting the entire basin led to an average increase in peak streamflow of 27.4 percent over all events and all basins. Basinwide average increases as high as 71 percent for the 1 Feb 1995 event and average increases over all events as high as 38 percent (over the N.F. Snoqualmie) were predicted due to complete clearcutting. The smallest basinwide average increase was predicted for the 10 Jan 1990 event (4.5 percent). The smallest increase averaged over all events was predicted for the Foss River (17.9 percent).

Table 7.7. Average predicted increase in peak streamflow (as compared to the simulation with historic vegetation cover) over all test basins for each flood.

Event	All Harvested	Band Harvested	GAP 1991
11/10/1989	47.2	12.1	4.0
12/06/1989	34.6	8.8	4.7
01/10/1990	4.5	0.9	0.6
11/10/1990	18.1	2.2	1.9
11/25/1990	9.9	1.1	0.7
02/01/1995	71.0	11.9	8.5
02/17/1995	31.8	4.3	4.1
11/09/1995	32.9	2.5	3.5
11/30/1995	10.1	0.9	1.1
02/09/1995	13.8	4.1	1.9
Average	**27.4**	**4.9**	**3.1**

Table 7.8. Average predicted increase in peak streamflow (as compared to the simulation with historic vegetation cover) over all storm events for each test basin.

Event	All Harvested	Band Harvested	GAP 1991
Snohomish	25.5	3.9	2.3
Carnation	26.2	4.7	4.6
Snoqualmie Falls	25.7	4.6	3.4
Gold Bar	25.1	3.3	0.8
Foss River	17.9	1.9	0.0
Beckler River	30.1	3.5	1.8
Tolt River	37.4	9.3	8.9
N.F. Snoqualmie	38.0	7.3	2.2
M.F. Snoqualmie	22.9	4.1	1.8
S.F. Snoqualmie	25.2	6.1	5.3
Average	**27.4**	**4.9**	**3.1**

The effect of forest harvesting at current (1991 GAP) levels resulted in predicted basinwide average increases of 3 percent over all events, with basinwide average increases as high as 8.5 percent for the 1 Feb 1995 event and average increases over all events as high as 8.9 percent for the Tolt River. The smallest basinwide average increase due to current harvest was predicted for the 10 Jan 1990 event (0.6 percent) while the smallest increase over all events was predicted for the Foss River (0 percent). Note that the GAP, 1991 harvest scenario indicated that no harvest had occurred for the Foss River drainage, which accounts for the absence of change.

The removal of all canopy between 700 and 900 meters elevation is predicted to result in an average increase in peak streamflow of 4.9 percent over all basins and all events. Basinwide average increases of 11.9 percent are predicted for the 1 Feb 1995 event with maximum average increases over all events of 9.3 percent for the Tolt River. The smallest basinwide average increase due to the band harvest was predicted for the 10 Jan 1990 and 30 Nov 1995 events (0.9 percent) while the smallest increase over all events was predicted for the Foss River (1.9 percent). Small increases in peak streamflow were predicted for the flood of record (25 Nov 1990). Complete canopy removal resulted in an average increase in peak streamflow over all basins of 9.9 percent. Predicted increases due to more realistic levels of forest harvest were limited to an

average of only 0.7 percent over all basins with a maximum of 1.6 percent predicted for the Tolt River.

The lowest average increase over all basins was predicted for the Foss River. Complete canopy removal resulted in a predicted increase of 17.9 percent over all events. Complete harvest between 700 and 900 m elevation resulted in a predicted increase of less than 2 percent. These results are partially explained by the relatively high elevation of Foss River. Of all the basins investigated, Foss River has the lowest fraction of its area between an elevation of 300 and 1200 meters, which is the standard definition for the transient snow zone in the central Washington Cascades (WFPA 1994).

7.4.3.2. Contribution of changes in initial soil moisture to predicted streamflow increases

For all events except 10 Nov 1989, the predicted increases in peak streamflow were not due to increased antecedent soil moisture due to a reduction in transpiration. The effect of reduced transpiration was investigated by comparing the basin wide soil moisture for each harvest scenario to that predicted with historic vegetation. This comparison was performed for each 100 meter elevation band over the basin. For all but the 10 Nov 1989 event, early fall precipitation events quickly replenished the soil moisture over the basin and erased any differences due to changes in transpiration. For a majority of events, soil moisture levels immediately before a snowmelt event were greater in the historic vegetation simulation than in the completely clearcut simulation. This increase in antecedent soil moisture is due to the modeled melt of intercepted snow.

7.4.3.3. Relationship between basin factors, event size and percent changes in streamflow

The relationship between predicted percent increase and various basin and event factors is explored qualitatively in Figure 7.13. Due to the small number of events and test basins, no attempt is made to form predictive equations from these results or to assess any statistical significance of the suggested trends.

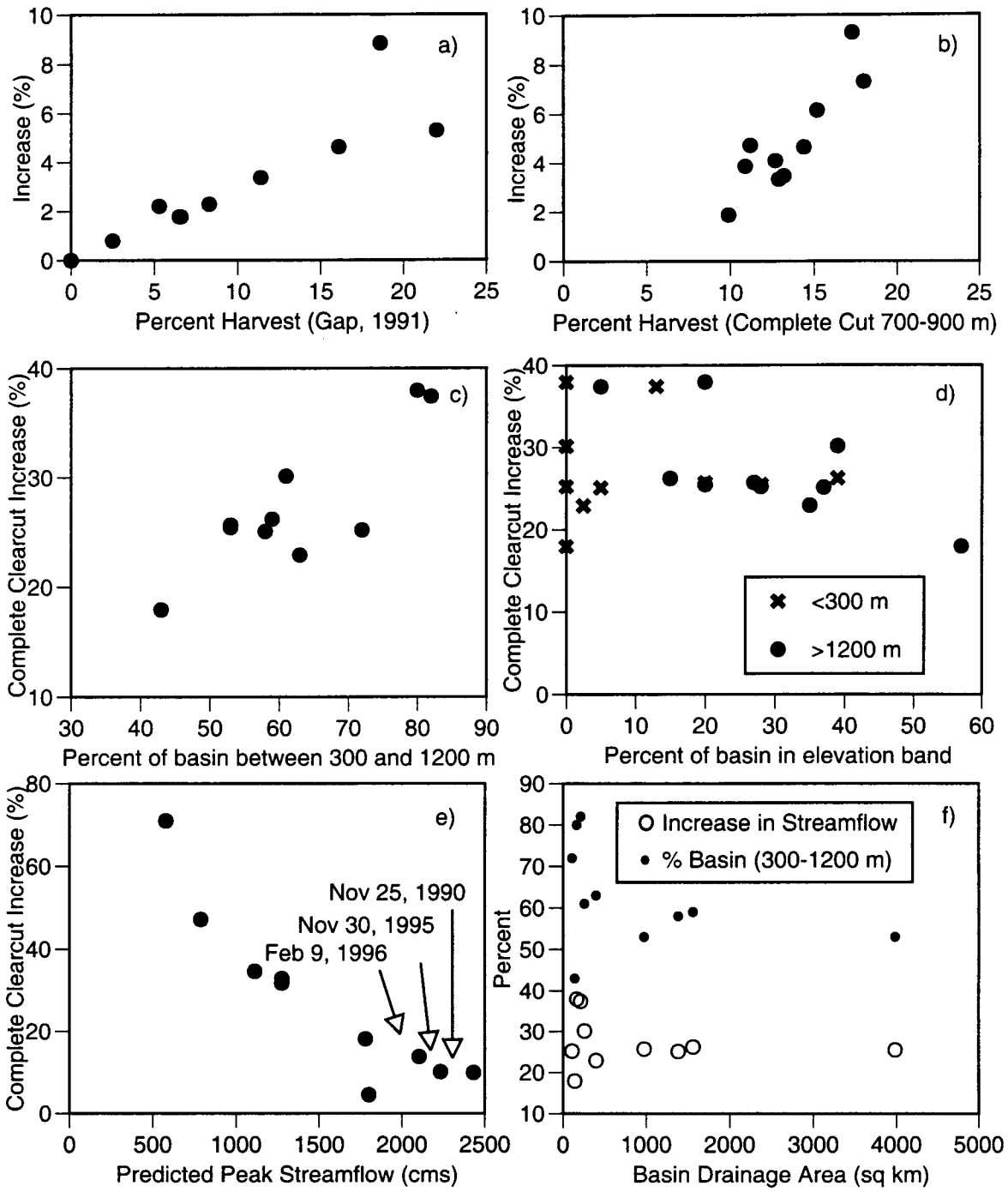

Figure 7.13. Effect of various characteristics on average percent increase in streamflow observed over 10 flood events. a) Recent harvest, b) Band harvest, c) Percent of basin area between an elevation of 300 to 1200 m elevation, d) same as c, but for elevations below 300 m or above 1200 m, e) Effect of flood size on percent increase in streamflow over all basins, and f) same as e, but for basin size (f also shows percent basin area between 300-1200 m vs. basin size). Event size is based on predicted peak streamflow in the Snoqualmie River at Carnation.

Despite the small sample size, several relationships are seen in Figure 7.13. The clearest relationship is that the predicted change in peak streamflow increases as the harvest fraction increases. This tendency is evident for both the 1991 GAP harvest data (Figure 7.13 a) and the 700-900 m elevation band cut (Figure 7.13 b).

Several relationships are suggested between predicted increase in streamflow and basin elevation. The predicted change in streamflow due to complete clearcutting increases as the percent of basin area between an elevation of 300 and 1200 m increases (Figure 7.13 c). No such clear relationship is seen between change in streamflow and the fraction of basin area below 300 meters (Figure 7.13 d). However, the simulations do suggest a weak downward tendency in predicted increase as the fraction of basin area above an elevation of 1200 meters increases (Figure 7.13 d).

Model predicted percent change in streamflow decreases strongly as event size increases (Figure 7.13 e). As event size increases, the relative importance of snowmelt in the overall flood response diminishes and, consequently, the percent increase due to changes in total snow melt decreases. This trend becomes especially evident by contrasting two events of similar snow cover but different precipitation intensities. During the heavy precipitation event of 9 Feb 1996 (313 mm in 74 hours), the overall increase due to forest canopy removal was, on average 13.8 percent for a complete clearcut. In contrast, during the event of 1 Feb 1995 (138 mm of precipitation over 84 hours), the overall increase due to forest canopy removal was, on average, 71.0 percent for a complete clearcut. Both of these events were characterized by an extensive low elevation snow cover.

Any relationship between basin size and predicted increase in streamflow is less clear (Figure 7.13 f). Although no strong trend is evident, the predicted increase is highly variable over small basins (due to the large variability of elevation ranges between small basins) and seems to converge to a constant value for the largest basins. This convergence is most likely due to the fact that as these basins become progressively larger by including more area at low elevation, the total area in the transient snow zone (300-1200 meters) becomes fixed. Therefore, increasing basin

size further does not result in a significant increase in area contributing enhanced snow melt due to canopy removal. A plot of percentage area in the transient snow zone against basin size is shown in Figure 7.13 f.

7.4.4. Flood of 9 February 1996

Additional insight into possible increases in peak streamflow due to forest canopy removal can be obtained by a more detailed analysis of the 9 February 1996 flood event. This event was characterized by an extensive low elevation snow pack that completely melted during the storm. Despite this low elevation snow pack and the strong control of a forest canopy on snow melt rates, an increase in streamflow of only 13 percent is predicted due to complete forest canopy removal over the basin. An explanation for the relatively small predicted increase during the flood peak can be found by comparing the observed micrometeorology, streamflow and predicted snow melt over the basin during the event (Figure 7.14).

Prior to the onset of precipitation (6 Feb), rapid warming occurred at low elevations (as evidenced by air temperature at Sea-Tac) followed by rapid melt of the low- and mid-elevation snow pack, especially in the entirely clearcut simulation. The initial snowmelt phase was followed by two distinct precipitation events. The first occurred on 6- Feb, the second began on 8-Feb. The first period of precipitation, combined with the rapid snowmelt, caused a distinct initial peak in the hydrograph. This initial peak preceded the main flood peak by approximately two days and exceeded flood stage on most rivers in the basin.

Figure 7.15 shows the hourly observed streamflow on the Snoqualmie River at Carnation (Figure 7.15 a) and Snoqualmie Falls (Figure 7.15 b) along with model predictions (3 hour streamflow) for both locations with the GAP 1991 land cover. The initial flood peak is evident at both locations. The effect of various forest harvest scenarios on the initial flood peak is dramatic (Table 7.9, Appendix C). Complete forest canopy removal increases peak streamflow by 89 percent at the Snoqualmie at Carnation (Figure 7.15 c) and by 87 percent at Snoqualmie Falls (Figure 7.15 d). Current levels of forest harvest are predicted to have increased the initial flood

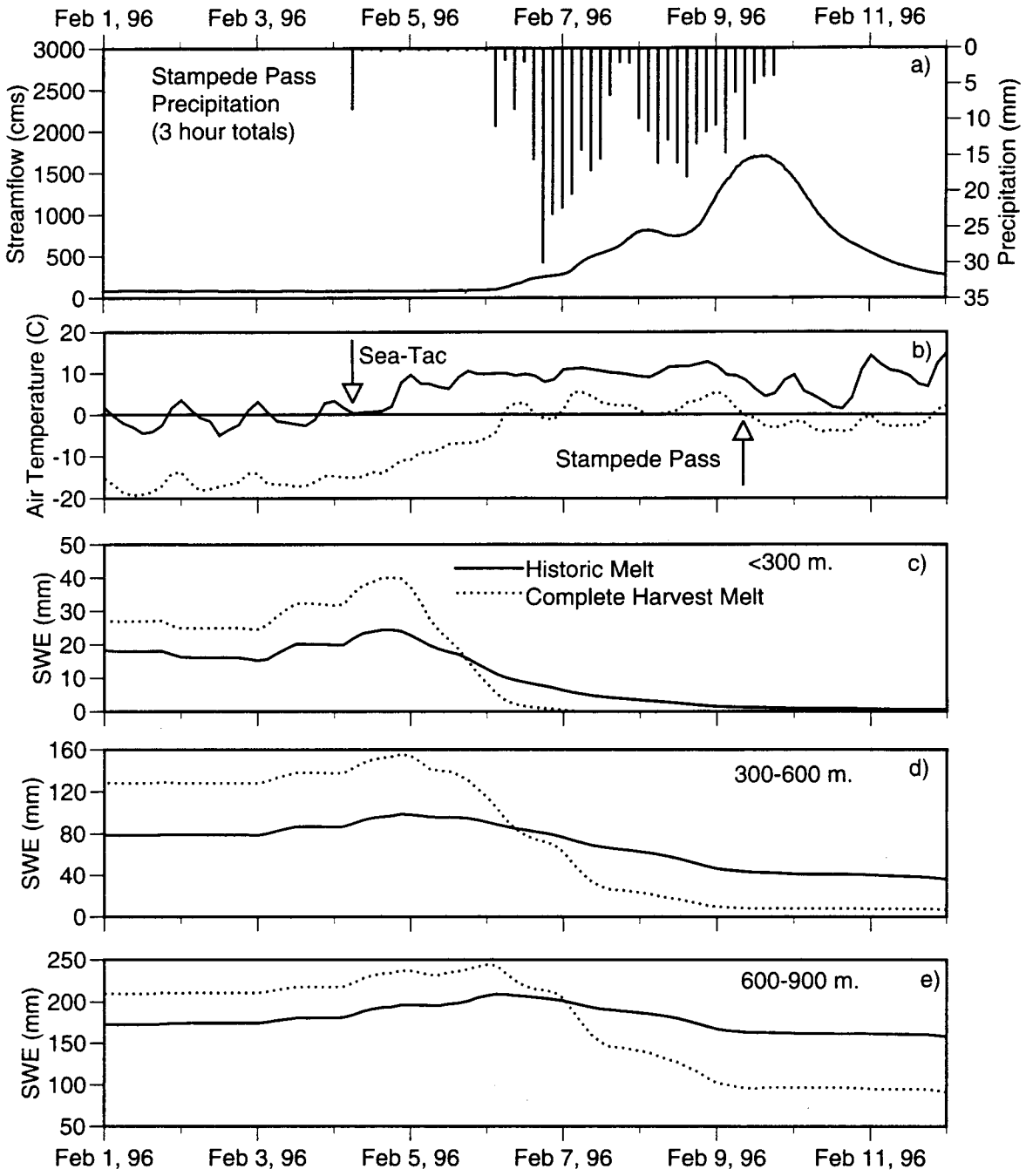

Figure 7.14. Observed micrometeorology, streamflow and predicted snowmelt during the February 1996 ROS event: a) Observed precipitation at Stampede Pass and observed streamflow at Snoqualmie at Carnation, b) observed air temperature at Seattle Tacoma International Airport and Stampede Pass, c) Predicted snow melt for the historic vegetation cover and complete harvest scenario at elevations less than 300 meters, d) same as c, but for the 300-600 m elevation band, e) same as c and d, but for the 600-900 m elevation band.

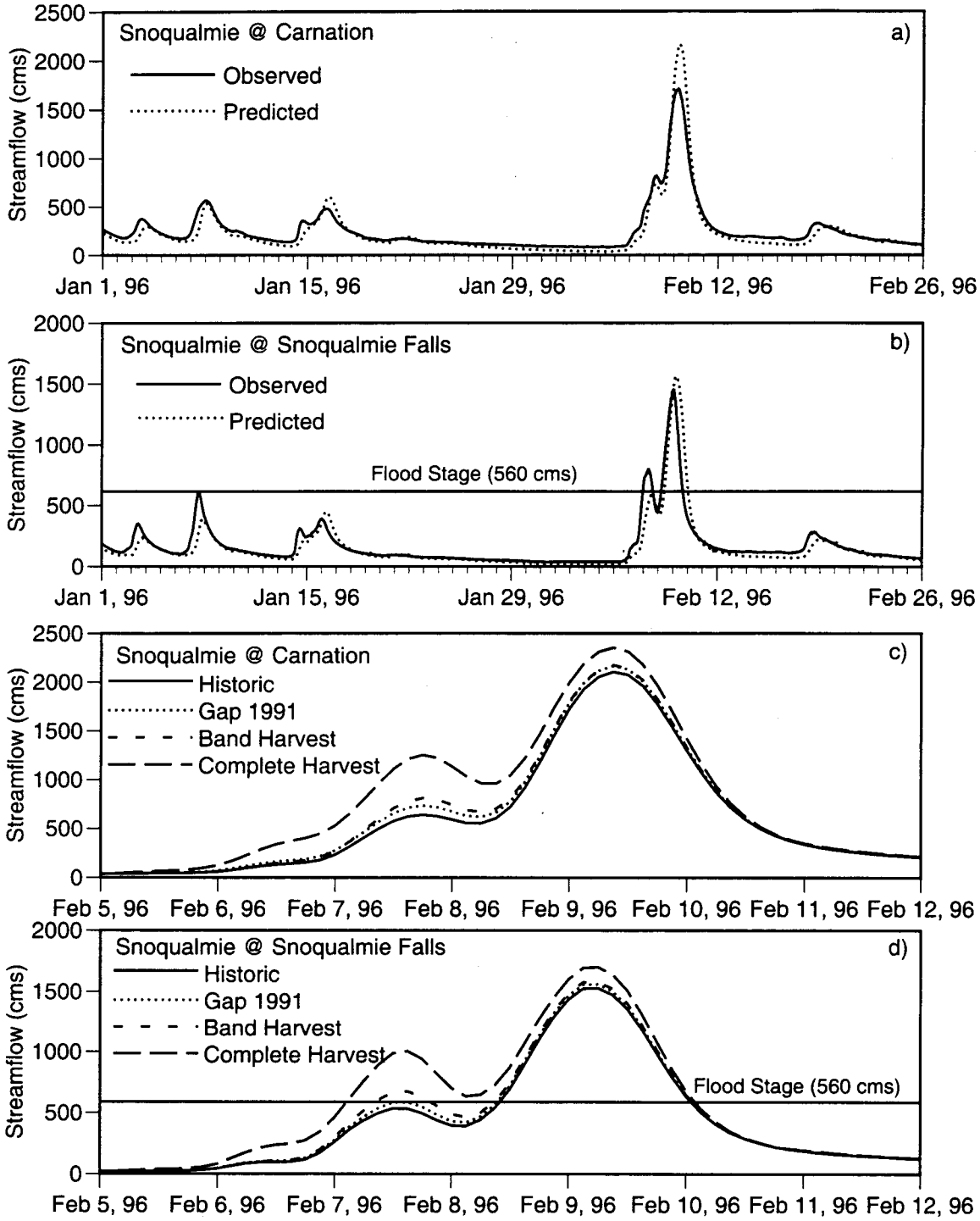

Figure 7.15. Effect of forest harvest on streamflow during February 1996 flood event to forest harvest: a) Streamflow with GAP landcover compared to observed at the Snoqualmie at Carnation, b) same as a, but for the Snoqualmie at Snoqualmie Falls, c) Effect of various levels of forest harvest on streamflow as predicted for the Snoqualmie at Carnation, d) same as c, but for the Snoqualmie at Snoqualmie Falls

peak by 12 percent at Carnation and 10 percent at Snoqualmie Falls. Complete canopy removal between 700 and 900 m is predicted to cause a 23 and 26 percent increase at Carnation and Snoqualmie Falls, respectively. The most dramatic increase in this initial flood event is predicted for the Tolt River (see Appendix C), where current levels of forest harvest are predicted to have caused an increase of 51 percent in the initial flood peak.

These modeled scenarios demonstrate the importance of antecedent conditions and specific storm micrometeorology on the expected increase in peak streamflow due to forest harvest. Due to the presence of low elevation snow, the effect of forest canopy removal on the initial flood was significant. However, since much of the low elevation snow pack melted prior to the second precipitation event, which directly caused the main flood peak, the effect of forest canopy removal on the main flood peak was considerably less.

Table 7.9. Basinwide average predicted increase in peak streamflows due to forest canopy removal for the initial flood peak during the February 1996 event.

Flood Peak	All Harvested	Band Harvested	GAP 1991
02/09/1995	13.8	4.1	1.9
02/08/1995	109.5	36.6	11.6

7.4.5. Relative contributions of increased melt rates and increased snow accumulation to peak streamflow enhancement

This dissertation has shown that the forest canopy can exert a strong influence on both the accumulation and melt of the ground snow pack. The remainder of this chapter investigates the relative contribution of changes in initial snow accumulation and changes in snow melt rates to increased water delivery to the soil during peak streamflow events. If changes in initial snow accumulation beneath the forest canopy do not significantly enhance runoff response during peak streamflow events, the analysis of forest harvest scenarios on peak streamflows can be simplified by focusing only on those parameters that control the attenuation of wind and radiation through the canopy (i.e. those factors that control the energy balance). However, if changes in antecedent

snow accumulation are found to be a significant contributor to increased runoff response, assessment of forest harvest scenarios must consider not only changes in the energy balance of the snow pack but those canopy factors that control antecedent snow accumulation as well.

To determine the relative contribution of changes in melt rates and changes in antecedent snow accumulation, the modeled total snowmelt was calculated over the duration of each of the ten flood events over each 100 meter elevation band ranging from sea level to 2300 meters. Total modeled snowmelt was calculated for both the historic vegetation cover and the completely harvested scenario. To determine the increase in snowmelt due to modeled antecedent conditions, the predicted increase in snowmelt due to clearcutting was compared to the maximum possible snowmelt in each elevation band during the simulation of historic vegetation cover (i.e. snowmelt occurring due to complete melt of the snowpack under the historic vegetation cover in each elevation band). Increases in snowmelt due to harvest beyond the maximum possible melt with the historic vegetation cover are attributed directly to changes in antecedent conditions. Table 7.10 shows a series of demonstration calculations. In hypothetical event A, complete melt occurred during both simulations. Therefore, the entire increase over the event is due to differences in antecedent snow accumulation. In hypothetical event B, the same relative amounts of melt occurred as in event A, however the greater initial snow accumulation beneath the forest canopy leads to incomplete melt of the below canopy snowpack. Although snow melt in the clearcut exceeds total possible melt under a forest canopy, only 60 percent of the increase in total melt is due to increased antecedent snow accumulation.

Table 7.10. Example calculations for determining percent of increased melt due to differences in antecedent snow accumulation for two hypothetical events.

Event	Snow accumulation beneath forest canopy	Snow accumulation in clearing	Snow melt beneath canopy	Snowmelt in clearing	Increase in melt	Percent Increase due to accumulation differences
A	25 mm	50 mm	25 mm	50 mm	25 mm	(50-25)/25=100.0
B	35 mm	50 mm	25 mm	50 mm	25 mm	(50-35)/25 = 60.0

The basin-wide average results of this analysis are shown in Table 7.11. Figures 7.16 a-j show the results by elevation band for each event. The structure of Figure 7.16 is best explained by example. In Figure 7.16b, approximately 90 mm of snowmelt was predicted between an elevation of 1000 and 1100 meters during the entirely clear-cut simulation (total length of bottom bar). Approximately 30 mm of snow melt was predicted during the historic simulation in the same elevation (shaded portion of bottom bar). (Although not shown on Figure 7.16b, 35 mm of SWE was available for melt during the historic simulation in this elevation band.) The increase in melt is approximately 60 mm (total height of top bar) and 25 mm (60 minus 35) of this increase (the black portion of top bar) was caused by differences in antecedent snow accumulation (DDTA in Figure 7.16).

In five of the ten events the total contribution of differences in antecedent snow accumulation to the predicted increase in total melt are less than five percent, with four events showing almost no contribution of antecedent conditions. However, for four of the flood events, the total contribution of differences in antecedent snow accumulation exceeded 20 percent of the total increase in snow melt with a maximum of 32.3 percent during the 25 Nov 1990 flood. The total contribution of differences in snow accumulation for the 9 Feb 1996 flood is approximately 27 percent of the total increase in snow melt.

The effect of differences in antecedent snow accumulation is most pronounced at lower elevations. For the 25 Nov 1990 event (Figure 7.16 e) antecedent conditions account for the entire increase in melt due to forest harvest below an elevation of 1000 meters. In those elevation bands with the greatest overall increase in melt (above 1200 meters), antecedent conditions do not effect melt rates during the 1990 event. During the 9 Feb 1996 event (Figure 7.16 j), increases due to changes in antecedent conditions are limited to elevations below 600 meters. Above an elevation of 600 meters, the entire increase in total melt is due to an increase in melt rates and is not affected by antecedent snow conditions. This result is expected due to the relatively high accumulations of SWE prior to this event at high elevation site (400 mm SWE observed at the Cougar Mountain SNOTEL Site).

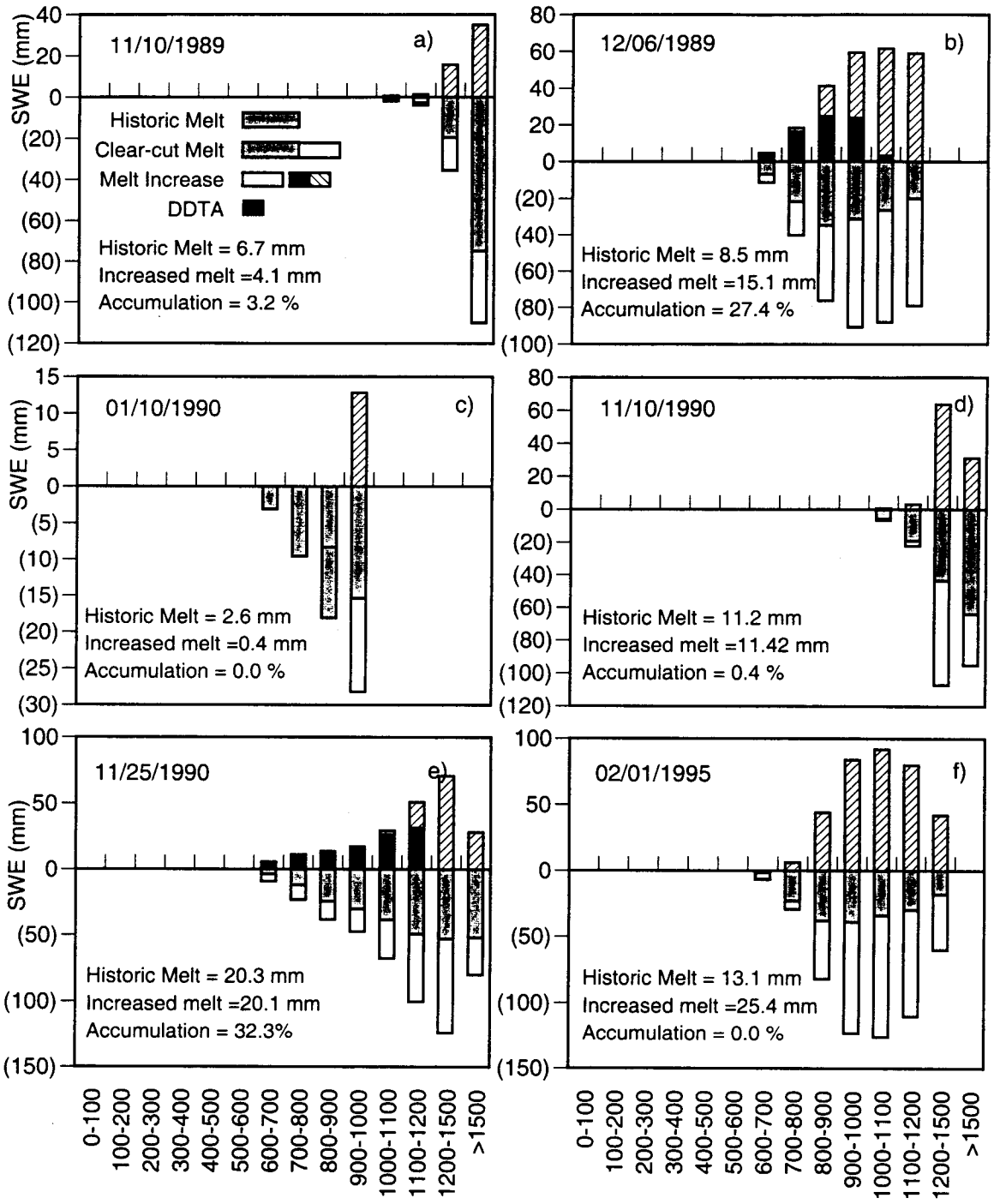

Figure 7.16 a-f. Increase of snow melt due to complete canopy removal during rain-on-snow events over the Snohomish basin from 10 Nov 1989 to 1 Feb 1995. Individual bars represent average values over each elevation range. Totals are calculated w.r.t. the entire Snohomish Basin. DDTA is the difference in the snow melt increase due to differences in antecedent snow accumulation.

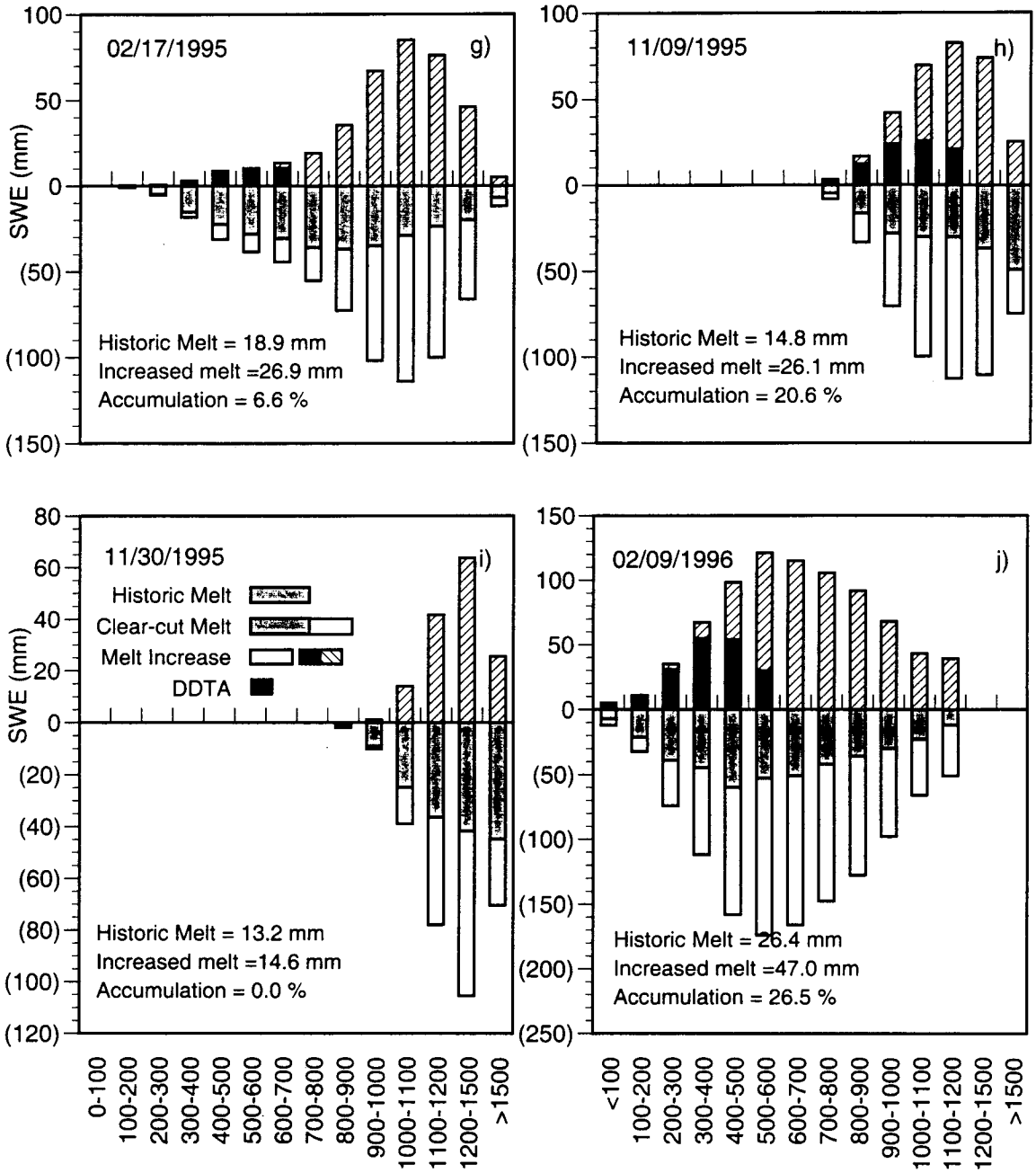

Figure 7.16 g-j. Increase of snow melt due to complete canopy removal during rain-on-snow events over the Snohomish basin from 17 Feb 1995 to 9 Feb 1996. Individual bars represent average values over each elevation range. Totals are calculated w.r.t. the entire Snohomish Basin. DDTA is the difference in the snow melt increase due to differences in antecedent snow accumulation.

These results suggest strongly that differences in antecedent snow accumulation can be responsible for a significant portion of the total increase in snowmelt due to forest canopy removal. However, the relative contribution of differences in antecedent snow accumulation varies over different events and depends strongly on the spatial distribution of snow cover.

Table 7.11. Increase of total water delivery to the soil expressed as a percentage of total observed precipitation over the entire Snohomish Basin. The relative basinwide contribution of differences in antecedent snow accumulation to the predicted increase is also shown.

Event	Precip-itation (basin average in mm)	Historic Vegetation (basin average snow melt in mm water equivalent)	Completely Clear-Cut (basin average snowmelt in mm water equivalent)	% increase in snowmelt relative to precipitation	% of increase due to differences in antecedent snow accumulation
11/10/1989	112	6.7	10.8	3.7	3.2
12/06/1989	163	8.5	23.6	9.3	27.4
01/10/1990	256	2.6	3.0	0.1	0.0
11/10/1990	166	11.2	22.6	6.9	0.4
11/25/1990	296	20.3	40.4	6.8	32.3
02/01/1995	138	13.1	38.5	18.4	0.0
02/17/1995	100	18.9	45.8	27.0	6.6
11/09/1995	170	14.8	40.9	15.4	20.6
11/30/1995	264	13.2	27.8	5.5	0.0
02/09/1995	313	26.4	73.4	15.0	26.5

Chapter 8. Summary and conclusions

This dissertation has investigated the effect of forest canopy removal on peak streamflows in the Pacific Northwest. Two science questions have guided this work: a) Has forest canopy removal increased peak streamflow events during rain-on-snow (ROS) floods? and b) To what extent are changes in antecedent snow accumulation associated with canopy removal responsible for these increases?

These questions arose from analysis of results from previous watershed and plot-scale studies of forest harvest effects on peak streamflow and water delivery to the soil during ROS events. Previous watershed-scale studies have shown increases in streamflow due to forest canopy removal for smaller peak streamflow events (those that occur several times per year) but, due to large natural variability and small sample sizes, these studies have been largely inconclusive regarding major floods (Bowling et al. 2000). Plot-scale studies have shown that total water delivery to the soil during ROS events increases due to canopy removal (e.g. Beaudry and Golding 1983, Berris and Harr 1987, Storck et al. 1999). The increase is due to two main factors: an increase in the snowmelt rate during the event caused by an increase in energy transfer to the snow surface, and an increase in antecedent snow accumulation. While the mechanisms responsible for the increased melt rate are well understood (see e.g. USACE 1956, Harr 1981, Berris and Harr 1987, Marks et al. 1998), the mechanisms controlling snow accumulation below forest canopies in the Pacific Northwest have not been well understood due primarily to a lack of field data.

8.1. Summary

To address the science questions posed in this dissertation, a multi-scale investigation of forest canopy effects on snow accumulation and melt was conducted. During a three year field investigation at a site in the Umpqua National Forest, OR (elevation 1200 m), weighing

lysimeters and cut-tree experiments (described in Chapter 4) were used to measure the processes controlling snow interception and its fate while providing continuous observations of below-canopy snowpack evolution. These data (described in Chapter 5) were used to construct, calibrate, and test an energy balance model of snow interception by the forest canopy as well as snow accumulation and melt beneath the forest canopy for use in distributed hydrology models (Chapter 6). A computationally efficient atmospheric stability correction was developed. The model was calibrated against one year of weighing lysimeter data and was tested at the plot scale against two years of weighing lysimeter data and at the stand scale against three years of snow course data taken over an area of 26 ha. Scaling from the plot to the stand scale was facilitated by inclusion of a fractional canopy coverage parameter.

This model was incorporated into a previously developed distributed hydrology model (DHSVM, Wigmosta et al. 1994) to explore the effect of forest canopy removal on floods during ROS events in maritime climates like the Pacific Northwest. A sensitivity analysis of the 10 largest floods that occurred between 1988 and 1996 on the Snohomish River, which drains the western slopes of the Cascade Mountains in Washington State, was conducted (Chapter 7). The modeled effects of various patterns of forest harvest on peak streamflow were explored. The contribution of increased snow accumulation and increased snowmelt rates resulting from forest harvest was determined for each flood as a function of elevation.

8.2. Conclusions

1) Snow interception by a mature forest canopy in a maritime climate is an important process with an apparent maximum interception capacity of approximately 40 mm SWE and is well described as a linear function (60 percent) of snowfall (for snowfall depths less than 50 mm SWE). Additional data are needed to adequately define the upper asymptote. Melt of intercepted snow and subsequent drip of meltwater to the beneath-canopy snowpack is the dominant removal mechanism of intercepted snow from the canopy in the transient snow zone of maritime climates.

The maximum interception capacity and the linear growth form were inferred from differences in beneath-canopy and clearing snow accumulation as measured by the weighing lysimeters. These conclusions were supported by direct observations of intercepted snow from the cut-tree experiments. Comparisons of total water (SWE plus accumulated outflow) from the weighing lysimeters showed that, under conditions common in the transient snow zone, meltwater drip and mass release dominated sublimation with meltwater drip accounting for the removal of up to 70% of intercepted snow. During periods when air temperature remained below freezing after snowfall, sublimation was an important mechanism for removal of intercepted snow with average annual losses of approximately 100 mm SWE (average observed over two winter seasons)

2) For the events and conditions observed here, micrometeorological effects on the rate of snow interception and the snow interception capacity can be ignored and morphological differences between Douglas-fir, ponderosa pine, white fir and lodgepole pine trees do not affect the rate, magnitude or disposition of intercepted snow.

No difference in the rate of intercepted snow between events was observed during 36 snowfall events over three winter seasons of weighing lysimeter data. Direct observations of intercepted snow load on cut-trees during snowfall events showed no pattern of increased rate or maximum capacity for snow interception by different species. Additional data are needed before the conclusions made here can be generalized to other species or climates.

3) A simple linear snow interception model combined with an energy balance model of intercepted snow disposition and ground snowmelt predicted the accumulation and melt of snow at the plot-scale beneath a mature forest canopy and at the scale of a forest stand.

Good agreement between model predictions and observations during three seasons of weighing lysimeter and snow course data was seen. The model was scaled from the plot to the stand scale by incorporating a fractional canopy coverage parameter. Model predictions at all scales were found to be strongly affected by the formulation of the atmospheric stability correction. A computationally efficient formulation which does not completely suppress turbulent exchange under stable conditions yielded the best agreement with observations.

4) Current levels of forest harvest have increased modeled peak streamflow relative to the peak streamflow obtained with a historic representation of forest canopy cover during major floods on the Snohomish River Basin.

A sensitivity analysis of peak streamflows during floods to varying levels of forest harvest was performed. The modeled average peak streamflows over the subbasins of the Snohomish considered here have increased by approximately three percent due to current levels of forest harvest relative to the peak streamflows obtained with a historic representation of forest canopy cover. The Tolt River subbasin (211 km^2) yielded the largest predicted increase, an average of 8.9 percent over all ten flood events. The maximum predicted increase in peak streamflow for the Snohomish River at Monroe (4000 km^2) was 4.8 percent during the flood of 1 February 1995. Increases of over ten percent were predicted for this flood at the Snoqualmie at Carnation (1561 km^2). The smallest basinwide average increase was predicted for the 10 Jan 1990 event (0.6 percent). The maximum predicted increase over all ten flood events and all subbasins was 24.7 percent for the Tolt River (1 Feb 1995). Even more dramatic increases in peak streamflow were predicted for the initial peak streamflow event during the February 1996 flood (up to 51 percent for the Tolt River). Small increases in streamflow were predicted for the flood of record (November 25, 1990). Larger increases in peak streamflow were predicted for a concentrated harvest in the transient snow zone and complete canopy removal over the basin.

The average increase in peak streamflow due to current levels of forest harvest at the watershed scale is below the minimum detectable difference of paired catchment studies (Bowling et al. 2000). Therefore, hydrologic modeling of the effect of forest canopy removal may be the only effective mechanism for investigating changes in peak streamflow during major flood events at the watershed scale.

5) Changes in antecedent snow accumulation must be considered to assess the impact of forest harvest at the watershed scale adequately.

Differences in antecedent snow accumulation due to forest harvest are responsible for up to 32 percent of the increased total snowmelt during ROS flood events at the scale of the entire Snohomish River. The relative contribution of differences in antecedent snow accumulation depends strongly on the initial snow distribution over the watershed and the micrometeorology during the event.

8.3. Unanswered questions

This work has quantified and modeled processes controlling snow accumulation and melt beneath forest canopies in the transient snow zone of maritime mountainous climates like the Pacific Northwest. The analysis of forest canopy removal on peak streamflow presented here considered only those effects related directly to forest canopy removal and was focused on major ROS floods. Therefore, several questions remain unanswered. These include:

1) How effectively does the snow interception and ablation model developed here predict snow interception and its disposition in cold climates and at higher elevations in maritime climates?

2) What is the combined effect of forest roads and canopy removal at the watershed scale on floods equal to or greater than the mean annual flood and is the predicted increase greater than the minimum detectable difference of paired catchment studies?

3) What is the combined effect of forest roads and canopy removal at the watershed scale on smaller peak streamflow events (i.e. those that occur on average several times per year) and is the predicted increase greater than the minimum detectable difference of paired catchment studies?

4) How do changes in antecedent snow accumulation due to forest harvest contribute to possible increases in peak streamflow during radiation-dominated melt events which occur in late spring and early summer?

These questions could be addressed through a combination of field studies and modeling investigations. Evaluation of the canopy-snow model presented here in colder climates (or at higher elevation) will require, at a minimum, a complete suite of measurements of the near-surface meteorology in a clearing (air temperature, humidity, windspeed, incoming short- and long-wave radiation, and precipitation) as well as robust measures of snow accumulation and melt both in a clearing and beneath the forest canopy. In cold climates and high elevation maritime climates, melt of intercepted snow is rare. Given the current model formulation, mass release will not occur without snowmelt and the intercepted snow will remain in the canopy where it is vulnerable to sublimation. While this representation is qualitatively correct, model predictions of beneath-canopy SWE at high elevation sites should be verified. Specific attention should be given to quantifying the role of wind transport of intercepted snow both during and after snowfall events. Ideally, such a field study would attempt to measure processes directly via a field campaign similar to that described here. However, for the purpose of model testing, a series of weekly snow courses combined with micro-meteorological observations may be sufficient.

To explore the combined effect of roads and canopy removal will require a limited field experiment to test the representation of roads over these large basins. Specific attention should be given to the spacing of culverts along the road network and the connectivity of these culverts to the natural stream network. A more detailed description of soil properties and a higher resolution terrain model will also be required. Given an accurate representation of the road network, a full analysis of forest harvest effects on all sizes and types of peak streamflow events should be straightforward and can proceed in a manner similar to that described in Chapter 7 to investigate the effect of forest canopy removal.

To explore the effect of canopy removal on radiation dominated melt events will require a more careful examination of snow albedo. At a minimum, the current formulation should be tested against observations of albedo during mid-winter and early-spring radiation dominated melt events. Preferably, the current albedo formulation, should be enhanced to consider physical processes, such as snow crystal metamorphosis, explicitly.

References:

Adams, R. S., D. L. Spittlehouse, and R. D. Winkler, The effect of a canopy on the snowmelt energy balance, in *Proc. 64th Western Snow Conf.*, Colorado State University, Fort Collins, 1996.

Anderson, E. A., A point energy and mass balance model of a snow cover, *NWS Technical Report 19*, National Oceanic and Atmospheric Administration, Washington, DC. 150 pp, 1976.

Anderson, H. W., and R. L. Hobba, Forests and floods in the northwestern United States, *IAHS Publ.* **48**:30-39, 1959.

Aubry, K. B., M. P. Amaranthus, C. B. Halpern, J. D. White, B. L. Woodward, C. E. Peterson, C. A. Logoudakis, and A. J. Horton, Evaluating the effects of varying levels and patterns of green-tree retention: experimental design of the DEMO study, *Northwest Science*, **73**:12-26, Special Issue,1999.

Beaudry, P. G., and D. L. Golding, Snowmelt during rain-on-snow in coastal British Columbia, in *Proc. 51th Western Snow Conf.*, pp. 55-66, Colorado State University, Fort Collins, 1983.

Berris, S. N., Comparative snow accumulation and melt during rainfall in forest and clearcut plots in western Oregon, *M.S. Thesis*, Oregon State University, Corvallis, 152 pp., 1984.

Berris, S. N., and R. D. Harr, Comparative snow accumulation and melt during rainfall in forested and clear-cut plots in the western Cascades of Oregon, *Water Resources Research*, **23**(1):135-142, 1987.

Black, T. A., J. M. Chen, X. Lee, and R. Sagar, Characteristics of shortwave and longwave irradiances under a Douglas-fir forest stand. *Can J. For. Res.*, **21**:1020-1028, 1991.

Bowling, L. C., and D. P. Lettenmaier, The effects of forest roads and harvest on catchment hydrology in a mountainous maritime environment, in *The Influence of Land Use on the Hydrologic-Geomorphic Response of Watersheds*, M. Wigmosta and S. Burges, eds., AGU, Washington, D.C., 2000.

Bowling L.C., P. Storck, and D. P. Lettenmaier, Hydrologic effects of logging in western Washington. *Water Resources Research*, in review, 2000.

Bunnell, F. L., R. S. McNay, and C. C. Shank, Trees and snow: the deposition of snow on the ground - a review and quantitative synthesis, *IWIFR-17*. Research Branch, Ministries of Environment and Forests, Victoria, BC., 449 pp., 1985.

Calder, I. R., *Evaporation in the Uplands*, Wiley, Chichester, 144 pp., 1990.

Chen, J., Edge effects : microclimatic pattern and biological responses in old-growth Douglas-fir forests, Ph.D. Thesis, University of Washington, 174 pp., 1991.

Christner, J., and R. D. Harr, Peak streamflows form the transient snow zone, Western Cascades, Oregon, in *Proc. 50th Western Snow Conf.*, pp. 27-38, Colorado State University, Fort Collins, 1982.

Coffin, B., and R. D. Harr, Effects of forest cover on volume of water delivery to soil during rain-on-snow, *Timber-Fish-Wildlife Report SH1-92-001*, Washington Department of Natural Resources, Olympia, Washington, 118 pp., 1992.

Connelly, B. A., T. W. Cundy, and D. P. Lettenmaier, Implications of forest practices on downstream flooding: Phase I Interim Report, Washington Forest Protection Association, unpublished, 1993.

Daly C., A statistical topographic model for mapping climatological precipitation over mountainous terrain, *Journal of Applied Meteorology,* **33**(2):140-158, 1994.

Denmead, O. T., and E. F. Bradley, Flux-gradient relationships in a forest canopy. In, Hutchinson, B. A., and B. B. Hicks (eds), *The Forest-Atmosphere Interaction*, D. Reidel publishing co., pp. 421-442, 1985.

Dingman, S. L., *Physical Hydrology*, Prentice Hall, 575 pp., 1994.

Entekhabi, D., and P. S. Eagleson, Land surface hydrology parameterization for atmospheric general circulation models: Inclusion of subgrid scale spatial variability and screening with a simple climate model, *Ralph M. Parsons Lab Rep. 325*, 195 pp., Mass. Inst. of Technology, Cambridge, 1989

Fitzharris, B. B., Snow accumulation and deposition on a wet coast, mid-latitude mountain. *Ph.D. Thesis*, University of British Columbia, Vancouver, 367 pp., 1975.

Halpern, C. B, S. A. Evans, C. R. Nelson, D. McKenzie, D. A. Liguori, D. E. Hibbs, and M. G. Halaj, Response of forest vegetation to varying levels and patterns of green-tree retention: an overview of a long-term experiment, *Northwest Science*, **73**:27-44, 1999.

Harr, R. D., Some characteristics and consequences of snowmelt during rainfall in western Oregon, *J. Hydrol.*, **53**,:277-304, 1981.

Harr, R. D., Effects of clearcut logging on rain-on-snow runoff in western Oregon: New look at old studies, *Water Resour. Res.*, **22**(7):1095-1100, 1986.

Harr, R. D., and F. M. McCorison, Initial effects of clearcut logging on size and timing of peak flows in a small watershed in western Oregon, *Water Resour. Res.*, **15**(1):90-94, 1979.

Hartman, R.K., A. A. Rost, and D. M. Anderson, Operational processing of multi-source snow data. Presented at the *Third International Conference/Workshop on Integrating Geographic Information Systems and Environmental Modeling*, Santa Fe, New Mexico, 1996.

Hedstrom, N. R., and J. W. Pomeroy, Measurement and modelling of snow interception in the boreal forest, *Hydrological Processes*, **12**, 1611-1625, 1998.

Hoover, M. D., and C. F. Leaf, Process and significance of interception in Colorado subalpine forest, in Sopper , W. E. and H. W. Lull (eds.), *Forest Hydrology*, Pergamon Press, New York. Pp. 213-223, 1967.

Horton, R. E., Rainfall interception, *Monthly Weather Rev.*, **47**:603-623, 1919.

Ishikawa, N., and Y. Kodama, Transfer coefficients of sensible heat on a snowmelt surface., *Meteorol. Atmos. Phys.* **53**:233-240, 1994.

Japanese Government Forest Experiment Station, Laboratory of snow damage in division of forest calamity prevention: study of fallen snow on the forest trees (the first report), (in Japanese), Bulletin **54**:115-164, 1952.

Johnson, R. C., The interception, throughfall and stemflow in a forest in highland Scotland and the comparison with other upland forests in the U.K., *Journal of Hydrology*, **118**:281-187, 1990.

Johnson, W. M., The interception of rain and snow by a forest of young ponderosa pine. *Trans. Am. Geophys. Union*, **23**:566-570, 1942.

Jones, J. A., and G. E. Grant, Peak flow responses to clear-cutting and roads in small and large basins, western Cascades, Oregon, *Water Resour. Res.*, **32**:959-974, 1996.

Jordan, R., A one-dimensional temperature model for a snow cover: technical documentation for SNTHERM.89, *Special Report 91-16*, US Army Corps of Engineers Cold Regions Research and Engineering Laboratory, Hanover, NH, 49 pp., 1991.

Kittredge, J., Influence of forests on snow in the ponderosa-sugar pine-fir zone of the central Sierra Nevada, *Hilgardia*, **22**(1):1-96, 1953.

Kobayashi, D., Snow accumulation on a narrow board, *Cold Regions Sc. Technol.*, **13**:239-245, 1987.

Kolesov, A. F., Interception of snow by the forest canopy, *Soviet Soil Science*, **17**(4):123-126, 1985.

Lamarche, J., and D. P. Lettenmaier, Forest road effects on flood flows in the Deschutes river basin, Washington, Water Resources Technical Report, Department of Civil Engineering, University of Washington, 178 pp., 1998.

Lundberg, A., Evaporation of intercepted snow - review of existing and new measurement methods. *Journal of Hydrology,* **151**:267-290, 1993.

Lundberg, A., Ian Calder, I., and R. Harding, Evaporation of intercepted snow: measurement and modelling. *Journal of Hydrology*, **206**:151-163, 1998.

Marks, D., and J. Dozier, Climate and energy exchange at the snow surface in the alpine region of the Sierra Nevada: 2. Snow cover energy balance, *Wat. Resour. Res.*, **28**:3043-3054, 1992.

Marks, D., J. Kimball, D. Tingey, and T. Link, The sensitivity of snowmelt processes to climate conditions and forest cover during rain-on-snow: a case study of the 1996 Pacific Northwest flood, *Hydrological Processes*, **12**:1569-1587, 1998.

Maxson, R.W., M. W. Allen, and T. L. Szeliga, Image classification by comparison of angles created between multi-channel vectors and an empirically selected reference vector. 1996 North American Airborne and Satellite Snow Data CD-ROM, Chanhassen, Minnesota: National Weather Service, 1996.

McGurk, B. J., Propylene glycol and ethanol as a replacement antifreeze for precipitation gauges: dilution, disposal and safety. In *Proc. 60th West. Snow Conf.*, Colorado State University, Fort Collins, pp. 56-65, 1992.

Merriam, R. A., A note on the interception loss equation, *J. Geophys. Res.*, **65**:3850-3851, 1960.

Miller, D. A., and R. A. White, A Conterminous United States Multi-Layer Soil Characteristics Data Set for Regional Climate and Hydrology Modeling, *Earth Interactions*, American Geophysical Union, 1998; http://EarthInteractions.org.

Miller, D. H., Snow in the trees - where does it go? In *Proc West. Snow Conf.*, Colorado State University, Fort Collins, pp 21- 29, 1962.

Miller, D. H., Interception processes during snowstorms. *Research Paper PSW-18*, USDA Forest Service, Pacific Southwest Forest and Range Experiment Station, Berkeley, CA, 24 pp., 1964.

Miller, D. H., Transport of intercepted snow from trees during snowstorms. *Res. Pap. PSW-33*, 30 pp., U.S. Dep. Agric. For. Serv., Berkeley, Calif., 1966.

Miller, D. H., Sources of energy for thermodynamically-caused transport of intercepted snow from forest crowns. in Sopper, W. E. and H. W. Lull (eds.), *International Symposium on Forest Hydrology*, pp. 201-211, Pergamon, New York, 1967.

Nijssen, B., I. Haddeland, and D. P. Lettenmaier, Point evaluation of a surface hydrology model for BOREAS, *Journal of Geophysical Research-Atmospheres*, **102**:29367-29378, 1997.

Ohta, T., T. Hashimoto, and H. Ishibashi, Energy budget comparison of snowmelt rates in a deciduous forest and open site, *Annals of Glaciology*, **18**:53-59, 1993.

Perkins, W.A., M.S. Wigmosta, B. Nijssen, Development and testing of road and stream drainage network simulations within a distributed hydrologic model, *Eos Trans. AGU*, **77**(46), Fall Meet. Suppl., F453, 1996.

Piehl, B. T., R. L. Beschta, and M. R. Pyles, Ditch Relief Culverts and Low-Volume Forest Roads in the Oregon Coast Range, *Northwest Science* **62**(3):91-98, 1998.

Price, A. G., Prediction of snowmelt rates in a deciduous forest. *Journal of Hydrology*, **101**:145-157, 1988.

Price, A. G., and T. Dunne, Energy balance computations of snowmelt in a subarctic area, Water Resources Research, **12**:686-694, 1976.

Rothacher, J., Does harvest in the west slope Douglas-fir increase peakflow in small forest streams? *For. Serv. Res. Pap. PNW-163*, U.S. Dep. Agric., Pac. Northwest For. Range Exp. Stn., Portland, Oregon, 13 pp., 1973.

Rowe, P. B., and T. M. Hendrix, Interception of rain and snow by second-growth ponderosa pine. *Trans. Am. Geophys. Union* **32**: 903-908, 1951.

Satterlund, D. R. and H. F. Haupt, Snow catch by conifer crowns. *Water Resour. Res.*, **3**:1035-1039, 1967.

Satterlund, D. R., and H. F. Haupt, The disposition of snow caught by conifer crowns, *Water Resour. Res.*, **6**(2):649-652, 1970.

Schmidt, R. A., Sublimation of snow intercepted by an artificial conifer, *Agricultural and Forest Meteorology*, **54**:1-27, 1991.

Schmidt, R. A., and D. R. Gluns, Snowfall interception on branches of three conifer species, *Can. J. For. Res.*, **21**:1262-1269, 1991.

Schmidt, R. A., and C. A. Troendle, Snowfall into a forest and clearing, *Journal of Hydrology*, **110**:335-348, 1989.

Scott, J.M., and M.D. Jennings, Large-area mapping of biodiversity. *Annals of the Missouri Botanical Garden*, **85**:34-47, 1998.

Storck, P., L. Bowling, P. Wetherbee, and D. Lettenmaier, Application of a GIS-based distributed hydrology model for the prediction of forest harvest effects on peak streamflow in the Pacific Northwest, *Hydrological Processes*, **12**:889-904, 1998.

Storck, P., T. Kern, and S. Bolton, Measurement of differences in snow accumulation, melt and micrometeorology due to forest harvesting, *Northwest Science*, **73**:87-100, 1999.

Storck, P., D. P. Lettenmaier, B. A. Connelly, and T. W. Cundy, Implications of forest practices on downstream flooding: Phase II Final Report, Washington Forest Protection Association, *TFW-SH20-96-001*, 100p., 1995.

Tarboton, D. G., T. G. Chowdhury, and T. H. Jackson, A spatially distributed energy balance snowmelt model, in Tonneson, K. A., W. Williams, and M. Tranter (eds), *Biogeochemistry of Seasonally Snow Covered Catchments, IAHS-AIHS Publication 228*, International Association of Hydrological Sciences, Wallingford, pp. 141-155, 1995.

Thomas, R. B., and W. F. Megahan, Peak flow response to clear-cutting and roads in small and large basins, western Cascades, Oregon: A second opinion, *Water Resources Research*, **34**(12):3393-3403, 1998.

US Army Corps of Engineers (USACE), Snow Hydrology: Summary report of the snow investigations, North Pacific Division, Portland, Oregon. 437 pp., 1956.

US Geological Survey, *Water Resources Data for Washington: Water Year 1982,* USGS Report # WRD-HD-85-220, Tacoma, Washington, 1985.

US Geological Survey, National Elevation Dataset, Fact Sheet 148-99, Reston, VA, 1999.

Van de Griend, A. A, and J. A. van Boxel, Water and surface energy balance model with a multi-layer canopy representation for remote sensing purposes, *Water Resources Research*, **25**(5): 949-971, 1989.

Van Heeswijk, M., J. Kimball, and D. Marks, Simulation of water available for runoff in clearcut forest openings during rain-on-snow events in the western Cascade Range of Oregon and Washington, *Water-Resources Investigations Report 95-4219*, US Geological Survey, Tacoma, Washington, 67 pp., 1996.

Washington Forest Practices Board, Standard methodology for conducting watershed analysis (version 2.1). *Forest Practices Board Manual*, Olympia, Washington, 1994.

Webb, E. K., Profile relationships: the log-linear range, and extension to strong stability. Quart. *J. R. Met. Soc.*, **96**:67-90, 1970.

Wetherbee, P. K., A comparison of observed and predicted snowpack outflow during rain-on-snow, Umpqua National Forest, Oregon, *M.S. Thesis*, University of Washington, 100 pp., 1995.

Wigmosta, M. S., D. P. Lettenmaier, and L. W. Vail, A distributed hydrology-vegetation model for complex terrain, *Water Resources Research,* **30**(6):1665-1679, 1994.

Wigmosta M. S. and W. A. Perkins, Simulating the effect of forest roads on watershed hydrology, in *The Influence of Land Use on the Hydrologic-Geomorphic Response of Watersheds*, M. Wigmosta and S. Burges, eds., AGU, Washington, D.C., 2000.

Westrick, K. J., C. F. Mass, B. Nijssen, D. McDonnal, P. Storck, and D. P. Lettenmaier, Description and evaluation of a high resolution hydrometeorological forecast system configured for real-time application, in review, *Weather Analysis and Forecasting*, 2000.

Yague, C., and J. L. Cano, The influence of stratification on heat and momentum turbulent transfer in Antarctica. *Boundary Layer Meteorology*, **69**:123-136, 1994.

Appendix A. Calculation of wind, and radiation profiles for driving the full canopy snow model

A.1. Estimation of above canopy meteorology from meteorology in a clearing.

Observations of above-canopy meteorology are seldom available. Given ground based (usually at the 2 meter reference height) observations of micrometeorology, the following transformations are made. Near surface temperature, humidity, incoming (i.e. downward) short and longwave radiation and precipitation measured at an open site (free from the effects of vegetation or structures) are taken as the above canopy values for the same terms. The near-surface and canopy reference heights are shown schematically in Figure 6.1. Wind speed (U) at the ground reference height (z_a) is scaled to the above canopy reference height (z_r) assuming neutral stability conditions and a logarithmic velocity profile as follows.

$$U(z_r) = U(z_a)\frac{\ln\left(\frac{z_r - d_s}{z_0}\right)}{\ln\left(\frac{z_a - d_s}{z_0}\right)} \tag{A.1}$$

where d_g is the snow displacement height (i.e snow depth) and z_o is the surface roughness.

A.2. Wind Profile

The wind profile through the canopy is modeled assuming neutral atmospheric conditions. While it is possible to include the effects of atmospheric stability on the profile itself, such a method requires iteration to determine the sensible heat flux and is too computationally expensive. The effects of stability on the sensible and latent heat fluxes at the snow surface are incorporated via the bulk Richardson's number (see Section 6.2). The wind profile above the canopy is assumed to follow a logarithmic profile

$$U(z) = U_r\frac{\ln\left(\frac{z - d_c}{z_{0,c}}\right)}{\ln\left(\frac{z_r - d_c}{z_{0,c}}\right)} \tag{A.2}$$

where U_r is the velocity at the reference height (z_r),k is Von Karman's constant, $z_{0,c}$ is the roughness length of canopy layer and d_c is the displacement height of the canopy layer. Immediately below this layer exists a roughness sublayer in which the vertical velocity gradients are smaller than those found by extrapolation of the semi-logarithmic profile in the inertial layer. These smaller velocity gradients are a result of wake diffusion effects caused by the canopy roughness elements. The profile here takes the shape:

$$U(z) = U_w - \frac{U_r}{\ln\left[\frac{z_r - d_c}{z_{0,o}}\right]}\left(1 - \frac{z - d_c}{z_w - d_c}\right) \tag{A.3}$$

where U_w is the wind speed at z_w (the height of the boundary between the inertial and roughness sublayers). Van de Griend and van Boxel (1989) suggest that

$$z_w = 1.5h - 0.5d_c \tag{A.4}$$

where h is the full height of the canopy. The wind profile within the canopy is assumed to be exponential, taking the form

$$U(z) = U_h e^{\beta\left(\frac{z}{h} - 1\right)} \tag{A.5}$$

where U_h is the wind speed at the top of the canopy andβ is a dimensionless extinction coefficient. Below the canopy of the overstory, i.e. within the trunk space, the wind profile is once again assumed to be logarithmic, taking the form

$$U(z) = U_t \frac{\ln\left(\frac{z - d_g}{z_{0,g}}\right)}{\ln\left(\frac{z_t - d_g}{z_{0,g}}\right)} \tag{A.6}$$

where U_t is the wind speed at the top of the trunk space ($z = z_t$), d_g and $z_{0,g}$ are the ground/understory displacement height and roughness length, respectively.

A.3. Aerodynamic resistance

Given the wind profile, the aerodynamic resistance between two levels h_1 and h_2 is given by

$$r_a = \int_{h_1}^{h_2} \frac{1}{K(z)} dz \tag{A.7}$$

where K(z) is the eddy diffusivity. The eddy diffusivity in the inertial layer above the canopy is a linear function of height given by

$$K(z) = \frac{k^2 U_r (z - d_o)}{\ln\left[\frac{z_r - d_o}{z_{0,o}}\right]} \tag{A.8}$$

In the roughness sublayer, diffusivity is assumed to be constant and equal to its value at z_w.

$$K(z) = K(z_w) = \frac{k^2 U_r (z_w - d_o)}{\ln\left[\frac{z_r - d_o}{z_{0,o}}\right]} \tag{A.9}$$

Following van de Griend and van Boxel (1989), the eddy diffusivity profile within the canopy takes the same shape as the wind profile, and is given by:

$$K(z) = K_h \frac{U(z)}{U_h} = K_h e^{\beta\left(\frac{z}{h}-1\right)} \tag{A.10}$$

where K_h is the eddy diffusivity at the top of the canopy. Below the canopy, the eddy diffusivity profile within the trunk space is once again defined by the logarithmic velocity profile, and is given by:

$$K(z) = \frac{k^2 U_t\left(z - d_g\right)}{\ln\left[\frac{z_t - d_g}{z_{0,g}}\right]} \tag{A.11}$$

The aerodynamic resistance for the overstory is calculated between the above-canopy reference height and the effective canopy height, z_c, and includes three distinct sections of the wind/eddy diffusivity profile.

$$r_{a,o} = \int_{z_c = d_c + z_{0,c}}^{z_r} \frac{1}{K(z)} dz = \int_{z_w}^{z_r} \frac{1}{K(z)} dz + \int_{h}^{z_w} \frac{1}{K(z)} dz + \int_{z_c}^{h} \frac{1}{K(z)} dz \tag{A.12}$$

The aerodynamic resistance for the soil surface, snow or understory is calculated by integrating Equation 11 along the lower 2 meters of the logarithmic velocity profile:

$$r_{a,g} = \int_{d_g + z_{0,g}}^{z_a = 2 + d_g + z_{o,g}} \frac{1}{K(z)} dz = \frac{\ln\left[\frac{z_a - d_g}{z_{0,g}}\right]^2}{k^2 U(z_a)} \tag{A.13}$$

where d_g and $z_{0,g}$ are the displacement and roughness height, respectively, for the snow surface.

A.4. Radiation Profile

Incoming shortwave (S_i) and longwave (L_i) radiation are specified above the canopy. Incoming shortwave radiation at the canopy reference level is assumed to be identical to S_i. Shortwave radiation absorbed by the intercepted snow is given by:

$$S_c = S_i\ (1-\alpha_i) \tag{A.14}$$

Where α_i is the intercepted snow albedo (assumed constant at 0.85). Shortwave radiation is transmitted to the near surface reference height via Beer's Law:

$$S_s = S_i \exp\ (-k\ *LAI) \tag{A.15}$$

where LAI is the leaf area index of the canopy and k is the radiation attenuation coefficient. Shortwave radiation absorbed by the snow surface is adjusted for snow albedo (see Section 6.4).

Longwave radiation absorbed by the intercepted snow $L_{i,c}$) is given by

$$L_{c,i} = L_i + L_{s,o} - 2\,L_{c,o} \qquad \text{(A.16)}$$

Where $L_{s,o}$ is the longwave radiation emitted by the ground snow pack and $L_{c.o}$ is the longwave radiation emitted by the canopy. The longwave radiation emitted by the canopy is given by:

$$L_{c,o} = \sigma T^4 \qquad \text{(A.17)}$$

where Tc is the temperature of the canopy (assumed equivalent to the air temperature or temperature of intercepted snow, when present). The longwave radiation emitted by the ground snow pack is given by:

$$L_{s,o} = \sigma T_s^4 \qquad \text{(A.18)}$$

where T_s is the snow surface temperature. Longwave radiation absorbed by the snow surface is given by

$$L_{s,i} = F * L_{c,o} + (1\text{-}F) * L_i \qquad \text{(A.19)}$$

where F is the effective canopy coverage.

A.5. Temperature and Humidity.

The effect of the canopy on temperature and humidity are not considered. The values for these forcings at all three levels are assumed identical.

Appendix B Linear storage reservoir channel routing model

A distributed routing model is used by DHSVM to route water intercepted by the channel and road networks. In this model, the channel network consists of a series of linked reaches modeled with a linear storage function. For each channel segment, continuity dictates that:

$$\frac{dS}{dt} = I - Q \tag{B.1}$$

where S is the storage in the reach, I is the inflow to the reach (including lateral inflow), Q is the outflow from the reach and t is time. It is assumed that storage is linearly related to the outflow from the reach by:

$$S = kQ \tag{B.2}$$

The factor of proportionality (k) can be approximated based on Manning's equation of flow for a rectangular channel:

$$Q = \frac{DWR^{2/3}S_o^{1/2}}{n} \tag{B.3}$$

where D is the flow depth in the channel, W is the width of the channel, R is the hydraulic radius (approximated by 0.75*D), S_o is the local channel slope, and n is Manning's roughness. Storage in the channel can be approximated by:

$$S = LWD \tag{B.4}$$

where L is the length of the local channel reach. Combining Eq's B.2 - B.4, k becomes:

$$k = \frac{Ln}{R^{2/3}S_o^{1/2}} \tag{B.5}$$

Assuming that inflow to the reach and k are constant over a given time interval, the following differential equation can be solved, which is a combination of Eq's B.1 and B.2.

$$\frac{dS}{dt} = I - \frac{S}{k} \tag{B.6}$$

The solution of Eq. B.6 given initial boundary conditions of S at time t and S_i at time t=0 is:

$$S = Ik + (S_i - Ik)\exp(-\frac{1}{k}t) \tag{B.7}$$

The final storage in the reach can be directly calculated from Eq. B.7 given the initial storage in the reach and the inflow during the time step. Outflow from the reach is calculated from Eq. B.1.

Appendix C: Complete listing of predicted increase in peak streamflows

Table C.1. Predicted increase in peak streamflow for 11 events,10 watersheds and three forest harvest scenarios. Values are a percent increase with respect to the historic vegetation cover. The February 7, 1996 event was not used to calculate the averages in Section 7.4.3.

Snohomish at Monroe

Event Date	All Cut	Band Cut	GAP 1991
11/10/89	37.06	8.11	2.41
12/6/89	32.26	6.19	3.40
1/10/90	6.31	1.04	0.99
11/10/90	18.79	2.30	1.65
11/25/90	10.61	1.06	0.93
2/1/95	58.55	7.50	4.78
2/17/95	29.20	2.94	3.00
11/9/95	31.61	3.10	2.67
11/30/95	11.71	1.14	1.07
2/9/96	18.43	5.25	1.98
2/7/96	86.03	24.43	7.52

Snoqualmie at Carnation

Event Date	All Cut	Band Cut	GAP 1991
11/10/89	33.12	8.38	3.54
12/6/89	32.10	8.92	7.19
1/10/90	6.20	0.95	1.66
11/10/90	19.65	2.50	3.32
11/25/90	9.76	1.11	1.43
2/1/95	70.58	13.04	12.72
2/17/95	30.00	4.52	5.85
11/9/95	37.38	3.22	5.65
11/30/95	10.99	1.05	2.06
2/9/96	12.35	3.50	2.95
2/7/96	88.78	22.85	11.58

Snoqualmie at Snoqualmie Falls

Event Date	All Cut	Band Cut	GAP 1991
11/10/89	27.91	7.34	2.21
12/6/89	34.04	10.18	5.64
1/10/90	3.85	0.81	0.50
11/10/90	17.19	2.09	2.03
11/25/90	8.68	0.95	0.65
2/1/95	73.76	12.90	9.90
2/17/95	31.71	4.76	4.63
11/9/95	38.34	3.02	4.51
11/30/95	10.10	0.86	1.51
2/9/96	11.38	3.51	2.17
2/7/96	86.77	25.69	9.77

Snohomish at Gold Bar

Event Date	All Cut	Band Cut	GAP 1991
11/10/89	40.05	9.04	1.08
12/6/89	34.36	6.15	1.21
1/10/90	3.81	0.94	0.11
11/10/90	15.84	1.66	0.49
11/25/90	9.83	0.92	0.33
2/1/95	59.91	5.68	2.05
2/17/95	30.13	1.07	1.06
11/9/95	29.81	1.61	0.79
11/30/95	10.92	0.87	0.27
2/9/96	16.27	5.30	0.47
2/7/96	106.03	34.58	2.51

Foss River

Event Date	All Cut	Band Cut	GAP 1991
11/10/89	22.86	4.09	0.00
12/6/89	30.72	3.91	0.00
1/10/90	2.36	0.81	0.00
11/10/90	13.09	0.93	0.00
11/25/90	7.46	0.63	0.00
2/1/95	43.93	3.18	0.00
2/17/95	19.52	0.15	0.00
11/9/95	19.66	0.86	0.00
11/30/95	8.39	0.54	0.00
2/9/96	11.32	3.57	0.00
2/7/96	78.61	27.17	0.00

Beckler River

Event Date	All Cut	Band Cut	GAP 1991
11/10/89	61.40	14.04	3.18
12/6/89	32.64	3.18	2.01
1/10/90	3.26	0.87	0.11
11/10/90	20.73	1.44	1.30
11/25/90	14.32	0.91	1.01
2/1/95	70.69	5.87	4.40
2/17/95	34.31	1.11	1.93
11/9/95	35.68	1.53	1.89
11/30/95	11.41	0.72	0.78
2/9/96	16.91	4.97	1.13
2/7/96	105.29	32.33	5.46

Table C.1. continued. Predicted increase in peak streamflow for 11 events,10 watersheds and three forest harvest scenarios. Values are a percent increase with respect to the historic vegetation cover. The February 7, 1996 event was not used to calculate the averages in Section 7.4.3.

Tolt River

Event Date	All Cut	Band Cut	GAP 1991
11/10/89	117.72	33.16	20.76
12/6/89	34.34	11.54	10.27
1/10/90	10.41	1.51	1.86
11/10/90	24.08	4.80	4.28
11/25/90	12.36	2.50	1.63
2/1/95	87.25	23.38	24.68
2/17/95	35.08	6.58	10.85
11/9/95	26.37	3.19	7.17
11/30/95	9.85	1.39	2.20
2/9/96	16.76	4.95	4.81
2/7/96	216.25	81.84	51.24

N.F. Snoqualmie

Event Date	All Cut	Band Cut	GAP 1991
11/10/89	94.14	27.20	3.97
12/6/89	38.71	13.25	1.75
1/10/90	6.31	0.92	0.05
11/10/90	20.19	3.64	2.29
11/25/90	9.12	2.01	0.84
2/1/95	115.94	14.53	6.09
2/17/95	43.95	3.88	2.40
11/9/95	27.63	3.47	2.82
11/30/95	9.57	1.31	0.97
2/9/96	14.06	2.80	0.82
2/7/96	190.94	75.54	7.79

M.F. Snoqualmie

Event Date	All Cut	Band Cut	GAP 1991
11/10/89	20.60	5.25	1.01
12/6/89	37.28	10.28	3.74
1/10/90	1.55	0.37	0.23
11/10/90	15.16	1.37	0.93
11/25/90	7.29	0.65	0.20
2/1/95	64.47	11.92	5.55
2/17/95	30.32	6.00	2.44
11/9/95	35.67	1.35	1.67
11/30/95	7.95	0.53	0.51
2/9/96	8.81	3.15	1.41
2/7/96	63.91	18.10	5.84

S.F. Snoqualmie

Event Date	All Cut	Band Cut	GAP 1991
11/10/89	16.95	4.21	2.02
12/6/89	40.00	14.02	11.96
1/10/90	1.06	0.39	0.06
11/10/90	16.51	1.76	2.45
11/25/90	9.61	0.60	0.23
2/1/95	64.68	21.43	14.68
2/17/95	34.13	11.56	9.02
11/9/95	47.17	3.30	7.61
11/30/95	10.30	0.57	1.78
2/9/96	11.77	3.57	3.10
2/7/96	72.75	23.04	14.62